

ALMA MATER STUDIORUM · UNIVERSITY OF BOLOGNA

School of Science
Department of Physics and Astronomy
Master Degree in Physics

Y-Systems And Wall Crossing

Supervisor:
Prof. Francesco Ravanini

Submitted by:
Stefano Franzoni

Co-Supervisor:
Prof. Davide Fioravanti

Academic Year 2022/2023

Abstract

The Thermodynamic Bethe Ansatz (TBA) equations have proved to be crucial to provide exact results in many areas of modern physics. The scope of its applications extends from lattice models for condensed matter physics to Integrable Quantum Field Theories (IQFTs). Research is also very active on its Ordinary Differential Equations (ODE) application, in particular, in the light of the correspondence between Integrable Models (IMs) and the ODEs associated to some classes of Schrödinger-like problems (ODE-IM correspondence). The possibility to formulate TBA systems in terms of functional relations known as Y-systems has brought to an alternative formulation of the problem and insights into the properties of its solutions. This thesis mainly focuses on the ODE side of the correspondence, and it investigates the formulation of Y-systems and TBA-systems of Schrödinger problems with polynomial potentials after wall crossing. Building on the results shown in [IMS19], an iterative procedure is proposed, so as to directly obtain the Y-system associated to a given chamber of the moduli space.

Contents

Introduction	3
1 TBA Equations and Y-Systems for Integrable Field Theories	6
2 The ODE-IM Correspondence: a Brief Overview	11
3 Resurgent Quantum Mechanics for the Stationary Schrödinger Equation	17
3.1 WKB Formalism	17
3.2 Borel Resummation	20
3.3 The Exact WKB Approach and the Delabaere-Pham Formula	22
3.4 The WKB Triangulation and Its Mutations	30
3.5 From the Delabaere-Pham Formula to a TBA System	37
3.6 TBA Deformation In the Minimal Chamber	42
3.7 Intermission: TBA Derivation with a ODE-IM Correspondence Perspective	43
3.8 Brief Overview of Exact Quantisation Conditions	47
4 TBA System for Polynomial Potentials Out of the Minimal Chamber	51
4.1 Warm Up: the Cubic Potential	52
4.2 Quartic Potential	64
5 Y-System Out of the Minimal Chamber	79
5.1 Y-System Deformation: Cubic Potential	79
5.2 Y-System Deformation: Quartic Potential	82
5.3 General Procedure	84
Conclusion	87
Acknowledgments	88

A Description of the Python Code	89
A.1 Code Description	90
A.2 Code Validation	94
List of Figures	97
Bibliography	99

Introduction

The Thermodynamic Bethe Ansatz (TBA) equations have been extensively used in the last thirty years to obtain exact results in a very wide range of physical applications. First introduced in 1969 by C. Yang and C.P. Yang [YY69] to describe the thermodynamics of non-relativistic interacting gases, the TBA equations were generalized at the beginning of the 90s to relativistic Integrable Quantum Field Theories (IQFTs) in the crucial works by Al.B. Zamolodchikov [Zam91, Zam90], and T.R. Klassen and E. Melzer [KM91, KM90]. In this context, a TBA system allows to extract the thermodynamics of the theory, and to exactly compute either the finite-volume ground state energy or the finite-temperature free energy. Even though the mirroring argument devised by Zamolodchikov to connect the free energy and the ground state energy works just for the ground state, methods to obtain integral equations for excited states based on the analytic continuation of the coupling constant were advanced by P. Dorey and R. Tateo in [DT96]. So far, no formal proof exists to show that any excited state may be reached with this method. Despite that, it remains a remarkable and potentially very profound result the fact that integral equations governing the ground state of an IQFT encapsulate information of many (if not all) excited states of the same theory. Within this IQFT-oriented approach to TBA equations, Zamolodchikov also underlined the possibility to translate the TBA system into a set of functional equations, the so-called Y-system, whose periodicity and shape may be put in close connection with an underlying description in terms of Lie algebras in the ADE series.

In parallel with the development of these tools, much work was devoted to understanding the role of other functional relations arising in both Integrable Models (IMs) and Ordinary Differential Equations (ODEs). Such functional relations are known as TQ-systems and TT-systems, and their introduction and development were mainly due to R.J. Baxter [Bax72], and Bazhanov, Lukyanov and Zamolodchikov [BLZ96, BLZ97, BLZ99]. These functional equations were originally studied by Baxter for integrable models on a lattice. In that context, lattice models in 2-dimensions are defined on a periodic lattice with generalized, twisted boundary conditions. The problem may be exactly solved for a wide class of models that will be referred to as integrable: this class of models is successfully applied to the description of magnets or condensed matter in general, with the possi-

bility to capture also their thermodynamic properties (in particular, phase transitions). In addition, it was also found out that TQ-relations may be turned into discretized versions of second-order, ordinary differential equations, providing a first hint of a possible connection between IMs and ODEs once the continuum limit is suitably taken. It was first realized by Dorey and Tateo in [DT99b, DDT07], that a full correspondence between integrable models and some classes of second order differential operators (ODE-IM correspondence) was possible by linking the TQ-systems with the functional relations studied by Y. Sibuya [SC73, Sib75] and A. Voros [Vor83] for a quartic quantum oscillator. For that connection to be realized, as anticipated, a continuum limit of the lattice model has to be performed, considering a fixed, dimensionful lattice width and a renormalization group procedure. Equally relevant for this thesis, in both the IM and the ODE contexts, TBA systems and Y-systems may be obtained from the TQ and the TT-systems, and the ODE-IM correspondence can be successfully employed to compute exact quantities and to prove important results in both fields.

The present thesis focuses on the ODE-side of the correspondence, and it is based on the exact WKB approach to the problem, developed by A. Voros [Vor83, Vor93], and E. Delabaere, H. Dillinger and F. Pham [DDP97, HD93]. In 2019, Katsushi Ito, Marcos Mariño and Hongfei Shu presented a set of TBA equations governing the WKB periods associated to generic polynomial potentials [IMS19], providing a generalization of the ODE-IM correspondence in the context of the exact WKB formalism. Even though the initial formulation of the TBA system they propose is limited to the case in which the roots of the polynomial potential are distinct and lie on the real axis (minimal chamber of the moduli space), they advance a generalization to the other sectors in the moduli space (non-minimal chambers) based on a deformation of the initial TBA. Such deformations occur in correspondence of the so-called wall-crossings, where the singularities in the kernels of the TBA equations cross the integration path, and residues need to be picked up after contour deformation. In this thesis, the cubic and the quartic oscillator are presented in detail, with a particular focus on the Stokes graphs mutations underlying the TBA deformation and the possibility to associate a Y-system also in this context. The Y-systems in the intermediate and in the maximal chamber are then obtained: the number of Y functions increases by one at each wall-crossing, in the same way as the number of equations in the TBA system. Looking for a periodicity in the Y-system, we verify that the periodicity is lost in all the non-minimal chambers. Then, we propose a procedure to obtain the Y-system associated to an arbitrary chamber, which is not based on the underlying deformed TBA-system, and it relies on a simple set of building-block rules and on the knowledge of the sequence of wall-crossing required to reach the given chamber. In addition, a Python code is developed in order to systematically keep track of the sequence of wall-crossings involved and to consistently apply the proposed procedure.

- In Chapter 1, a brief introduction to TBA systems for integrable quantum field theories is given. The canonical derivation of the TBA system for an S-Matrix-based, integrable QFT in $(1 + 1)$ -dimensions is presented. This is the most straightforward way to formulate a TBA-system with all the typical features of this type of coupled integral equations. Finally, the TBA system for scattering theories in the ADE series is reformulated in terms of a set of functional equations, the Y-system.
- In Chapter 2, a brief review of the link between integrable models and ordinary differential equations is provided.
- In Chapter 3, a review of the exact WKB method is presented. The formal WKB solution and the associated differential form and Riemann surface are introduced; the concepts of Borel transform and resummation are defined. The Stokes graph, its cycles, the relevant theorems that guarantee Borel summability, and the WKB triangulations are presented: this theory will be crucial in the following chapters of this thesis, where the Delabaere-Pham formula presented here will be one of the two possible starting points for the derivation of the TBA equations in [IMS19].
- In Chapter 4, the results presented in [IMS19] are introduced, starting from the case of a cubic potential in Sect.4.1, the first and simplest example exposed in the article. Then, the case of a quartic potential is discussed in Sect.4.2. The details of the passages needed to deform the TBA out of the minimal chamber are presented for the cubic case, and then generalized and applied also to the quartic potential.
- In Chapter 5, the Y-systems in the the intermediate and maximal chambers are derived, and their periodicity properties are described. Then, a procedure is proposed, so as to directly derive the Y-system for an arbitrary polynomial potential in a generic chamber in the moduli space.
- In the Appendix A, the Python code to numerically compute, plot and analyze the Stokes graph of a generic potential in an arbitrary direction is briefly described. In particular, the code allows to compute the sequence of wall crossings encountered along a path on the complex energy plane, and to analyse the cycle content in each chamber.

Chapter 1

TBA Equations and Y-Systems for Integrable Field Theories

In this chapter, we will start introducing the set of integral equations that will be central in the present thesis, the TBA equations. As anticipated in the Introduction, the TBA equations were first introduced in 1969 by C. Yang and C.P. Yang [YY69] to describe the thermodynamics of non-relativistic interacting gases, and later generalized to relativistic Integrable Quantum Field Theories (IQFTs) by A.I.B. Zamolodchikov [Zam91, Zam90], and T.R. Klassen and E. Melzer [KM91, KM90]. In this latter context, the TBA equations describe the thermodynamics of the integrable quantum field theory, and they allow to compute either the finite-volume ground state energy or the finite-temperature free energy. Due to its historical importance and rather simple derivation, we shall present here a brief overview of the TBA system, as obtained by Zamolodchikov, Klassen and Melzer for IQFTs. This presentation should provide a fairly accessible introduction to the features of this system of integral equations, and it will also fix some of the ideas and terminologies that will be used in the later discussion. In particular, the connection to a Y-system description will be established.

Let us start the derivation by stating the main assumptions. We shall restrict ourselves to relativistic quantum field theories in $(1 + 1)$ -dimensions. In this context, fields are operator-valued distributions acting on an infinite dimensional Hilbert space. The integrability property may be defined as follows:

Definition 1.1 *A $(1 + 1)$ -dimensional relativistic QFT is integrable if there exist infinitely many, pairwise commuting, local conserved charges.*

Examples of integrable QFTs in $(1 + 1)$ -dimensions are given by Sine-Gordon, Sinh-Gordon models, or, more in general, Toda field theories. In addition to the trivially integrable Conformal Field Theories (CFTs), also a few perturbations thereof by relevant operators have proved to be integrable [Mus20]. In particular, so far, only some

perturbations by a single relevant operator have been found to preserve integrability: for example, the Tricritical Ising Model (TIM) perturbed by the energy operator, or the Ising model perturbed by the magnetization operator are both integrable. Integrability plays a crucial role in the derivation of a TBA system, as it severely constrains the dynamics, and it allows to compute exactly many properties. In particular, it is very convenient to describe IQFTs in terms of their scattering data, as integrability poses the following constraints on the S-matrix:

1. only purely elastic processes take place, with no particle production, nor destruction;
2. the set of rapidities of the incoming state must coincide with that of the outgoing state, with permutations allowed only within internal symmetry multiplets;
3. scattering processes $n \rightarrow n$ are completely factorizable in a product of $n(n-1)/2$ two-particle scattering amplitudes.

In addition, a common assumption on the S-matrix shape is that of diagonality, which requires that, for a $2 \rightarrow 2$ process between the particle types $\{a_1, b_1\} \rightarrow \{a_2, b_2\}$, the associated S-matrix element $S_{a_1, a_2}^{b_1, b_2}$ satisfies $S_{a_1, a_2}^{b_1, b_2} = \delta_{a_1}^{b_1} \delta_{a_2}^{b_2} S_{a_1, a_2}$. We are now ready to summarize the main steps to get to the TBA equations. Let us fix the particle content by specifying the masses m_a , with a running over the particle types. Using the dimensionality of the theory, the rapidity θ may be used to parameterize energy and momentum:

$$E_a(\theta) = m_a \cosh(\theta) \ , \quad p_a(\theta) = m_a \sinh(\theta) \ . \quad (1.1)$$

Now, let us first consider Lorentz invariance. Let us suppose that the theory is defined on a flat torus generated by the circumferences C_L along the x -direction and C_R along the y -direction, of length L and R , respectively. Then, thanks to Lorentz invariance, two quantisation schemes are available. Denoting with $T_{\mu\nu}$ the stress-energy tensor of the theory, in the so called L -channel, the Hamiltonian reads:

$$H_R = \frac{1}{2\pi} \int_{C_R} dx T_{yy} \ , \quad (1.2)$$

whereas in the R -channel:

$$H_L = \frac{1}{2\pi} \int_{C_L} dy T_{xx} \ . \quad (1.3)$$

The partition function may be then equivalently expressed in the two schemes as

$$\mathcal{Z}(L, R) = \text{Tr}_{\mathcal{H}_R} e^{-LH_R} = \text{Tr}_{\mathcal{H}_L} e^{-LH_L} \quad (1.4)$$

Considering now taking the limit $L \rightarrow +\infty$, the physical interpretation is different in the two channels: while in the L -channel, this corresponds to take the time evolution

to infinity, in the R -channel it coincides with the thermodynamic limit. Using then the equivalent expressions for the partition function, the following fundamental relation may be obtained, that connects the finite-size ground state energy with the finite-temperature $T \equiv 1/R$ free energy density:

$$E_0(R) = Rf(R) . \quad (1.5)$$

The argument we just exposed is due to Zamolodchikov, and it is referred to as the Zamolodchikov's mirroring argument. Crucially, it holds just for $(1+1)$ -dimensional theories and it applies only to the ground state. Let us now focus on the R -channel, where L represents the volume. Then, being prepared to take $L \rightarrow +\infty$, short distance processes may be neglected, and asymptotic states called Bethe states constitute a basis for the Hilbert space \mathcal{H}_R . Denoting with N the number of particles, and considering n particle types labeled by a and with mass m_a , the associated wave function (coordinate Bethe Ansatz) reads:

$$\Psi(x_1, \dots, x_N) = e^{i \sum_{j=1}^N p_j x_j} \sum_{Q \in S_N} B(Q) \Theta(x_Q) , \quad (1.6)$$

where S_N is the permutation group, B are amplitude coefficients, and

$$\Theta(x_Q) = \begin{cases} 1 & \text{if } x_{Q_1} < \dots < x_{Q_N} \\ 0 & \text{otherwise} \end{cases} . \quad (1.7)$$

Since in the R -channel, L is large but still finite, suitable boundary conditions must be imposed at the domain boundaries, which translate into quantisation conditions that select the set of allowed rapidities. Using a diagonal, factorised S-matrix, the logarithm of the quantisation condition may be expressed as follows:

$$Lm_{a_i} \sinh(\theta_i) + \sum_{j \neq i} \delta_{a_i, a_j} (\theta_i - \theta_j) = 2\pi n_i , \quad i = 1, \dots, N , \quad (1.8)$$

where $n_i \in \mathbb{Z}$ if the i -th particle is a boson, $n_i \in \mathbb{Z} + 1/2$ if it is a fermion. Now, $\{n_i\}$ specify the set of allowed rapidities. From the unitarity condition on the S-matrix, additional constraint follow for the set of possible rapidities, depending on the statistics obeyed by each particle type. So far, the only consistent QFTs seem to be the ones that require distinct n_i for identical particles with the same rapidity. It is interesting to notice the close interplay between statistics and dynamics, as no particle exchange is possible without scattering in a theory with just one spatial dimension. Let us now take the last step in the derivation, namely, the Thermodynamic Limit (TL). As usual, this corresponds to taking $L \rightarrow +\infty$, $N \rightarrow +\infty$, keeping the density N/L constant and finite. As a consequence, it may be proved that the set of allowed rapidities tends to a continuous spectrum, and occupied states (also called roots) may be conveniently and

consistently described by a density distribution $\rho_a^{(r)}(\theta)$. Analogously, the unoccupied states (or holes) may be described by a density distribution $\rho_a^{(h)}(\theta)$. Taking then the TL of Eq.1.8, the configuration at thermodynamic equilibrium is given by that minimizing the free energy functional. With this last piece of information, the thermodynamic limit of Eq.1.8 reads:

$$\varepsilon_a(\theta) = m_a R \cosh(\theta) - \sum_{b=1}^n \int_{\mathbb{R}} \frac{d\theta'}{2\pi} \phi_{ab}(\theta - \theta') \ln\left(1 + e^{-\varepsilon_b(\theta')}\right), \quad (1.9)$$

with $\varepsilon_a \equiv -\log(\rho_a^{(r)}/\rho_a^{(h)})$ called pseudoenergies, and $\phi_{ab} \equiv -i \frac{d}{d\theta} \ln(S_{ab})$. The system of integral equations in Eq.1.9 is the celebrated Thermodynamic Bethe Ansatz (TBA) system for a diagonal IQFT in $(1+1)$ -dimensions. The interactions in ϕ_{ab} couple the integral equations. In the trivial case of a free theory, $\phi_{ab} \equiv 0$, and the pseudoenergies decouple: this is the reason for their name, as their value would reduce to the energy of a free, relativistic particle, as in Eq.1.1. Solving the system, the ground state energy of the theory may be exactly computed as:

$$E_0(R) = Rf(R) = - \sum_{b=1}^n \int_{\mathbb{R}} \frac{d\theta'}{2\pi} m_b \cosh(\theta') \ln\left(1 + e^{-\varepsilon_b(\theta')}\right). \quad (1.10)$$

As already pointed out, the mirroring argument applies just to the ground state. However, as anticipated in the Introduction, P. Dorey and R. Tateo in [DT96] found out that by analytically continuing the variable $r \equiv mR$ in the complex plane, some excited states of the theory may be reached. In particular, one-particle and two-particles excited states were obtained for the scaling Lee-Yang model, with excellent agreement with the results from truncated conformal approaches. The procedure should not present obstructions in the generalizations to any IQFT, even though no formal proof exists to show that any excited state may be reached with this method. As we shall see in Chpt.4 and in the rest of this dissertation, the idea of deforming the TBA system through a smooth path in the space of its parameters (moduli space) will be applied also in the field of Resurgent Quantum Mechanics in order to get a TBA description for different states of the theory starting from an initial, simpler one. In those chapters, the ideas here just roughly touched upon will be fully developed. At this stage, it is interesting to notice how the same mathematical description allows to describe very different physical systems, and, in particular, that analogous techniques to manipulate the equations find useful application in such different contexts.

Let us conclude this section by mentioning the possibility to classify a set of diagonal integrable theories in terms of simply laced, affine Lie algebras of the ADE series (for an introduction to ADE Lie algebras, see [FMS99]). To be specific, a S-matrix theory associated to a \mathcal{A} -algebra in the ADE series, the number of particles n in the spectrum

coincides with its rank, while the mass spectrum is proportional to the positive eigenvector of its Cartan matrix. In addition, the poles in the physical strip of the associated S-matrix are simple and evenly spaced by $\Delta\theta = 2\pi/h(\mathcal{A})$, $h(\mathcal{A})$ being the Coxeter number of \mathcal{A} . Remarkably, Al.B. Zamolodchikov in [Zam90] (then generalized by F.Ravanini, R.Tateo and A.Valleriani in [RVT93]) showed that the general TBA system in Eq.1.9 may be transformed into the universal form

$$\varepsilon_a(\theta) = m_a R \cosh(\theta) - \sum_{b=1}^n I_{ab} \int \frac{d\theta'}{2\pi} \phi_h(\theta - \theta') \left[m_b R \cosh(\theta') - \ln \left(1 + e^{-\varepsilon_b(\theta')} \right) \right], \quad (1.11)$$

with I_{ab} being the incidence matrix of \mathcal{A} , and ϕ_h being the universal kernel:

$$\phi_h(\theta) = \frac{h}{\cosh(h\theta/2)}. \quad (1.12)$$

In addition, using the poles structure of the system, it is possible to show that the solution to Eq.1.11 is a particular solution of the following functional system:

$$Y_a \left(\theta + i\frac{\pi}{h} \right) Y_a \left(\theta - i\frac{\pi}{h} \right) = \prod_{b=1}^n [1 + Y_b(\theta)]^{I_{ab}}. \quad (1.13)$$

This is an example of functional systems known as Y-systems, which will be central in the discussion in the later chapters. Finally, it is also important to underline that Eq.1.13 exhibits a nice periodicity, which is given by:

$$Y_a \left(\theta + i\pi \frac{h+2}{h} \right) = Y_a(\theta) \quad (1.14)$$

for the D_r and E series, and

$$Y_a \left(\theta + i\pi \frac{h+2}{h} \right) = Y_{r-a+1}(\theta) \quad (1.15)$$

for the A_r series. Let us mention that additional symmetries in the A_r series imply that $Y_a(\theta) = Y_{r-a+1}(\theta)$: thus, 1.14 holds also in this case.

The TBA equations and the Y-system we showed in this chapter present all the fundamental features of the systems that will be derived in the following chapters in the context of Resurgent Quantum Mechanics. The periodicity property in Eq.1.14 will also provide a useful reference to compare the Y-systems arising in that context.

Chapter 2

The ODE-IM Correspondence: a Brief Overview

In this chapter we will give a brief overview of the ODE-IM correspondence, developed by P. Dorey and R. Tateo in [DT99a, DT00], and later reviewed by P. Dorey, C. Dunning and R. Tateo in [DDT07]. This exposition clearly does not aim at completeness, as the topic is itself very wide and puts in relationship very different physical and mathematical formalisms. Rather, we would like to provide a minimal description of this correspondence, so as to better appreciate the theoretical context in which the main topics of this thesis are situated.

Let us start from the IM side of the correspondence, and let us consider the case of integrable lattice models. In this context, the models are defined on a 2-dimensional, $N \times N'$ lattice, with $N/2$ even. Taking as a paradigmatic example the six-vertex model, sites represent atoms, and links represent bonds in terms of arrows. The underlying physical picture is that of oxygen atoms bonded together by hydrogen ions, lying closer to an atom or to the other one depending on the verse of the arrow. The lattice configuration is given in terms of the Boltzmann weights associated to allowed site configurations. These are commonly defined as

$$\begin{aligned} W \left[\begin{array}{c} \rightarrow \uparrow \rightarrow \\ \vdots \\ \rightarrow \downarrow \rightarrow \end{array} \right] &= W \left[\begin{array}{c} \leftarrow \downarrow \leftarrow \\ \vdots \\ \leftarrow \uparrow \leftarrow \end{array} \right] = a(\nu, \eta) = \sin(\eta + i\nu) \\ W \left[\begin{array}{c} \rightarrow \downarrow \rightarrow \\ \vdots \\ \rightarrow \uparrow \rightarrow \end{array} \right] &= W \left[\begin{array}{c} \leftarrow \uparrow \leftarrow \\ \vdots \\ \leftarrow \downarrow \leftarrow \end{array} \right] = b(\nu, \eta) = \sin(\eta - i\nu) \\ W \left[\begin{array}{c} \rightarrow \uparrow \leftarrow \\ \vdots \\ \rightarrow \downarrow \leftarrow \end{array} \right] &= W \left[\begin{array}{c} \leftarrow \downarrow \rightarrow \\ \vdots \\ \leftarrow \uparrow \rightarrow \end{array} \right] = c(\nu, \eta) = \sin(2\eta) , \end{aligned} \tag{2.1}$$

where η is the anisotropy, and ν is the spectral parameter. Then, provided that suitable boundary conditions are specified, the partition function is computed as usual by

summing over all possible configurations σ , and it reads:

$$\mathcal{Z} = \sum_{\{\sigma\}} \prod_{\text{sites}} W[\cdot\cdot] . \quad (2.2)$$

Let us impose twisted boundary conditions: starting from periodic boundary conditions on both lattice directions, this translates into the substitution of the N -th column of lattice sites with the following, φ -rotated versions:

$$\begin{aligned} W \left[\beta_{N\alpha_N}^{\alpha'_N} \rightarrow \right] &\Rightarrow e^{-i\varphi} W \left[\beta_{N\alpha_N}^{\alpha'_N} \rightarrow \right] \\ W \left[\beta_{N\alpha_N}^{\alpha'_N} \leftarrow \right] &\Rightarrow e^{i\varphi} W \left[\beta_{N\alpha_N}^{\alpha'_N} \leftarrow \right] . \end{aligned} \quad (2.3)$$

Then, the computation of the partition function is usually attacked with the transfer matrix formalism, defining the transfer matrix \mathbb{T} as:

$$\mathbb{T}_\alpha^{\alpha'} \equiv \sum_{\{\beta_i\}} e^{\pm i\varphi} W \left[\beta_{1\alpha_1}^{\alpha'_1} \beta_2 \right] W \left[\beta_{2\alpha_2}^{\alpha'_2} \beta_3 \right] \dots W \left[\beta_{N\alpha_N}^{\alpha'_N} \beta_1 \right] \quad (2.4)$$

so that $\mathcal{Z} = \text{Tr} \left[\mathbb{T}^N \right]$. The diagonalization of the transfer matrix is possible through the Bethe Ansatz, here adapted to a lattice model. In this context, each eigenvector depends on a finite set of n parameters ν_1, \dots, ν_n , called roots. The Ansatz is found to provide legitimate solutions provided that the Bethe Ansatz equations are satisfied by the roots:

$$(-1)^n \prod_{j=1}^n \frac{\sinh(2i\eta - \nu_k + \nu_j)}{\sinh(2i\eta - \nu_j + \nu_k)} = -e^{-2i\varphi} \frac{a^N(\nu_k, \eta)}{b^N(\nu_k, \eta)} \quad (2.5)$$

A generic eigenvalue t may be then expressed as:

$$t(\nu) = e^{-i\varphi} a^N(\nu, \eta) \prod_{j=1}^n g(\nu_j - \nu) + e^{i\varphi} b^N(\nu, \eta) \prod_{j=1}^n g(\nu_j - \nu) , \quad (2.6)$$

where $g(\nu, \eta) \equiv a(\nu - i\eta, \eta)/b(\nu - i\eta, \eta)$. It must be underlined that the models considered so far are classical models. However, crucially, a very useful connection exists with quantum spin chains, that allows to study these one-dimensional quantum systems just in terms of classical two-dimensional lattice models. As an example of this link, the six-vertex model considered above is in direct correspondence with the spin-1/2 XXZ spin chain, also known as the Heisenberg-Ising chain. Now, let us turn back to the transfer matrix: a fundamental observation due to Baxter, is that \mathbb{T} commutes at different values of the spectral parameter, allowing for simultaneous diagonalization. In addition, Baxter proved the existence of an auxiliary function $q(\nu)$ for each eigenvalue $t(\nu)$ of \mathbb{T} , that is entire and $i\pi$ periodic in the ground state, and such that it satisfies:

$$t(\nu) q(\nu) = e^{-i\varphi} a^N(\nu, \eta) q(\nu + 2i\eta) + e^{i\varphi} b^N(\nu, \eta) q(\nu - 2i\eta) . \quad (2.7)$$

The system above is called TQ-system, and it encapsulates in its analytic structure the full Bethe Ansatz equations. The TQ-system is at the heart of the correspondence with ordinary differential equations. A hint for such link may be found by slightly manipulating Eq.2.7. Using the parity of the ground state eigenvector t_0 in the twist angle φ , the TQ-system may be translated into the following functional equation:

$$t_0(\nu, |\varphi|) \tilde{q}_0(\nu) = a^N(\nu, \eta) \tilde{q}_0(\nu + 2i\eta) + b^N(\nu, \eta) \tilde{q}_0(\nu - 2i\eta) , \quad (2.8)$$

where $\tilde{q}_0(\nu, \varphi) \equiv \exp(-\nu\varphi/(2\eta))q_0(\nu, \varphi)$. This is a finite-difference analogue of a second-order differential equation, and it is possible to associate to it the analogue of a Wronskian, the so-called quantum Wronskian $\mathscr{W}(\nu)$. This quantity is very important, as it may be proved to fit into a hierarchy of relations, called the fusion hierarchy. In addition, it may be shown that a truncation phenomenon occurs when η/π is rational, providing the finite set of functional equations called TT-system, usually associated to simply-laced Dynkin diagrams. In turn, the TT-system may be translated into a Y-system and a TBA system, with analogous features to the ones introduced in Chpt.1. To conclude this bird's eye tour on the tools to attack lattice IMs, let us underline that the discretized second-order differential equation in Eq.2.8 suggests that a continuum limit should be taken in order to start making contact with proper ODEs. This may be achieved considering a fixed, dimensionful lattice width and a renormalization group procedure. This method rests on the assumption that the lattice model sits close enough to a second order phase transition, so that the resulting field theory is conformal. As an example, let us write here two functional relations, as they emerge once the continuum limit is taken. The first one is the analogue of Eq.2.8, and it reads:

$$t_0(E) q_0(E) = e^{i\varphi} q_0(\omega^2 E) + e^{-i\varphi} q_0(\omega^{-2} E) , \quad (2.9)$$

with E a carefully chosen function of ν , and $\omega^2 = e^{-4\pi i\eta}$. As it will be clear in a moment, this last relation will provide the contact point with ODE formalism that we will summarize in the next paragraph. The second example here is the continuum version of a TT-system associated to a rank r , simply-laced Dynkin diagram with incidence matrix I_{ab} :

$$T_a(\omega^{-1}s) T_a(\omega s) = 1 + \prod_{b=1}^r (T_b(s))^{I_{ab}} , \quad a = 1, \dots, r , \quad (2.10)$$

where s is analogous to E above, and it is a carefully chosen function of ν . Defining the Y-functions Y_a as:

$$Y_a(s) \equiv 1 + \prod_{b=1}^r (T_b(s))^{I_{ab}} , \quad a = 1, \dots, r , \quad (2.11)$$

then, Eq.2.10 may be translated into the Y-system

$$Y_a(\omega^{-1}s) Y_a(\omega s) = \prod_{b=1}^r (1 + Y_b(s))^{I_{ab}} , \quad a = 1, \dots, r , \quad (2.12)$$

which precisely coincides with the one in Eq.1.13 up to a suitable change of variables. Indeed, using the asymptotics of Eq.2.12, the Y-system may be put in contact with the TBA system presented in Eq.1.11. As underlined in [DDT07], the TBA found here in the context of IM would correspond to an ultraviolet limit of Eq.1.11, where the overall mass scale is taken to zero.

Let us now move to the ODE side, and let us see how to connect the ideas developed in the last paragraph with this new perspective. The starting point here is the solution of eigenvalue problems represented by second-order differential equations on the real line. The first ordinary differential operators to be associated to integrable models were the stationary Schrödinger operators on the complex plane with monic polynomial potential

$$V(z) = (iz)^{2M} , \quad M > 0 . \quad (2.13)$$

The original problem (C.M. Bender and S. Böttcher [BB98]) was that of finding the spectrum of a PT-symmetric hamiltonian for a non-relativistic particle. Each eigenvalue E , in general complex, can be considered in the spectrum if the associated eigenfunction suitably decays at spatial infinity. It was then realized the need to extend the problem to the complex plane in order to find a smooth continuation among spectra through all the values of M , in particular, from $M < 2$ to $M > 2$. The theory on the complex plane has been extensively studied by Sibuya in [Sib75]. At this stage, we will only describe the fundamental points of the theory, since, in Sect.3.7, an example of the application of these ideas will be presented. In particular, here we will concentrate in making contact with the TQ-relation in Eq.2.7, so as to understand the basics of the ODE-IM correspondence. The key aspect of Sibuya's approach is to consider the asymptotics of a given eigenfunction approaching infinity along a generic ray $\rho e^{i\theta}$, and not just along the real axis. The standard WKB approach provides uniquely-identified subdominant and dominant solutions Ψ_{\pm}

$$\Psi_{\pm} \sim \frac{1}{(V - E)^{1/4}} \exp \left[\pm \frac{1}{M + 1} e^{i\theta(1+M)} \rho^{1+M} \right] , \quad (2.14)$$

exchanging roles on the so-called anti-Stokes lines. These lines correspond to the condition

$$\Re [e^{i\theta(1+M)}] = 0 , \quad (2.15)$$

and they decompose the complex plane into wedges, called Stokes sectors. The difficulty encountered when trying to overcome the value $M = 2$ is associated to an anti-Stokes line crossing the real axis, and it can be avoided by considering a distorted version of the problem, where the integration contours in the WKB approximation are bent out of the real axis. As a result, the original spectral problem on the real axis is generalized to a set of spectral problems, each associated to eigenfunctions decaying at infinity on a pair

of Stokes sectors [DDT07]. Even though all these problems may seem to be unrelated, actually, they all may be put on equal footing by considerations of analytic continuation. Sibuya and Voros established such connections, and these precisely correspond to functional equations analogous to the TQ-systems that emerged in the context of integrable models. As an example, let us consider the monic potential in Eq.2.13. Having rotated $z \rightarrow z/i$ and $E \rightarrow -E$, the Schrödinger equation reads:

$$\left[-\frac{d^2}{dz^2} + z^{2M} - E \right] \Psi(z) = 0 \quad (2.16)$$

with the original, real integration contour now on the imaginary axis. The Stokes sectors may be now labeled as

$$\mathcal{S}_k \equiv \left| \arg(z) - \frac{\pi k}{M+1} \right| < \frac{\pi}{2M+2}, \quad k \in \mathbb{Z}. \quad (2.17)$$

Sibuya then proved that a fundamental function $y(z, E)$ exists, which corresponds to the WKB result in the sectors $\mathcal{S}_{-1} \cup \mathcal{S}_0 \cup \mathcal{S}_1$, with y being subdominant in \mathcal{S}_0 and dominant in \mathcal{S}_{-1} and \mathcal{S}_1 . Crucially, it may be shown that a subdominant solution to a second-order ODE in a given sector is unique up to a multiplicative finite constant. The subdominant solution y_k in a generic Stokes sector \mathcal{S}_k may be then generated from y using the invariance of Eq.2.16 under the so-called Symanzik rotation $z \rightarrow \omega z$, with $\omega = \exp(2\pi i/(2M+2))$, and it reads as follows:

$$y_k(z, E) \equiv \omega^{k/2} y(\omega^{-k} z, \omega^{2k} E). \quad (2.18)$$

The final step is based on the fact that any pair $\{y_k, y_{k+1}\}$ is a pair of linearly independent solutions. Thus, for example, y_{-1} can be expressed as a linear combination of y_0 and y_1 as follows:

$$y_{-1} = C(E) y_0 + \tilde{C}(E) y_1, \quad (2.19)$$

with $C, \tilde{C} \in \mathbb{C}$. The coefficients C and \tilde{C} are called Stokes multipliers, and they may be expressed in terms of the Wronskians between the solutions y_{-1} , y_0 and y_1 . Using this piece of information and evaluating the result at $z = 0$ (where all the solutions are well-behaved if the potential is non-singular there), then Eq.2.19 turns into the following so-called CD-relation:

$$C(E) D_{\mp}(E) = \omega^{\mp 1/2} D_{\mp}(\omega^{-2} E) + \omega^{\pm 1/2} D_{\mp}(\omega^2 E), \quad (2.20)$$

with $D_-(E) \equiv y(0, E)$, $D_+(E) \equiv y'(0, E)$. This is the sought-after contact point with the IM realm we introduced above. Indeed, comparing the CD-relation with the TQ-relation in Eq.2.9, it is clear that these two coincide if we let $\varphi = \pi/(2M+2)$. In addition, a first, yet incomplete, dictionary may be established between the two worlds:

in particular, the spectral parameter corresponds to the energy, the anisotropy to the degree of the potential, the transfer matrix to the Stokes multiplier C , and the Q operator to D_- . Without giving further details, let us mention that the dictionary from the IM to the ODE realms may be fully completed adding an angular-momentum-like contribution to the potential. By including this term, the set of possible values of the twist parameter φ becomes larger, as φ gets in correspondence with the value of the angular momentum.

Let us conclude this chapter by underlining the importance of the ODE-IM correspondence in proving important results in both ODE and IM contexts. For example, it was successfully used to prove conjectures on the reality of the spectra of the following class of PT-invariant Hamiltonians $H_{M,l}$:

$$H_{M,l} \equiv p^2 - (iz)^{2M} + \frac{l(l+1)}{z^2}, \quad M, l \in \mathbb{R}, M > 0. \quad (2.21)$$

The spectra of $H_{M,l}$ were proved to be real for $M \geq 1$ and $|2l+1| < M+1$ ([DDT01]). In addition, it provided new techniques to numerically calculate physically relevant quantities. For example, as we will see in the following chapters, energy levels of Schrödinger problems can be evaluated using non-linear integral equations, like TBA-like equations, Destri de Vega or Klümper-Batchelor-Pearce equations (known in general as Non-Linear Integral Equations, NLIEs). These approaches have proved to be very efficient numerically, and they provide exact, non-perturbative results.

Chapter 3

Resurgent Quantum Mechanics for the Stationary Schrödinger Equation

In this chapter, the mathematical formalism needed for the study of the resurgent approach to quantum mechanics is presented. The mathematical theory was studied in the works by A. Voros [Vor83, Vor93], E. Delabaere, H. Dillinger and F. Pham [DDP97, HD93], and then developed and reviewed in [DP99] and [IN14]. Their approach was built upon the WKB method, originally introduced in 1926 by Wentzel, Kramers and Brillouin to obtain perturbative solutions to the Schrödinger equation. An exact version of the WKB approximation was then introduced, using the concept of Borel resummation. The scope of application of this exact version of the WKB method is the solution of second order differential equations on compact Riemann surfaces, one typical example being that of a stationary Schrödinger problem with a meromorphic potential. The aim of the theory of resurgency and of the exact WKB approach may be synthesized in the attempt of reorganizing in a coherent way the semiclassical, WKB perturbative series, so as to get finite results and to provide methods to obtain, in principle, exact quantization conditions. Thus, the theory of resurgency may be a useful framework to attack the solution of a possibly wide range of quantum systems. Let us now briefly introduce the WKB formalism, before moving to its exact version.

3.1 WKB Formalism

Let us consider the Schrödinger problem on a compact Riemann surface Σ . For the purpose of this presentation, we may immediately fix $\Sigma = \mathbb{P}^1$, the Riemann sphere. A standard complex atlas may be defined as usual from the set of local coordinates z_1 and z_2 such that

$$z_1 : \mathbb{C} \rightarrow \mathbb{C}, \quad z_1(w) = w, \quad (3.1)$$

and

$$z_2 : \mathbb{P}^1 \setminus \{0\} \rightarrow \mathbb{C} , \quad z_2(w) = \begin{cases} \frac{1}{w} , & \text{if } w \neq \infty \\ 0 , & \text{if } w = \infty \end{cases} . \quad (3.2)$$

Then, denoting with z a local complex coordinate on Σ , the one-dimensional, stationary Schrödinger equation reads:

$$\left(\frac{d^2}{dz^2} - \eta^2 Q(z) \right) \Psi(z, \eta) = 0 , \quad (3.3)$$

where $\eta = \hbar^{-1}$ represents the inverse of the Planck constant, $Q(z) = V(z) - E$, with V a meromorphic potential and $E \in \mathbb{C}$ the energy. In the following discussion, we will be interested in polynomial potentials, so we may safely restrict the discussion to analytic potentials. Considering the effect of an arbitrary coordinate transformation on Eq.3.3, it can be seen that the function Q transforms as an analytic, quadratic differential on Σ , so that it is useful to define:

Definition 3.1 *The quadratic differential associated to the Eq.3.3 is the meromorphic quadratic differential on Σ locally given by*

$$\Phi = Q(z) dz^{\otimes 2} , \quad (3.4)$$

for a local coordinate z .

As it will be clear in a moment, the geometry of zeros, poles and trajectories of the quadratic differential play a crucial role in the exact WKB formalism. Let us call the zeros of the differential Φ the turning points, and collect them in the set P_0 . Then, let us call P_∞ the set of poles (for our choice of potential, this will coincide with $\{\infty\}$), and denote $P = P_0 \cup P_\infty$. We shall then assume the following:

Assumption 3.1 *Let Φ be the quadratic differential associated to Eq.3.3. The following assumption are made:*

1. Φ has at least one zero, and at least one pole.
2. all zeros are simple.
3. the order of any pole is more than or equal to 2.

For the case of a polynomial potential of degree $N \geq 1$, the first and last assumptions trivially hold: the only assumption needed is that of non-coalescing zeros. This request will be fundamental to have a well-defined triangulation and for the Theorem 3.4 to

hold, for example. We may then proceed to translate Eq.3.3 into the Riccati equation, by making the following Ansatz:

$$\Psi(z, \eta) = \exp\left(\int^z S(z', \eta) dz'\right), \quad (3.5)$$

obtaining then:

$$\frac{dS}{dz} + S^2 = \eta^2 Q(z). \quad (3.6)$$

Then, a formal, power-series solution is built by expanding S as a Laurent series in powers of η^{-1} :

$$S(z, \eta) = \sum_{n=-1}^{\infty} \eta^n S_n(z) = \eta S_{-1}(z) + S_0(z) + \eta^{-1} S_1(z) + \dots \quad (3.7)$$

By plugging in the expansion in Eq.3.6, the following set of recursive relation is obtained:

$$\begin{cases} S_{-1}^2(z) = Q(z) \\ 2S_{-1}S_{n+1} + \sum_{n_1+n_2=n, 0 \leq n_j \leq n} S_{n_1}S_{n_2} + \frac{dS_n}{dz} = 0, \quad n \geq -1 \end{cases} \quad (3.8)$$

As a consequence of the quadratic initial condition on the coefficients of the series, one gets a double family of solutions, which we shall label with $\{S_n^{(\pm)}\}_{n \geq -1}$ depending on the sign of $S_{-1} = \pm \sqrt{Q(z)}$. By direct inspection of Eq.3.8, one realizes that the functions $\{S_n^{(\pm)}\}_{n \geq -1}$ are singular on P and multi-valued and holomorphic on $\Sigma \setminus P$. In addition, introducing the odd part and the even part of $S(z, \eta)$ as:

$$S_{odd}(z, \eta) = \frac{1}{2} (S^{(+)}(z, \eta) - S^{(-)}(z, \eta)), \quad S_{even}(z, \eta) = \frac{1}{2} (S^{(+)}(z, \eta) + S^{(-)}(z, \eta)), \quad (3.9)$$

then, the following holds [KT05]:

Proposition 3.1 *The equality $S^{(\pm)}(z, \eta) = \pm S_{odd}(z, \eta) + S_{even}(z, \eta)$ holds, and the even part may be expressed as logarithmic derivative of the odd part:*

$$S_{even}(z, \eta) = -\frac{1}{2S_{odd}} \frac{dS_{odd}(z, \eta)}{dz}. \quad (3.10)$$

Hence, we are ready to define the formal WKB solutions of Eq.3.3.

Definition 3.2 *We define the following formal solutions:*

$$\Psi_{\pm}(z, \eta) = \frac{1}{\sqrt{S_{odd}(z, \eta)}} \exp\left(\pm \int^z S_{odd}(z', \eta) dz'\right), \quad (3.11)$$

as the formal WKB solutions of Eq.3.3, where the integral is understood as term-wise integration in powers of η .

This formal definition allows for a formal expansion in powers of η^{-1} :

$$\Psi_{\pm}(z, \eta) = \eta^{-1/2} \exp\left(\pm \eta \int^z \sqrt{Q(z')} dz'\right) \sum_{k=0}^{\infty} \eta^{-k} \Psi_{\pm, k}(z) , \quad (3.12)$$

whose principal term

$$\Psi_{\pm}(z, \eta) = \frac{\eta^{-1/2}}{Q(z)^{1/4}} \exp\left(\pm \int^z \sqrt{Q(z')} dz'\right) \quad (3.13)$$

yields the well-known WKB approximation for the solution to the Schrödinger equation in Eq.3.3. The series in Eq.3.12 is known to be in general divergent ([IN14]), and its resummation will be the main topic of the next section. Given the multi-valuedness of the integrand in Eq.3.11 on $\Sigma \setminus P$, the integration is to be considered on the Riemann surface $\widehat{\Sigma} = \{(z, w) \mid w^2 = \Phi\}$ associated to the form $\sqrt{Q(z)} dz$. Then, $\widehat{\Sigma}$ may be projected on Σ by the double-covering projection map $\pi : \widehat{\Sigma} \rightarrow \Sigma$, whose branching points coincide with the zeros of Φ in P_0 . Let us indicate with $\tau : \widehat{\Sigma} \rightarrow \widehat{\Sigma}$ the covering involution, exchanging the branches so that, if z belongs to one of them, then $z^* = \tau(z)$ lives on the other one. Using the formalism we just introduced, it is immediate to recognize that $S_{odd}(z^*, \eta) = -S_{odd}(z, \eta)$ holds, and the following normalization at a turning point $a \in P_0$ may be introduced for the formal WKB solution in Eq.3.11:

Definition 3.3 *The normalization of the formal WKB solution at a turning point $a \in P_0$ is defined as follows:*

$$\Psi_{\pm}(z, \eta) = \frac{1}{\sqrt{S_{odd}(z, \eta)}} \exp\left(\pm \int_a^z S_{odd}(z', \eta) dz'\right) , \quad (3.14)$$

where the integration from the point a is defined using the anti-invariant property of S_{odd} mentioned above:

$$\int_a^z S_{odd}(z', \eta) dz' = \frac{1}{2} \int_{\gamma_z} S_{odd}(z', \eta) dz' , \quad (3.15)$$

with γ_z a path in $\widehat{\Sigma}$, starting at z , ending at z^* , and looping once around a .

With this machinery at hand, we are ready to tackle the problem of translating the diverging, formal WKB series into analytic functions, and to understand which hypothesis are required for this transformation to be possible. This will be the topic of the next section.

3.2 Borel Resummation

Let us introduce and summarize the theory of Borel resummation. This will be the tool we use to get analytic functions out of the diverging WKB series. Let us start by defining Borel summability and its Borel sum:

Definition 3.4 Let $f(\eta) = \sum_{n=0}^{\infty} \eta^{-n} f_n$ be a formal power series. Then, $f(\eta)$ is said to be Borel summable if the formal power series

$$f_B(y) = \sum_{n=1}^{\infty} f_n \frac{y^{n-1}}{(n-1)!} \quad (3.16)$$

is convergent in a neighborhood of the origin $y = 0$, it can be analytically continued to $\Omega \subset \mathbb{C}$ with Ω containing the ray from 0 to $\infty e^{i\theta}$ for some real θ , and satisfies

$$|f_B(y)| \leq C_1 e^{C_2 |y|}, \quad y \in \Omega, \quad C_{1,2} > 0 \quad (3.17)$$

We shall then call $f_B(y)$ the Borel transform of $f(\eta)$ around the direction θ .

Definition 3.5 Given a Borel summable series $f(\eta) = \sum_{n=0}^{\infty} \eta^{-n} f_n$ around the direction θ (see above, Def.3.4), its Borel sum in the direction θ is defined by the following Laplace integral

$$\mathcal{S}_\theta[f](\eta) = f_0 + \int_0^{\infty e^{i\theta}} e^{-\eta y} f_B(y) dy. \quad (3.18)$$

Thanks to Eq.3.17, the integral converges and provides an analytic function of η in the region $\{\eta \in \mathbb{C} \mid |\arg(\eta) - \theta| < \pi/2, |\eta| \gg 1\}$. The Borel sum induces a map from the set of Borel summable formal series to a set of analytic functions, the Borel resummation operator \mathcal{S} . In the case of a formal series with a prefactor $f(\eta) = e^{\eta s} \eta^{-\rho} \sum_{n=0}^{\infty} \eta^{-n} f_n$, if $g(\eta) = \sum_{n=0}^{\infty} \eta^{-n} f_n$ is Borel summable in the above sense, then the Borel sum of $f(\eta)$ is by definition $\mathcal{S}_\theta[f](\eta) = e^{\eta s} \eta^{-\rho} \mathcal{S}_\theta[g](\eta)$, $\mathcal{S}_\theta[g](\eta)$ being the Borel sum of $g(\eta)$ in the direction θ .

The definitions above generalise the usual Borel summability and Borel sum, defined on the real axis for $\theta = 0$. Such generalisation is necessary to overcome the obstructions to Borel summability on the real axis that may arise when poles in the Borel transform hit the ray of integration of the Borel sum. Before considering this problem, let us briefly mention some of the most useful properties enjoyed by the Borel transform and the Borel sum.

Properties 3.1 1. If a formal power series $f(\eta)$ converges and defines a holomorphic function near $\eta = \infty$, then $f(\eta)$ is Borel summable and its Borel sum coincides with the original function

2. If $f(\eta)$ is Borel summable, then its Borel sum enjoys an asymptotic expansion to $f(\eta)$ for $|\eta| \rightarrow \infty$

3. The Borel resummation operator commutes with addition and multiplication, and it is compatible with the composition with convergent power series. For example, $\mathcal{S}_\theta[\exp(f)] = \exp(\mathcal{S}_\theta[f])$ (Ref.[Nik23]).

From 2 in Prop.3.1, it is apparent that the Borel sum allows to convert a formally divergent series into an analytic one, keeping contact with the original series with asymptotic expansions. Thus, the Borel resummation formalism is suitable to regulate divergent series, and, despite not being unique in the choice of the Borel transform, it still remains a natural way to achieve the goal.

Let us now consider the issues arising when Borel summability is lost along a given direction θ . In this case, one considers the Borel resummation along slightly tilted directions $\theta \pm \delta$, for a small $\delta > 0$. Usually, if δ is taken sufficiently small, the Borel summability is restored in both the distorted directions $\theta \pm \delta$, allowing to define then $\mathcal{S}_{\pm\delta}[f] \equiv \mathcal{S}_{\theta\pm\delta}[f]$. Now, both $\mathcal{S}_{\pm\delta}$ share the same asymptotic expansion $f(\eta)$ as $|\eta| \rightarrow \infty$ in the wedge of definition. However, in general, the two resummed functions do not coincide, since the two paths of integration in the Laplace transform are not homotopic due to the presence of poles in the integrand: such ambiguity is an instance of the so-called Stokes phenomenon. If $f(\eta)$ is Borel summable in a given range $[-\delta, \delta]$, then $\mathcal{S}_\varepsilon[f](\eta) = \mathcal{S}[f](\eta)$ for any $\varepsilon \in [-\delta, \delta]$. Hence, the absence of singular points in the Borel transform is intimately connected with the absence of a Stokes phenomenon. Finally, in what follows, it is important to remark that the request of Borel summability in a given direction θ of $f(\eta)$ is totally equivalent to the Borel summability of $f(e^{-i\theta}\eta)$ in the positive real-axis direction.

3.3 The Exact WKB Approach and the Delabaere-Pham Formula

Let us now turn our attention to the study of Borel summability of the WKB solutions in Eq.3.12. This is what the exact WKB is all about, as the goal is to reorganize the sum of the diverging series using the Borel resummation. For this aim, we fix the coordinate z on Σ and analyze the formal power series in η . As a consequence, Borel summability of the solution imposes constraints on the values that z may take. An efficient way to analyze the allowed regions on Σ is to study the Stokes graph associated to the differential form in Eq.3.4. So, let us introduce the trajectories of the differential and the Stokes graph.

Definition 3.6 *A trajectory of the differential Φ in Eq.3.4 in the direction θ is a leaf of the foliation on $\Sigma \setminus P$ given by:*

$$\Im \left(e^{-i\theta} \int^z \sqrt{Q(z')} dz' \right) = \text{constant} . \quad (3.19)$$

The important features of these trajectories are their uniqueness through any point in $\Sigma \setminus P$ and the fact that they do not intersect with each other. It is also useful to define an orientation for the trajectories, that is well defined on $\widehat{\Sigma} \setminus \pi^{-1}P$. Indeed, the inverse

image of the foliation in Eq.3.19 by the projection π induces a foliation on $\widehat{\Sigma} \setminus \pi^{-1}P$, so that each lift of a trajectory in $\widehat{\Sigma}$ by π may be regarded as a trajectory in $\widehat{\Sigma}$. Using the single-valuedness of the differential form Φ on $\widehat{\Sigma}$, a positively-oriented trajectory may be defined requiring that the real part of $\int^z \sqrt{Q(z')} dz'$ increases along the trajectory. Notice that, due to the sign exchange in the covering involution, the projection exhibits discontinuities across branch cuts. Now, let us introduce a special class of trajectories, the Stokes curves, that originate from a turning point in P_0 :

Definition 3.7 *A Stokes curve of the differential Φ in the direction θ is a trajectory of Φ in the direction θ whose one of the end-points is a turning point of Φ . Specifically, given $a \in P_0$ and a coordinate z on Σ , Stokes curves are defined as follows:*

$$\left\{ z \in \Sigma \mid \Im \left[e^{-i\theta} \int_a^z \sqrt{Q(z')} dz' \right] = 0 \right\} . \quad (3.20)$$

For a polynomial function Q with distinct roots, the set of turning points is finite and its cardinality is equal to the degree N of the polynomial. The local behavior of the Stokes curves around each turning point is known, and it is characterized by exactly three emanating trajectories. On the other hand, at infinity the differential has a pole $p_\infty \in P_\infty$ of order $N + 4$, and the trajectories are asymptotic to $N + 2$ rays emanating from the point at infinity. From a global perspective, under the same assumptions on Q , the following classification of the trajectories of Φ in a given direction is possible:

1. A generic trajectory starts and ends at the point in P_∞ .
2. A separating trajectory connects a point in P_0 to the point in P_∞ .
3. A (regular) saddle trajectory connects two turning points in P_0 .

From this classification, one observes that Stokes curves may be either separating trajectories or saddle trajectories. Using the equivalence of the Borel summability of $f(\eta)$ in a given direction θ to the Borel summability of $f(e^{-i\theta}\eta)$ in the positive real-axis direction, it is clear that the Stokes curves associated to the latter are precisely the Stokes curves in the direction θ defined in Def.3.7. These may be linked to a deformed Schrödinger problem:

$$\left(\frac{d^2}{dz^2} - \eta^2 e^{-2i\theta} Q(z) \right) \Psi = 0 , \quad (3.21)$$

with associated differential $\Phi_\theta = e^{-2i\theta}\Phi$. Such remark is intended to clarify the definition of the Stokes curves in an arbitrary direction in Def.3.7. We are now ready to define the Stokes graph G_θ in a direction θ , associated to the differential Φ_θ .

Definition 3.8 *The Stokes graph G_θ associated to the differential Φ_θ is the set of Stokes curves associated to Φ in the direction θ .*

The Stokes graph is a crucial tool to study the Borel summability of the solutions, as it encapsulates all the information needed to test if sufficient conditions for Borel summability hold. In particular, it will be clear in a moment that the change in topology of G_θ varying θ is associated to the appearance of saddle trajectories at specific directions: such saddle trajectories prevent Borel summability, forcing the introduction of lateral Borel resummation and allowing to prove the fundamental Delabaere-Pham formula. Let us then state the relevant theorems in this regard.

Let us consider the problem of Borel summability of solutions in Def.3.3 for a fixed direction $\theta \in \mathbb{R}$, assuming that the Stokes graph G_θ for the differential Φ_θ contains at most one saddle trajectory. Let D be any of the so-called Stokes regions, a connected component $D \subset \Sigma$ bounded by trajectories in the Stokes graph G_θ , and be z a point in D with a suitable coordinate choice whose domain contains D . It is important to stress that, since the Stokes regions are coordinate-independent, also the notion of Borel summability is coordinate-independent, which is a desirable property. The criterion for Borel summability proposed by T. Koike and R. Schäfke requires the introduction of the notion of admissible paths:

Definition 3.9 *Let $\widehat{P}_0 = \pi^{-1}(P_0)$, $\widehat{P}_\infty = \pi^{-1}(P_\infty)$ and $\widehat{P} = \widehat{P}_0 \cup \widehat{P}_\infty$. A path β on $\widehat{\Sigma} \setminus \widehat{P}_0$ is said to be admissible in the direction θ if its projection to Σ by π either never intersects with the Stokes graph G_θ , or intersects with G_θ only at points in P_∞ .*

For a path that is not admissible, one may find a decomposition of the path into a finite number of admissible paths if the hypothesis of the following lemma are satisfied:

Lemma 3.0.1 *Let β be a path on $\widehat{\Sigma} \setminus \widehat{P}_0$ with end-points $\widehat{z}_1, \widehat{z}_2 \in \widehat{\Sigma} \setminus \widehat{P}_0$, satisfying the following conditions:*

1. *Each of \widehat{z}_1 and \widehat{z}_2 either does not lie on G_θ or is a point in \widehat{P}_∞ .*
2. *β never intersects with a saddle trajectory in G_θ .*

Then, β has a decomposition into a finite number of paths $\beta = \beta_1 + \dots + \beta_N$ in the relative homology group $H_1\left(\widehat{\Sigma} \setminus \widehat{P}_0, \widehat{P}_\infty \cup \{\widehat{z}_1, \widehat{z}_2\}; \mathbb{Z}\right)$ and each summand β_i , $i \in \{1, \dots, N\}$ is admissible in the direction θ .

Then, the following criterion of the Borel summability holds:

Theorem 3.1 *If the Stokes graph G_θ is saddle-free, then the WKB solution normalized as in Eq.3.15 is Borel summable in the direction θ at any point z in each Stokes region. The Borel sums of the WKB solutions give analytic solutions to Eq.3.3 in each Stokes region, which are also analytic in η on wedge $\{\eta \in \mathbb{C} \mid |\arg \eta - \theta| < \pi/2, |\eta| \gg 1\}$.*

Now, let us mention another Borel summability criterion, that will prove to be useful later in the discussion of Borel summability of Voros symbols. Such theorem applies to a slightly modified version of the solutions, that makes use of $S_{odd}^{reg}(z, \eta) \equiv S_{odd}(z, \eta) - \eta\sqrt{Q(z)}$, and it reads as follows:

Theorem 3.2 *Let β be a path on $\widehat{\Sigma} \setminus \widehat{P}_0$ and end-points $\widehat{z}_1, \widehat{z}_2 \in \widehat{\Sigma} \setminus \widehat{P}_0$ satisfying the same hypothesis as in Lemma 3.0.1. Then, the formal power series $\int_{\beta} S_{odd}^{reg}(z, \eta) dz$ is Borel summable in the direction θ .*

Now, let us move back to Th.3.1. From this result, it is clear that, in general, the appearance of a saddle trajectory spoils the Borel summability of the WKB solutions, as the path associated to a solution normalized at a turning point (see Eq.3.14) cannot be decomposed into a sum of admissible paths. On the other hand, if θ is varied within an interval such that no saddle-trajectories appear, the Borel sum of the solutions is invariant on the interval. Now, given a direction with no saddle trajectories, the WKB solutions associated to different Stokes regions are connected by connection formulae found by Voros (see [Vor83]). The same formulae also describe the Stokes phenomenon that characterizes the solutions. Let us first present the connection theorem in this latter perspective, as it should highlight the effect of the Stokes phenomenon on the resummed solutions. The setting is as follows. Let $z \in \widehat{\Sigma} \setminus \widehat{P}$. Let $D_{1,2}$ be two Stokes regions separated by a Stokes curve C emanating from a turning point a , with D_2 coming next to D_1 in anti-clockwise direction around the turning point a .

Theorem 3.3 *Let θ_0 be a direction such that, for a sufficiently small $\varepsilon > 0$, the following holds:*

1. G_{θ} are saddle free for any $\theta \in [\theta_0 - \varepsilon, \theta_0 + \varepsilon]$
2. z lies on C in the direction θ_0 and it does not lie on a Stokes curve for any $\theta \in [\theta_0 - \varepsilon, \theta_0 + \varepsilon]$, with $\theta \neq \theta_0$

Denoting with Ψ_{\pm} the WKB solution normalized at the point a and with $\Psi_{\pm}^{(\theta_0 - \varepsilon)}$ (resp., $\Psi_{\pm}^{(\theta_0 + \varepsilon)}$) the Borel sum of Ψ_{\pm} in the direction $\theta_0 - \varepsilon$ (resp., $\theta_0 + \varepsilon$), then the following relations hold in a neighbourhood of z :

$$\begin{cases} \Psi_{+}^{(\theta_0 - \varepsilon)} = \Psi_{+}^{(\theta_0 + \varepsilon)} + i\Psi_{-}^{(\theta_0 + \varepsilon)} \\ \Psi_{-}^{(\theta_0 - \varepsilon)} = \Psi_{-}^{(\theta_0 + \varepsilon)} \end{cases} \quad (3.22)$$

for C positively oriented out of a ;

$$\begin{cases} \Psi_{+}^{(\theta_0 - \varepsilon)} = \Psi_{+}^{(\theta_0 + \varepsilon)} \\ \Psi_{-}^{(\theta_0 - \varepsilon)} = \Psi_{-}^{(\theta_0 + \varepsilon)} + i\Psi_{+}^{(\theta_0 + \varepsilon)} \end{cases} \quad (3.23)$$

for C positively oriented towards a .

Going back to the connection formulae in their traditional formulation, the theorem may be stated as follows:

Theorem 3.4 *Let G_θ be a saddle-free Stokes graph. Denoting with Ψ_\pm the WKB solution normalized at a and with $\Psi_\pm^{D_j}$ ($j = 1, 2$) the Borel sum of Ψ_\pm in the region D_j ($j = 1, 2$), then the following relations hold for the analytic continuation of $\Psi_\pm^{D_1}$ to D_2 across C .*

1. *For C positively oriented out of a :*

$$\begin{cases} \Psi_+^{D_1} = \Psi_+^{D_2} + i\Psi_-^{D_2} \\ \Psi_-^{D_1} = \Psi_-^{D_2} \end{cases} \quad (3.24)$$

or, equivalently,

$$\begin{pmatrix} \Psi_+^{D_1} \\ \Psi_-^{D_1} \end{pmatrix} = M_+ \begin{pmatrix} \Psi_+^{D_2} \\ \Psi_-^{D_2} \end{pmatrix}, \quad (3.25)$$

with:

$$M_+ \equiv \begin{pmatrix} 1 & i \\ 0 & 1 \end{pmatrix}. \quad (3.26)$$

2. *For C positively oriented towards a :*

$$\begin{cases} \Psi_+^{D_1} = \Psi_+^{D_2} \\ \Psi_-^{D_1} = i\Psi_+^{D_2} + \Psi_-^{D_2} \end{cases} \quad (3.27)$$

or, equivalently,

$$\begin{pmatrix} \Psi_+^{D_1} \\ \Psi_-^{D_1} \end{pmatrix} = M_- \begin{pmatrix} \Psi_+^{D_2} \\ \Psi_-^{D_2} \end{pmatrix}, \quad (3.28)$$

with:

$$M_- \equiv \begin{pmatrix} 1 & 0 \\ i & 1 \end{pmatrix}. \quad (3.29)$$

The importance of the connection formulae above cannot be underestimated. Indeed, as shown in [KT05], they allow to express the global problems of differential equations in terms of characteristic exponents and the Borel sum of contour integrals of $S_{\text{odd}}(z, \eta) dz$ around cycles in $\widehat{\Sigma} \setminus \widehat{P}$. The exact quantisation conditions presented in Sect.3.8 are an example of application of these ideas. For example, in that context, the change in normalization of a WKB solution from a turning point to another one will be expressed in terms of characteristic exponents as follows:

$$\Psi_{\pm, a_1} = \exp\left(\pm \int_{a_1}^{a_2} S_{\text{odd}}(z) dz\right) \Psi_{\pm, a_2}, \quad (3.30)$$

where Ψ_{\pm, a_1} and Ψ_{\pm, a_2} are the resummed WKB solutions normalized at the turning points a_1 and a_2 , the exponential factor is called Voros multiplier and the path connecting a_1 and a_2 is contained in the Stokes region delimited by a_1 and a_2 . When computing exact quantisation conditions, it turns out that these exponents combine to form exponents of contour integrals of $S_{odd}(z, \eta) dz$ around cycles encircling turning points. These exponents are instances of the so-called Voros symbols, and they play a crucial role in the exact WKB approach. In fact, their importance is not limited to exact quantisation conditions, as their behavior under resummation allows to encapsulate the dynamics of the Schrödinger system in a very powerful way. For these reasons, let us now introduce the relevant quantities in a systematic way.

Let $H_1(\widehat{\Sigma} \setminus \widehat{P}) \equiv H_1(\widehat{\Sigma} \setminus \widehat{P}; \mathbb{Z})$ be the first homology group and $H_1(\widehat{\Sigma} \setminus \widehat{P}_0, \widehat{P}_\infty) \equiv H_1(\widehat{\Sigma} \setminus \widehat{P}_0, \widehat{P}_\infty; \mathbb{Z})$ the first relative homology group. Let us call the elements of $H_1(\widehat{\Sigma} \setminus \widehat{P})$ cycles and the elements of $H_1(\widehat{\Sigma} \setminus \widehat{P}_0, \widehat{P}_\infty)$ paths. As a consequence of the Lefschetz duality, the bilinear form

$$\langle \cdot, \cdot \rangle : H_1(\widehat{\Sigma} \setminus \widehat{P}) \times H_1(\widehat{\Sigma} \setminus \widehat{P}_0, \widehat{P}_\infty) \rightarrow \mathbb{Z} \quad (3.31)$$

exists, which gives the number of intersections between cycles and paths. A normalization $\langle x - axis, y - axis \rangle = +1$ is understood. This bilinear form also induces the bilinear form

$$(\cdot, \cdot) : H_1(\widehat{\Sigma} \setminus \widehat{P}) \times H_1(\widehat{\Sigma} \setminus \widehat{P}) \rightarrow \mathbb{Z} . \quad (3.32)$$

Let us now introduce the Voros symbol for a cycle γ as follows:

Definition 3.10 *Let $\gamma \in H_1(\widehat{\Sigma} \setminus \widehat{P})$ be a cycle. The formal series $\exp(V_\gamma)$ is by definition the Voros symbol for the cycle γ , where V_γ is the formal power series defined by $V_\gamma(\eta) = \oint_\gamma S_{odd}(z, \eta) dz$.*

Let us also define the so-called quantum periods, as they will be very useful in the next sections:

Definition 3.11 *Let V_γ be the formal power series defined by $V_\gamma(\eta) = \oint_\gamma S_{odd}(z, \eta) dz$, as in Def.3.10 above. Then the quantity Π_γ defined as $\Pi_\gamma(\eta) \equiv -\frac{i}{\eta} V_\gamma(\eta)$ is called the quantum period associated to the cycle γ .*

Let us remark that Voros symbols are formal power series with an exponential factor $\exp(\eta v_\gamma)$, with $v_\gamma = \oint_\gamma \sqrt{Q_0(z)} dz$, as in Def.3.5. Hence, their Borel summability follows from Th.3.1, 3.2 if the integration path does not cross any saddle trajectory. On the contrary, if a saddle trajectory appears, then, in general, Borel summability is lost,

and the Stokes phenomenon occurs.

With the motivations given above, let us consider more in detail the Stokes phenomenon for the Stokes symbols, and let us see how it is intimately connected with the mutations of the Stokes graph. For simplicity, let us assume that a Stokes graph $G_{\theta_c}(\Phi)$ at θ_c has a saddle trajectory l_{θ_c} . Then, we may find a class of cycles $\gamma_{\theta_c} \in H_1(\widehat{\Sigma} \setminus \widehat{P})$ such that its projection on Σ surrounds l_{θ_c} , choosing its orientation so that $\Re(v_{\gamma_{\theta_c}}) < 0$. Such class is referred to as the saddle class of the saddle trajectory l_{θ_c} . The ambiguity between the choice of γ_{θ_c} or $-\gamma_{\theta_c}^*$ is irrelevant for the definition of the associated Voros symbol $\exp(V_{\gamma_{\theta_c}})$, thanks to the anti-invariant property of S_{odd} described in Sect.3.1. Let us choose $r > 0$ small enough, so that for any $\delta > 0$, $0 < \delta \leq r$, one has $G_{\pm\delta} \equiv G_{\theta_c \pm \delta}$ free from saddle trajectories. We shall call both $G_{\pm\delta}$ the saddle reductions of G_{θ_c} , and we shall refer to the mutation from $G_{-\delta}$ to $G_{+\delta}$ through G_{θ_c} as to a flip. Such transformation affects the topology of the Stokes regions of the Stokes graph, and this geometrical perspective will prove to be very practical in Sect.3.4, where this transformation will be precisely defined in the context of WKB triangulations. Now, by Lemma 3.0.1, the cycles can always be decomposed into sum of admissible paths, and the Voros symbols are Borel summable. In addition, their Borel sum is invariant in any direction θ within each of the ranges $]0, r]$ and $[-r, 0[$, allowing to consistently define the resummed Voros symbols $\mathcal{S}_{\pm}[e^{V_{\gamma}}](\eta) \equiv \mathcal{S}_{\pm\delta}[e^{V_{\gamma}}](\eta)$ for some δ in $]0, r]$. We are now ready to state the fundamental Delabaere-Pham theorem (see [DDP97]).

Theorem 3.5 *Let G_{θ_c} be a Stokes graph with a single saddle trajectory with associated saddle class $\gamma_{\theta_c} \in H_1(\widehat{\Sigma} \setminus \widehat{P})$, and let $G_{\pm\delta}$ be two saddle reductions of G_{θ_c} . Then, the Borel sums $\mathcal{S}_{\pm}[e^{V_{\gamma}}]$ for any $\gamma \in H_1(\widehat{\Sigma} \setminus \widehat{P})$ satisfy the following equalities as analytic functions of η on a domain containing $\{\eta \in \mathbb{R} \mid \eta \gg 1\}$:*

$$\mathcal{S}_-[e^{V_{\gamma}}] = \mathcal{S}_+[e^{V_{\gamma}}] (1 + \mathcal{S}_+[e^{V_{\gamma_{\theta_c}}}])^{-(\gamma_{\theta_c}, \gamma)} . \quad (3.33)$$

At this point, it is very useful to rephrase the Delabaere-Pham formula also in terms of the so-called Stokes automorphisms. To this end, let us denote with $\mathbb{V} = \mathbb{V}(Q(z, \eta))$ the field of rational functions generated by the Voros symbols $e^{V_{\gamma}}$:

Definition 3.12 *Let us call Stokes automorphism the field automorphism $\mathfrak{S}_{\gamma_{\theta_c}} : \mathbb{V} \rightarrow \mathbb{V}$ defined as follows:*

$$\mathfrak{S}_{\gamma_{\theta_c}} : e^{V_{\gamma}} \mapsto e^{V_{\gamma}} (1 + e^{V_{\gamma_{\theta_c}}})^{-(\gamma_{\theta_c}, \gamma)} , \quad \gamma \in H_1(\widehat{\Sigma} \setminus \widehat{P}) . \quad (3.34)$$

Then, Eq.3.33 can be translated into

$$\mathcal{S}_- = \mathcal{S}_+ \circ \mathfrak{S}_{\gamma_{\theta_c}} \quad (3.35)$$

or, equivalently,

$$\mathcal{S}_+^{-1} \circ \mathcal{S}_- = \mathfrak{S}_{\gamma_{\theta_c}} . \quad (3.36)$$

Thus, applying the automorphisms to a generic Voros symbol e^{V_γ} , and taking then the logarithm, one obtains the following equivalent expression in terms of quantum periods:

$$\text{disc}_{\theta_c} [\Pi_\gamma] \equiv \mathcal{S}_+ [\Pi_\gamma] - \mathcal{S}_- [\Pi_\gamma] = -\frac{i}{\eta} (\gamma_{\theta_c}, \gamma) \log (1 + \mathcal{S}_+ [e^{i\eta\Pi_{\gamma_{\theta_c}}}]) . \quad (3.37)$$

The Delabaere-Pham formula in Th.3.5 can be also generalized to the case in which there is more than one saddle trajectory, and the associated saddle classes intersect with a given cycle $\gamma \in H_1(\widehat{\Sigma} \setminus \widehat{P})$ (see [IMS19]):

Theorem 3.6 *Let G_{θ_c} be a Stokes graph with N saddle trajectories with associated saddle classes $\gamma_i \in H_1(\widehat{\Sigma} \setminus \widehat{P})$, $i = 1, \dots, N$, and let $G_{\pm\delta}$ be two saddle reductions of G_{θ_c} . Then, the Borel sums $\mathcal{S}_\pm [e^{V_\gamma}]$ for any $\gamma \in H_1(\widehat{\Sigma} \setminus \widehat{P})$ satisfy the following identities as analytic functions of η on a domain containing $\{\eta \in \mathbb{R} \mid \eta \gg 1\}$:*

$$\mathcal{S}_- [e^{V_\gamma}] = \mathcal{S}_+ [e^{V_\gamma}] \prod_{\{\gamma_i\}_i} (1 + \mathcal{S}_+ [e^{V_{\gamma_i}}])^{-(\gamma_i, \gamma)} . \quad (3.38)$$

With completely analogous steps as for Eq.3.37, we may then translate the formula into the following equation in terms of quantum periods:

$$\text{disc}_{\theta_c} [\Pi_\gamma] \equiv \mathcal{S}_+ [\Pi_\gamma] - \mathcal{S}_- [\Pi_\gamma] = -\frac{i}{\eta} \sum_{\{\gamma_i\}_i} (\gamma_i, \gamma) \log (1 + \mathcal{S}_+ [e^{i\eta\Pi_{\gamma_i}}]) . \quad (3.39)$$

Let us briefly comment on the last results. The Delabaere-Pham formula explicitly describes the Stokes phenomenon affecting the Voros symbols as a flip occurs in the Stokes graph when the direction $\theta = \theta_c$ is crossed. The contribution coming from the flip is exponentially small in the limit $|\eta| \gg 1$, due to the asymptotic expansion dominated by the exponential factor $e^{\eta v_{\theta_c}}$: this is an example of a non-perturbative effect in the variable $\hbar = 1/\eta$. As it will be clear in the Sect.3.5, the formula allows to express the discontinuities of Voros symbols (or, equivalently, quantum periods) just in terms of other Voros symbols (or quantum periods). This will be crucial and it will allow to translate the problem of finding all the resummed quantum periods relevant for the Schrödinger problem to that of solving a closed TBA-like system. In the next section (Sect.3.4), we will also present a very efficient technique to describe the Borel summability of quantum periods in terms of the so-called WKB triangulations. This tool will be very practical to consistently obtain the set of fundamental cycles (and associated quantum periods) associated to the Schrödinger problem, and it will considerably help to simplify the analysis needed to deform the TBA system across the space of parameters of the problem.

3.4 The WKB Triangulation and Its Mutations

In this section we will present an overview on the WKB triangulation. This formalism will prove to be very practical when searching for the set of fundamental quantum periods that are relevant for the Schrödinger problem. It should be underlined that this topic is very rich and it opens a number of connections with very different areas of mathematics. For example, as pointed out in [IN14], the mutations of WKB triangulations may be described in terms of the seed mutation of the associated cluster algebra. The link between WKB triangulation and cluster algebra might be then used to gain insight into possibly many branches of mathematics, like representations theory of quivers and quantum groups, hyperbolic geometry, integrable systems, T-systems and Y-systems, and so on. However, for the scope of this thesis, we shall restrict the exposition to the minimal amount of notation and formalism required to tackle the case of a Schrödinger problem with a polynomial potential. Thus, we start with the general definitions and properties of triangulations, and then we will show how to associate a legitimate triangulation to a Stokes graph.

Let us start by considering a compact, connected, oriented surface \mathbf{S} , possibly with boundary, and a finite set \mathbf{M} of points in \mathbf{S} , that is called the set of marked points. Let us assume the following:

Assumption 3.2 *Let \mathbf{M} be the set of marked points of the surface \mathbf{S} . \mathbf{M} is assumed to be nonempty, and that at least one marked point lies on each boundary component of \mathbf{S} , with some of them possibly on the interior of the surface. In addition, the following cases of (\mathbf{S}, \mathbf{M}) are excluded:*

1. *a sphere with less than four punctures,*
2. *an unpunctured or once-punctured monogon,*
3. *an unpunctured digon,*
4. *an unpunctured triangle,*

where we refer to the points in \mathbf{M} in the interior of \mathbf{S} as to punctures, and to surfaces homeomorphic to a disk with marked points on the boundary as to a polygon.

The following definition of bordered surface is given:

Definition 3.13 *A pair (\mathbf{S}, \mathbf{M}) satisfying Assumption 3.2 is called a bordered surface.*

In order to define ideal triangulations by arcs, let us first define arcs and the notion of compatibility: then, the concept of triangulation will be enriched so as to deal with the additional structure that characterizes triangulations induced by Stokes graphs.

Definition 3.14 An arc α on a bordered surface (\mathbf{S}, \mathbf{M}) is a curve in \mathbf{S} such that:

1. the endpoints of α are points in \mathbf{M} ,
2. α cannot self-intersect but at its endpoints,
3. α cannot intersect punctures and boundaries but at its endpoints,
4. α is not isotopic to a marked point or to a boundary of \mathbf{S} .

Furthermore, arcs are defined up to isotopy in the class of the associated curves.

Definition 3.15 Given two arcs in a bordered surface (\mathbf{S}, \mathbf{M}) , they are said to be compatible if there are representatives in their respective isotopy classes such that they do not intersect each other in the interior of \mathbf{S} ,

Then, an ideal triangulation is introduced as follows:

Definition 3.16 Given a bordered surface (\mathbf{S}, \mathbf{M}) , an ideal triangulation $T = \{\alpha_i\}_{i \in I}$ is a maximal set of distinct, pairwise compatible arcs in (\mathbf{S}, \mathbf{M}) .

Let us now consider a transformation of ideal triangulations known as flip, that will play a crucial role when applied to WKB triangulation in identifying the appearance of saddle trajectories.

Definition 3.17 Let T be an ideal triangulation of a bordered surface (\mathbf{S}, \mathbf{M}) , and let α be an arc in T . If there exists another arc α' of (\mathbf{S}, \mathbf{M}) such that $T' = (T \setminus \{\alpha\}) \cup \{\alpha'\}$ is an ideal triangulation, then α' is called a flip of α , and T' is a flip of T at α .

It is important to underline that, in general, not all the arcs may be flipped, the only exception being arcs that are inner sides of self-folded triangles. However, the WKB triangulations generated by polynomial potentials considered in this thesis do not present this situation, and we can safely assume that any arc can be flipped. In general, it is also known that all ideal triangulations of a bordered surface are linked by a sequence of flips that preserve the cardinality of T . This important feature allows to consider labelled triangulations, where arcs are labelled by integers, and flips preserve the labelling of the arcs not affected by each flip. Hence, we may introduce the following notation:

Definition 3.18 Let T and T' be two triangulations of a bordered surface (\mathbf{S}, \mathbf{M}) , such that T' is a flip of T at the arc α_k . Noticing that also T is a flip of T' at α_k , we can denote the associated flips as follows:

$$T' = \mu_k(T) \quad \text{or} \quad T = \mu_k(T') \quad . \quad (3.40)$$

Now, the aim is to start making contact between the abstract triangulations described above and the properties of Stokes graphs introduced in Sect.3.3. To do so, it is important to update the definitions of both bordered surfaces and ideal triangulations, so as to include an additional set of special points, that of midpoints. As it will be clear in a moment, this additional structure is the triangulation-counterpart of the turning points of the WKB analysis, and it plays a non-negligible role in shaping the possible triangulations.

Definition 3.19 *Let (\mathbf{S}, \mathbf{M}) be a bordered surface, with a number m of triangles in any ideal triangulation T of (\mathbf{S}, \mathbf{M}) . Let us introduce a set $\mathbf{A} \subset \mathbf{S}$ with m points such that $\mathbf{A} \cap \partial\mathbf{S} = \mathbf{A} \cap \mathbf{M} = \emptyset$. Then, the triplet $(\mathbf{S}, \mathbf{M}, \mathbf{A})$ will be called a bordered surface, for brevity, and each $a \in \mathbf{A}$ a midpoint.*

The definition of arcs is updated accordingly, considering arcs that avoid the midpoints in \mathbf{A} :

Definition 3.20 *Let α be an arc in the bordered surface (\mathbf{S}, \mathbf{M}) . Then, α is also an arc in the extended bordered surface $(\mathbf{S}, \mathbf{M}, \mathbf{A})$ if it does not go through any of the midpoints in \mathbf{A} (in other words, if it is a curve in $\mathbf{S} \setminus \mathbf{A}$).*

Finally, the extended definition of ideal triangulations reads as follows:

Definition 3.21 *We shall call an n -tuple $T = \{\alpha_i\}_{i=1}^n$ of arcs in the bordered surface $(\mathbf{S}, \mathbf{M}, \mathbf{A})$ a labeled Stokes triangulation of $(\mathbf{S}, \mathbf{M}, \mathbf{A})$, if the following conditions hold:*

1. *The arcs in T are pairwise compatible, using the isotopy classes for arcs in $(\mathbf{S}, \mathbf{M}, \mathbf{A})$.*
2. *Let us denote with $\tilde{\cdot}$ the operation of considering an arc in $(\mathbf{S}, \mathbf{M}, \mathbf{A})$ as an arc in (\mathbf{S}, \mathbf{M}) . Then, we shall require that the n -tuple $\tilde{T} = \{\tilde{\alpha}_i\}_{i=1}^n$ defines a labeled ideal triangulation of (\mathbf{S}, \mathbf{M}) .*
3. *Every triangle of T contains exactly one midpoint.*

In the context of $(\mathbf{S}, \mathbf{M}, \mathbf{A})$ bordered surfaces, the concept of flip is slightly modified, too, as the operation, when possible, is no more uniquely fixed. Considering as "flippable" the arcs that are not inner arcs of a labeled Stokes triangulation T , then the generating operations of any flip are called signed flips, and they are defined as follows:

Definition 3.22 *Let T be a labeled Stokes triangulation with a flippable arc α_k , and let ε be a sign ($\varepsilon \in \{+, -\}$). Then, the signed flip $T' = \mu_k^{(\varepsilon)}(T)$ at k with sign ε is the labeled Stokes triangulation obtained from T by replacing the arc α_k as depicted in Fig.3.1. Namely, this corresponds to rotating the endpoints of α_k along an edge of the corresponding quadrilateral, clockwise (anticlockwise) if $\varepsilon = +$ (if $\varepsilon = -$).*

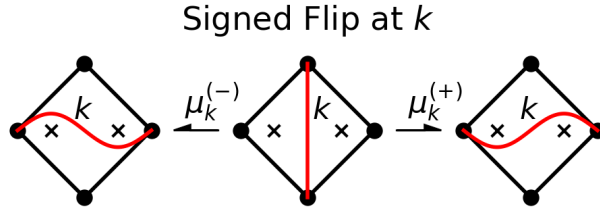


Figure 3.1: Signed flip $T' = \mu_k^{(\varepsilon)}(T)$ at k with sign ε .

For the sake of completeness, let us mention that another operation exists on labeled Stokes triangulations, namely that of signed pops (see [IN14]). These transformations affect triangulations that contain self-folded triangles, exchanging the self-folded arc with the one with an endpoint rotated either clockwise or anticlockwise around the corresponding midpoint. As already pointed out above, however, self-folded triangles do not appear in the WKB triangulations induced by Stokes graphs of polynomial differentials: hence, we will simplify the exposition and we will not further expand on this aspect.

We are finally ready to establish the anticipated link between the labeled Stokes triangulations presented above, and the Stokes graphs described in Sect.3.3. Let us consider the Stokes graph $G(\Phi)$ associated to the quadratic differential Φ on the compact Riemann surface Σ . We will always tacitly assume that Φ is a polynomial differential satisfying Assumption 3.1, and that Σ coincides with the Riemann sphere. In addition, we will also ask that the graph G is saddle-free: this hypothesis, as it will be clear in a moment, is necessary to build a legitimate WKB triangulation. Given these assumptions, it is known that G separates Σ into a finite number of Stokes regions, as defined in Sect.3.3. In particular, for a polynomial differential, two types of Stokes regions are relevant for the discussion:

- regular horizontal strip: Stokes region inside a quadrilateral defined by two simple zeros and two poles of order $m \geq 3$ (equivalent to a region $\{w \in \mathbb{C} \mid a < \Im w < b, a, b \in \mathbb{R}\}$);
- half plane: Stokes region inside a digon defined by a simple zero and a pole of order $m \geq 3$ (equivalent to a region $\{w \in \mathbb{C} \mid 0 < \Im w\}$).

Let us start the construction of a labeled Stokes triangulation by labeling the regular horizontal strips of $G(\Phi)$ as D_1, \dots, D_n . Then, following [IN14] and [GMN11], the labeled Stokes triangulation may be built as follows:

Procedure 3.1 1. Let p_1, \dots, p_s be the poles of Φ of orders $m_1, \dots, m_s \geq 3$. We define a bordered surface $\mathbf{S}(\Phi)$ by cutting from Σ a small hole around each pole p_i , without removing other poles or turning points.

2. Denoting with B_i each boundary associated to the removed circles, we insert $m_i - 2$ marked points on each B_i . Each marked point is picked to correspond to one of the $m_i - 2$ directions to which the Stokes trajectories are asymptotic in a neighbourhood of p_i . The labeling is chosen so as to order the points clockwise around the pole p_i . The set of marked points is then indicated with \mathbf{M} . Then, (\mathbf{S}, \mathbf{M}) is a bordered surface in the sense of Def.3.13.
3. The zeros of Φ (or turning points) constitute the set of midpoints $\mathbf{A}(\Phi)$. Then, $(\mathbf{S}, \mathbf{M}, \mathbf{A})$ is a bordered surface in the sense of Def.3.19.
4. Then, one isotopy class of arcs of $(\mathbf{S}, \mathbf{M}, \mathbf{A})$ is associated to each Stokes region D_i of $G(\Phi)$ in the following way. If the region is a regular horizontal strip, one considers the isotopy class of WKB trajectories connecting the two poles delimiting D_i . Then, the arc in D_i is identified with this class of WKB trajectories, regarded as ending on the corresponding marked points when approaching the poles at the endings. An analogous procedure is considered for a half plane region. In this case, the isotopy class of WKB trajectories is the one with curves starting and ending at the unique pole of the region, and the trajectories are asymptotic to two adjacent marked points. Then, the arc associated to the region is identified with this class of WKB trajectories, regarded as ending on the consecutive marked points.

We shall indicate with $T(\Phi) = (\alpha_i)_{i=1}^n$ the n -tuple of arcs of the bordered surface $(\mathbf{S}, \mathbf{M}, \mathbf{A})$.

In fact, the n -tuple constructed following Procedure 3.1 can be shown to be a labeled Stokes triangulation of $(\mathbf{S}, \mathbf{M}, \mathbf{A})$, and it will be referred to as the labeled Stokes triangulation induced by $G(\Phi)$. In addition, by construction, each triangle contains exactly one midpoint (alias turning point of Φ). Let us now specify the WKB triangulation associated to a generic polynomial potential of degree N . The only pole is the $N + 4$ -order essential singularity at infinity: hence, a single circle is cut out around $z = \infty$, and $N + 2$ marked points are taken on its boundary. Supposing that $\Phi \sim z^N dz^2$ in a neighborhood of $z = \infty$, the $N + 2$ rays to which the Stokes trajectories are asymptotic are located at

$$z_j = \left\{ z \in \mathbb{C} \mid \arg(z) = 2i \frac{\theta + \pi j}{N + 2} \right\}, \quad j = 1, \dots, N + 2. \quad (3.41)$$

As a final remark on this construction, it is now clear why the hypothesis of a saddle free Stokes graph is important. Indeed, for a Stokes graph with at least one saddle trajectory, it is not possible to associate a triangulation: the Stokes region that collapsed to originate the saddle trajectory is actually necessary to provide the associated arc and to complete the tessellation by triangles.

Let us conclude this exposition of WKB triangulation by introducing an additional element to the previous construction. Considering the quadratic differential Φ on Σ ,

let the cycles be the elements of $H_1(\widehat{\Sigma} \setminus \widehat{P})$ as in Sect.3.3. It is useful to generalize the idea of classes of cycles that are defined up to covering involution τ , as we did when introducing the saddle class associated to a saddle trajectory. Denoting with $*$ the image of a cycle through τ , let us denote with $\text{Sym}(H_1(\widehat{\Sigma} \setminus \widehat{P}))$ the following set:

$$\text{Sym}(H_1(\widehat{\Sigma} \setminus \widehat{P})) \equiv \{ \gamma \in H_1(\widehat{\Sigma} \setminus \widehat{P}) \mid \gamma^* = \gamma \}. \quad (3.42)$$

The $*$ -equivalence between cycles is defined by the condition $\gamma - \gamma' \in \text{Sym}(H_1(\widehat{\Sigma} \setminus \widehat{P}))$, so that $\gamma \sim -\gamma^*$. Then, the set of cycles modulo the $*$ -equivalence reads as follows:

$$\widetilde{\Gamma} \equiv H_1(\widehat{\Sigma} \setminus \widehat{P}) / \text{Sym}(H_1(\widehat{\Sigma} \setminus \widehat{P})). \quad (3.43)$$

In the following, the notion of cycles is updated, so as to identify them with elements of $\widetilde{\Gamma}$. Finally, limiting ourselves to the hypothesis of a polynomial differential, the simple cycles of the Stokes graph $G(\Phi)$ are introduced as follows:

Definition 3.23 *Let Φ be a saddle-free quadratic differential, with a labeled Stokes graph $G(\Phi)$ and let us denote with D_1, \dots, D_n the regular horizontal strip Stokes regions. Then we shall indicate with $\gamma_i \in \widetilde{\Gamma}$, $i = 1, \dots, n$, the simple cycles of G . These are defined so as to encircle once the two turning points delimiting each region D_i . The set Γ is the subset of $\widetilde{\Gamma}$ generated by the set of simple cycles $\{\gamma_i\}_{i=1}^n$.*

The set of simple cycles will be useful in the next sections to systematically obtain the set of cycles relevant to the Schrödinger problem. Let us briefly explain the reason. Let us consider again the deformed Schrödinger problem in Eq.3.21, whose associated quadratic differential is Φ_θ . For the sake of simplicity, let us refer to this deformation as to the $S^1(\theta)$ -action on the quadratic differential Φ . Let us assume that for $\theta = 0$ the Stokes graph G_0 has a single regular saddle trajectory l_0 and that it is saddle free for $\theta \in [-r, r]$ and $\theta \neq 0$, for some $r > 0$. Considering a sign $\varepsilon = \pm$ and the saddle reductions $G_{\pm\delta}$, $0 < \delta < r$, let us define $G = G_{\varepsilon\delta}$ and $G' = G_{-\varepsilon\delta}$, picking a labeling such that they are connected by a signed flip as $G' = \mu_k^{(\varepsilon)}(G)$. Being D_1, \dots, D_n the regular horizontal strip Stokes regions of the Stokes graph G , this last assumption indicates that the Stokes region collapsing to originate the regular saddle trajectory is labeled with the integer k , $1 \leq k \leq n$. Given that poles and zeros are not affected by the deformation in θ of Φ_θ , then $\Gamma_G = \Gamma_{G'}$, where the subscripts indicate the Stokes graph the subset of cycles generated by simple cycles is linked to. Accordingly, the simple cycles are indicated as $\gamma_i \in \Gamma_G$ and $\gamma'_i \in \Gamma_{G'}$, with $i = 1, \dots, n$. Then, the following results hold:

Theorem 3.7 *1. The saddle class γ_0 coincides with $\varepsilon\gamma_k$;*

2. Denoting with $b_{ij} \equiv (\gamma_i, \gamma_j)$, the simple cycles mutate according to:

$$\gamma'_i = \begin{cases} -\gamma_k, & \text{if } i = k \\ \gamma_i + [\varepsilon b_{ki}]_+ \gamma_k, & \text{if } i \neq k, \end{cases} \quad (3.44)$$

where $[x]_+ \equiv \max(x, 0)$.

3. The Voros symbols $\exp(V_i) \equiv \exp(V_{\gamma_i}^{(\varepsilon\delta)})$ and $\exp(V'_i) \equiv \exp(V_{\gamma'_i}^{(-\varepsilon\delta)})$ mutate as follows:

$$\lim_{\delta \rightarrow 0^+} \mathcal{S} [e^{V'_i}] = \begin{cases} \lim_{\delta \rightarrow 0^+} \mathcal{S} [(e^{V_k})^{-1}], & \text{if } i = k \\ \lim_{\delta \rightarrow 0^+} \mathcal{S} [e^{V_i} (e^{V_k})^{[\varepsilon b_{ki}]_+} (1 + (e^{V_k})^\varepsilon)^{-b_{ki}}], & \text{if } i \neq k, \end{cases} \quad (3.45)$$

where $[\cdot]_+$ is as above at 2.

Let us then draw a few conclusions. First, from the Delabaere-Pham formula in Th.3.5 and from the Borel summability criteria in Th.3.1 and Th.3.2, it is clear that the presence of a saddle trajectory is required to produce a non-trivial discontinuity in the Borel resummation of the Voros symbols. Second, by definition, to each saddle trajectory is associated a saddle class of cycles, which corresponds to a given simple cycle by Th.3.7, Point 1. This is rather intuitive, as saddle trajectories are by definition finite Stokes trajectories, hence connecting two turning points: considering the saddle reduction of this graph, this pair of turning points singles out a unique regular horizontal strip, and, by Def.3.23, a simple cycle is then associated to the original saddle trajectory. Third, let us consider the result in Th.3.7, Point 3. The theorem is a rephrasing of the Delabaere-Pham formula in Th.3.5, and it states that the Voros symbol associated to a given simple cycle admits a discontinuity in its Borel resummation expressed only in terms of other simple cycles, whose intersection with the given cycle is non-vanishing. Since the aim is to study the discontinuities in the Borel resummation of quantum periods, this motivates us to concentrate on simple cycles associated to a labeled Stokes triangulation. Thus, this poses a limit on the number of simple cycles that may be relevant. Finally, let us consider the result in Th.3.7, Point 2. This theorem governs the mutation of simple cycles in correspondence of a signed flip. In particular, neglecting the signs, it is important to notice that the simple cycles mutate either in themselves or in the sum of simple cycles, if their intersection is positive. Hence, considering the $S^1(\theta)$ -action on Φ , we expect that the mutations occurring in a given range of θ either do not introduce new cycles (always neglecting possible inversions) or they do introduce simple cycles, but just in terms of sums of pre-existing simple cycles. To summarize the last considerations, we may conclude that, in order to study the discontinuity structure of the quantum cycles, we may safely restrict to the study of the ones associated to the simple cycles that characterize the problem. In turn, the spectrum of simple cycles relevant to determine the

discontinuity structure of the problem may be determined by looking at the mutations of the labeled Stokes triangulation under the $S^1(\theta)$ -action on Φ over a π -wide range. From their definition in Def.3.23, it follows that the maximum number of cycles in the spectrum for a polynomial potential of degree $r+1$ is given by $r(r+1)/2$, corresponding to the case where all pairs of turning points are associated to a simple cycle. This may be rephrased in the language of graphs theory. Considering the $r+1$ turning points as vertices of an undirected graph, and simple cycles as edges connecting the associated vertices, then the situation above corresponds with a complete graph.

Using the structures introduced above, one may also rephrase the mutations of the Stokes graph mentioned in Sect.3.3 in the language of cluster algebras. Without further developing in this direction, let us just mention the important links found in [IN14]. As for the simple paths and simple cycles defined above, they transform as monomial x -variables and monomial y -variables, respectively. The associated Voros symbols also mutate accordingly, and their Borel resummation experience jumps in correspondence with signed flips (expressed by the Delabaere-Pham formula Eq.3.33) and signed pops (expressed by a similar formula, Th.3.7 in [IN14]). As a consequence, Voros symbols are found to mutate as x -variables and \hat{y} -variables in the extended seeds formalism. Finally, the vocabulary that translates the problem into the language of cluster algebra allows also to prove crucial identities between Stokes automorphisms (e.g. the pentagon identity $\mathfrak{S}_{\gamma_2}\mathfrak{S}_{\gamma_1} = \mathfrak{S}_{\gamma_1}\mathfrak{S}_{\gamma_1+\gamma_2}\mathfrak{S}_{\gamma_2}$). These results find useful applications also in the study of BPS spectra (see [GMN11]), in particular to find wall-crossing formulae.

Since the link between the resummed quantum periods and the TBA system is the main step to take next, we now turn our focus to apply the Delabaere-Pham formula in the context of polynomial potentials of arbitrary order, so as to obtain the associated TBA system and briefly comment on the quantization conditions that may be imposed then.

3.5 From the Delabaere-Pham Formula to a TBA System

In this section, we will see how to get a description of the discontinuities in the Borel resummation of the relevant quantum periods of the Schrödinger problem in terms of a set of TBA equations. Following [IMS19], we shall restrict to the case of polynomial potentials, where the analysis in terms of the Delabaere-Pham formula is the simplest if all the roots are aligned on the real axis. In this case, the relevant cycles are defined connecting nearest neighbour turning points and the TBA is easily read-off from the Delabaere-Pham formula and using the classical limit. The interesting point is to try

to generalize the TBA for quantum periods outside the minimal chamber, to get the re-summed quantum periods over all the range of physical energies. Having imposed exact quantisation conditions (see Sect.3.8), this allows to get in principle the exact energy spectrum of the stationary Schrödinger problem.

Let us start by presenting the setting of the problem. Let us consider a polynomial potential $V_{r+1}(z)$ of degree $r+1$, so that $Q(z) = V(z) - E$, for some energy $E \in \mathbb{C}$. The Riemann surface associated to Q is then a surface with genus $[r/2]$. Let us call the space of parameters characterizing Q the moduli space \mathcal{M} : basically, this consists in a $r+1$ -dimensional complex space, parameterized by the polynomial coefficients and the energy. Then, let us assume that Q is taken at a point of the moduli space where all the turning points z_i , $i = 1, \dots, r+1$ are real and distinct, choosing the labels so that $z_1 < z_2 < \dots < z_{r+1}$. Let us further assume that the point in the moduli space is such that the coefficient of z^{r+1} in the potential induces classically allowed intervals $[z_a, z_{a+1}]$ for a odd and classically forbidden ones for a even ($a = 1, \dots, r$). We take the just mentioned hypothesis on the point of the moduli space to be sufficient conditions for it to belong to the so-called minimal chamber, a subset of the moduli space whose actual boundaries will be specified later in Def.3.27. We will call the (non-unique) point satisfying these hypothesis a special point of the minimal chamber. Thus, we may introduce the cycles γ_a , $a = 1, \dots, r$, defined so that they encircle the interval $[z_a, z_{a+1}]$: in the hypothesis stated above, as we will see in a moment, these cycles correspond to the spectrum of simple cycles described at the end of Sect.3.4. Considering the quantum periods Π_{γ_a} associated to the cycles γ_a , let us define the masses m_a as proportional to the zero-order term in the formal expansion in $\hbar = 1/\eta$ of the quantum period Π_{γ_a} .

Definition 3.24 *Let γ_a be the cycles defined as above to encircle the intervals $[z_a, z_{a+1}]$, $a = 1, \dots, r$, z_i , $i = 1, \dots, r+1$, being a turning point. Let then Π_{γ_a} be the quantum period associated to the cycle γ_a . Then we call masses the following quantities:*

$$m_{2k-1} = \Pi_{\gamma_{2i-1}}^{(0)} = \oint_{\gamma_{2k-1}} \sqrt{E - V(z)} dz \quad (3.46)$$

$$m_{2k} = i\Pi_{\gamma_{2i}}^{(0)} = i \oint_{\gamma_{2k}} \sqrt{E - V(z)} dz , \quad (3.47)$$

for k integer, such that $1 \leq 2k-1 < 2k \leq r$. The orientation of the cycles is chosen so that m_a are all real and positive.

From the hypothesis above on the point in the moduli space, it is possible to explicitly identify the position of the saddle trajectories in the problem. Indeed, let us consider the classically forbidden intervals encircled by γ_a , a odd. Since they are classically forbidden, $V(x) - E > 0$ for a real x in the interval. Hence, $\sqrt{(V(x) - E)}$ is real and positive on the interval, which proves that a saddle trajectory lies over forbidden intervals if

we consider the Stokes graph in the direction $\theta = 0$. On the other hand, the opposite happens at $\theta = \pi/2$, as allowed and forbidden periods are swapped, so that γ_a , with a even, encircle saddle trajectories. Considering then the asymptotic behavior of $Q(z)$ as $|z| \rightarrow \infty$, it may be easily shown that Stokes trajectories must be asymptotic to $r + 3$ evenly spaced rays (for the general behavior of Stokes trajectories, see Sect.3.3, or [IN14] and [GMN11]). Now, let us consider a turning point from which a saddle trajectory emanates: the other two Stokes trajectories emanating cannot be saddle trajectories, otherwise the asymptotic behavior just described could not be matched. This argument applies both at $\theta = 0$ and $\theta = \pi/2$. In addition, since the $S^1(\theta)$ -action on Φ in a neighborhood of a turning point acts as a smooth rotation, we expect that no other saddle trajectory appears for $\theta \in]0, \pi/2[$ and $\theta \in]\pi/2, \pi[$. Finally, recalling that the $S^1(\theta)$ -action on Φ has a period π , we conclude that the set of cycles $\{\gamma_a\}_{a=1}^r$ encircle all the saddle trajectories appearing in the problem in a π -wide interval. Using this analysis on the Stokes graph, it follows from the Delabaere-Pham formula in Eq.3.39 that the quantum periods associated to classically forbidden intervals are Borel summable around the direction $\theta = 0$ (real, positive axis), hence with no discontinuity. On the other hand, $\Pi_{\gamma_{2k-1}}$ are not Borel summable at $\theta = 0$, and the Delabaere-Pham formula yields:

$$\text{disc}_0 [\Pi_{\gamma_{2k-1}}] = -i\hbar \log \left(1 + \exp \left(-\frac{i}{\hbar} \Pi_{\gamma_{2k-2}} \right) \right) - i\hbar \log \left(1 + \exp \left(-\frac{i}{\hbar} \Pi_{\gamma_{2k}} \right) \right). \quad (3.48)$$

From their definition in Def.3.11, it is also clear that quantum periods are even in \hbar or η : thus, a similar equation emerges also for $\theta = \pi$, though not providing further constraints on the periods. Crucially, an additional equation comes from the direction $\theta = \pi/2$ (or, equivalently, for $\theta = -\pi/2$), which is connected to the exchange between classically allowed and classically forbidden periods, as described above. The Delabaere-Pham formula here reads:

$$\text{disc}_{\pi/2} [\Pi_{\gamma_{2k}}] = -i\hbar \log \left(1 + \exp \left(-\frac{i}{\hbar} \Pi_{\gamma_{2k-1}} \right) \right) - i\hbar \log \left(1 + \exp \left(-\frac{i}{\hbar} \Pi_{\gamma_{2k+1}} \right) \right). \quad (3.49)$$

The analysis of the discontinuity structure of the Borel transform of quantum periods is an example of the application of the "scanning" technique described at the end of the last section. Indeed, at each fixed angle θ , the associated simple cycles are obtained. By varying θ , the appearance of saddle trajectories comes with the mutations of simple cycles and with the discontinuity of the quantum period associated to the saddle class. Hence, by this analysis, the set of relevant cycles, or the spectrum of simple cycles, coincides in this case with the set $\{\gamma_a\}_{a=1}^r$, conveniently introduced above. Moving on with the derivation of a TBA system, a unified description of the discontinuity structure of the problem may be obtained by introducing r auxiliary functions ε_a defined as follows:

Definition 3.25 *Let us define the complex functions ε_a , with $a = 1, \dots, r$, as follows:*

$$\varepsilon_{2k-1} \left(\theta + \frac{i\pi}{2} \pm i\delta \right) = \frac{i}{\hbar} \mathcal{S}_{\pm} [\Pi_{\gamma_{2k-1}}] (\hbar) \quad (3.50)$$

$$\varepsilon_{2k} (\theta) = \frac{i}{\hbar} \mathcal{S} [\Pi_{\gamma_{2k}}] (\hbar) , \quad (3.51)$$

where $e^{-\theta} = \hbar$, k is as in Def.3.24, and $0 < \delta \ll 1$ on the LHS of the first equation is associated to the saddle reduction appearing on the RHS (indicated with \pm). The functions ε_a will be referred to as pseudoenergies.

Remark 3.1 *Let us underline that θ has been tacitly redefined in Def.3.25 to make contact with the notation in [IMS19] and to produce the correct TBA-like equations, as it will be clear in a few passages. Hence, $\theta \in \mathbb{R}$ appearing before Def.3.25 now corresponds to $\Im\theta$.*

With Def.3.25 at hand, the discontinuities now read:

$$\text{disc}_{\pi/2} [\varepsilon_a] (\theta) = L_{a-1} (\theta) + L_{a+1} (\theta) , \quad a = 1, \dots, r , \quad (3.52)$$

where $L_a (\theta) = \log (1 + e^{-\varepsilon_a(\theta)})$, with $L_0 = L_{r+1} = 0$ by definition. Now, it is possible to rephrase the problem in terms of a Riemann-Hilbert problem, by taking into account the classical limit:

$$\varepsilon_a (\theta) = m_a e^{\theta} + \mathcal{O} (e^{-\theta}) , \quad \theta \rightarrow \infty . \quad (3.53)$$

Then, it is possible to verify that the problem is solved by the following TBA system:

$$\varepsilon_a (\theta) = m_a e^{\theta} - \int_{\mathbb{R}} \frac{L_{a-1} (\theta')}{\cosh (\theta - \theta')} \frac{d\theta'}{2\pi} - \int_{\mathbb{R}} \frac{L_{a+1} (\theta')}{\cosh (\theta - \theta')} \frac{d\theta'}{2\pi} , \quad a = 1, \dots, r . \quad (3.54)$$

The notation may be considerably simplified using the convolution product between functions f and g :

$$(f * g) (\theta) = \int_{\mathbb{R}} f (\theta - \theta') g (\theta') d\theta' . \quad (3.55)$$

Then, defining the kernel K as

$$K (\theta) = \frac{1}{2\pi} \frac{1}{\cosh (\theta)} , \quad (3.56)$$

the TBA system in Eq.3.54 may be recast as follows:

$$\varepsilon_a (\theta) = m_a e^{\theta} - K * L_{a-1} (\theta) - K * L_{a+1} (\theta) . \quad (3.57)$$

Thus, we managed to link the solution to a Schrödinger problem on the complex plane to the solution of a TBA system. The main feature of this system is that of being a

conformal-limit version of the usual TBA systems studied in Chp.1. Borrowing from the integrable field theory terminology of Chpt.1, we also see that the interaction appearing in Eq.3.54 connects nearest neighbour pseudoenergies, hence mimicking the link to a A_r -type, underlying Lie algebra. However, the link is not the same as in the ADE-classification of integrable systems studied by Zamolodchikov, and described in Chpt.1. To understand why, let us convert the TBA system into the associated Y-system. The Y-system is obtained performing a smooth shift $\theta \rightarrow \theta + i\pi/2$ on pseudoenergy, and then adding the result to the pseudoenergy shifted by $\theta \rightarrow \theta - i\pi/2$. Finally, defining the Y-functions as $Y_a(\theta) \equiv \exp(-\varepsilon_a(\theta))$, the Y-system reads:

$$Y_a\left(\theta + i\frac{\pi}{2}\right) Y_a\left(\theta - i\frac{\pi}{2}\right) = (1 + Y_{a+1}(\theta))(1 + Y_{a-1}(\theta)) , \quad (3.58)$$

with $Y_0 \equiv Y_{r+1} \equiv 0$ understood. We shall refer to this Y-system as to the minimal chamber Y-system, or, equivalently, to the α -chamber Y-system. This Y-system is periodic with period $i\pi(r+3)$, which gets enhanced to a period $i\pi(r+3)/2$ for r odd (i.e., polynomial potentials with even degree). Let us compare the Y-system in Eq.3.58 with the one for integrable models associated to A_r Lie algebras in Eq.1.13. In this case, the coxeter number is $h = r + 1$, and the incidence matrix I_{ab} is zero except from the first off-diagonal elements $(a, b) = (a, a + 1)$ and $(a, b) = (a, a - 1)$, being equal to one. Hence, the Y-system in Eq.1.13 reads as follows:

$$Y_a\left(\theta + i\frac{\pi}{r+1}\right) Y_a\left(\theta - i\frac{\pi}{r+1}\right) = (1 + Y_{a+1}(\theta))(1 + Y_{a-1}(\theta)) . \quad (3.59)$$

Specializing Eq.1.14 to A_r Lie algebras, the periodicity of Eq.3.59 is $i\pi(r+3)/(r+1)$. Comparing Eq.3.58 with Eq.3.59, it is immediate to notice that the θ -displacement in the latter is model dependent, whereas in the former is fixed to $i\pi/2$. This difference is substantial, and it may be traced back to the different physical origins of both displacements. Indeed, for integrable models it is connected to the pole structure of the associated S-matrix, with poles equally spaced by $\Delta\theta = 2\pi i/h$; on the other hand, for a Schrödinger problem with a polynomial potential with real turning points, it is associated with the directions where Borel summability is lost being $i\pi/2$ apart from each other. Thus, in the Schrödinger case, the θ -shift is independent on the degree of the potential. Let us turn our attention to the periodicity. Again, ultimately the difference is due to the different θ -shifts of the two Y-system.

Let us now turn back to the derivation of the TBA system above in Eq.3.54. It is important to underline the weight of the assumptions on the location in the moduli space that we took at the beginning of this section. To be precise, for this derivation to be as straightforward and as general as it is, it is crucial to assume that all the turning points are non-coalescing and aligned on the real axis. Indeed, if so, the Delabaere-Pham formula may be written down with generality for any polynomial potential, and

it seizes the behavior of the discontinuities in a rather simple way. On the other hand, if an arbitrary point in the moduli space is considered, then the discontinuity structure is difficult to be determined in general, since more fundamental cycles intervene, and such cycles and their intersections are hard to obtain in general. On top of that, in these situations the masses m_a get complex, and it is more difficult to synthesize the discontinuity equations from the Delabaere-Pham formula into a single constraint and then to translate it into a Riemann-Hilbert problem. For these reasons, it seems to be more efficient and convenient to start from a point in the minimal chamber and then consider a path in the moduli space that takes the problem to the required set of values of the parameters. In this perspective, the path through the moduli space is only required not to go through a point where turning points coalesce, as in that case one would lose most of the tools presented in the Sect.3.3 (in particular, the results on Borel summability of the solutions and of the quantum periods, and the Delabaere-Pham formula). On top of that, the coalescence of turning points would spoil the possibility to coherently define the triangulation in Sect.3.4, and to effectively use it to analyse the period content of the problem. For these reasons, we shall assume to move out of the special points in the minimal chamber via paths that do not lead to coalescence.

3.6 TBA Deformation In the Minimal Chamber

Following [IMS19], let us now present the issues emerging from the complexification of the masses m_a , introducing the relevant notations. This will be the most convenient starting point to specialize the method to the cubic and the quartic oscillator, and then to any polynomial potential. Let us start manipulating Eq.3.54, taking the masses m_a to be generic complex numbers with argument φ_a , namely $m_a = |m_a|e^{i\varphi_a}$, $a = 1, \dots, r$. With the aim to preserve a real classical limit, let us define the shifted pseudoenergies and L -functions:

Definition 3.26 *Let ε_a , $a = 1, \dots, r$ be the pseudoenergies, each with mass $m_a = |m_a|e^{i\varphi_a}$. Then, the shifted pseudoenergies are defined as follows:*

$$\tilde{\varepsilon}_a = \varepsilon_a(\theta - i\varphi_a) . \quad (3.60)$$

The shifted L -functions are introduced accordingly:

$$\tilde{L}_a(\theta) = L_a(\theta - i\varphi_a) = \log(1 + e^{-\tilde{\varepsilon}_a(\theta)}) . \quad (3.61)$$

With this definitions at hand, the TBA system in Eq.3.54 may be recast as follows:

$$\tilde{\varepsilon}_a(\theta) = |m_a|e^\theta - \int_{\mathbb{R}} \frac{\tilde{L}_{a-1}(\theta')}{\cosh(\theta - \theta' + i(\varphi_{a-1} - \varphi_a))} \frac{d\theta'}{2\pi} - \int_{\mathbb{R}} \frac{\tilde{L}_{a+1}(\theta')}{\cosh(\theta - \theta' + i(\varphi_{a+1} - \varphi_a))} \frac{d\theta'}{2\pi} . \quad (3.62)$$

It is apparent from this last expression that now the poles of the kernel are displaced, and their position depends on the phase difference between adjacent masses. As a consequence, as opposed to the case with real masses, it may happen that the poles in the kernels cross the real line of integration. To be precise, this first occurs when

$$|\varphi_{a\pm 1} - \varphi_a| = \frac{\pi}{2}, \quad (3.63)$$

and such equation poses a limit on the validity of the TBA system, as written in Eq.3.62. Using this constraint, we are then ready to define with due accuracy the already mentioned minimal chamber of the moduli space, or α -chamber:

Definition 3.27 *Let \mathcal{M} be the moduli space of the Schrödinger problem for a polynomial potential of degree $r + 1$. The subspace $A \subset \mathcal{M}$ such that*

$$|\varphi_{a\pm 1} - \varphi_a| < \frac{\pi}{2} \quad (3.64)$$

holds for all $a = 2, \dots, r - 1$ is called the minimal chamber, or α -chamber.

As it will be clear in the next chapter, the α -chamber notation is introduced ad-hoc in this thesis. It will be useful to efficiently label a sequence of chambers with greek letters (α -chamber, β -chamber, ...), when following a path in the moduli space. Now, from the considerations above, for the TBA system in Eq.3.62 to hold, it is necessary to ask that the point $p \in A \subset \mathcal{M}$ lies in the minimal chamber. With this assumption, having defined a modified kernel $K_{a,b}$ as

$$K_{a,b}(\theta) = \frac{1}{2\pi} \frac{1}{\cosh(\theta + i(\varphi_a - \varphi_b))}, \quad (3.65)$$

the TBA system may be synthesized in the following expression:

$$\tilde{\varepsilon}_a(\theta) = |m_a|e^\theta - (K_{a-1,a} * L_{a-1})(\theta) - (K_{a+1,a} * L_{a+1})(\theta). \quad (3.66)$$

For the sake of brevity, we shall refer to Eq.3.66 as to the TBA system in the minimal chamber.

3.7 Intermission: TBA Derivation with a ODE-IM Correspondence Perspective

In this section we will provide an alternative derivation of the TBA system in Eq.3.57 from a ODE-IM perspective, following [IMS19] and [AMSV10]. The procedure focuses on the analysis of the WKB asymptotics of the solutions to the Schrödinger equation in

Eq.3.3 for a polynomial potential. For convenience, let us explicitly state the equation, using a generic spectral parameter $\xi = 1/\eta$ playing the role of the Planck's constant \hbar :

$$\left(-\xi^2 \frac{d^2}{dz^2} + z^{r+1} - \sum_{a=1}^r u_a z^{r-a} \right) \Psi(z, u_a, \xi) = 0, \quad (3.67)$$

where $V(z) - E \equiv z^{r+1} - \sum_{a=1}^r u_a z^{r-a}$ (adopting a convenient rescaling for the highest order term in the potential), and u_a in $\Psi(z, u_a, \xi)$ indicate the implicit dependence from all the r complex constants u_a of the wave function Ψ . Considering the special case where $\xi \equiv 1$, then the asymptotic analysis of the WKB solution yields the following subdominant solution in a wedge containing the positive real axis:

$$\Psi(z, u_a) \sim \frac{1}{\sqrt{2i}} z^{n_r} \exp\left(-\frac{2}{r+3} z^{\frac{r+3}{2}}\right), \quad (3.68)$$

where n_r is defined as:

$$n_r = \begin{cases} -\frac{r+1}{4} & r+1 \text{ odd} \\ -\frac{r+1}{4} - B_{\frac{r+3}{2}} & r+1 \text{ even} \end{cases} \quad (3.69)$$

and the complex coefficient B_m is given by the expansion of

$$\left(1 - \sum_{a=1}^r u_a z^{-a-1} \right)^{1/2} \equiv 1 + \sum_{m=1}^{\infty} B_m z^{-m}. \quad (3.70)$$

The Stokes phenomenon due to the essential singularity of the potential at infinity determines the Stokes sectors \mathcal{S}_k , for $k = 0, \dots, r+2$

$$\mathcal{S}_k = \left\{ z \in \mathbb{C} \mid \left| \arg(z) - \frac{2k\pi}{r+3} \right| < \frac{\pi}{r+3} \right\}, \quad (3.71)$$

so that the solution in Eq.3.68 is subdominant in the sector \mathcal{S}_0 . Notice that the Eq.3.67 at $\xi = 1$ is invariant under the following Symanzik rotation

$$(z, u_a) \rightarrow (\omega z, \omega^{a+1} u_a), \quad \omega = e^{\frac{2\pi i}{r+3}}. \quad (3.72)$$

As a consequence, other solutions to the equation at $\xi = 1$ may be obtained by repeatedly applying the transformation in Eq.3.72:

$$\Psi_k(z, u_a) \equiv \omega^{k/2} \Psi(\omega^{-k} z, \omega^{-(a+1)k} u_a). \quad (3.73)$$

In particular, the solution $\Psi_k(z, u_a)$ has got the desirable property of being the subdominant one in the sector \mathcal{S}_k . Now, the solution in Eq.3.68 at the special point $\xi = 1$ may be generalized to a generic value of ξ defining

$$\Psi(z, u_a, \xi) \equiv \Psi\left(\xi^{-\frac{2}{r+3}} z, \xi^{-\frac{2(a+1)}{r+3}} u_a\right). \quad (3.74)$$

This solution is still the subdominant one in the sector \mathcal{S}_0 . The operation of recovering the general $\xi \neq 1$ Eq.3.67 from the special case $\xi = 1$ is equivalent to rescale the coordinate z and the parameters as follows:

$$z \rightarrow \xi^{\frac{2}{r+3}} z, \quad u_a \rightarrow \xi^{\frac{2(a+1)}{r+3}} u_a. \quad (3.75)$$

With this perspective in mind, the Symanzik rotations in Eq.3.73 may be reinterpreted as rotations in the spectral parameter ξ , so that the subdominant solution in the sector \mathcal{S}_k for a generic ξ reads:

$$\Psi_k(z, u_a, \xi) = \omega^{k/2} \Psi(z, u_a, e^{i\pi k} \xi). \quad (3.76)$$

Then, let us introduce the Wronskian for two subdominant solutions in the sectors k_1 and k_2 :

Definition 3.28 Let $\Psi_{k_1}(z, u_a, \xi)$ and $\Psi_{k_2}(z, u_a, \xi)$ be the subdominant solutions in the sectors \mathcal{S}_{k_1} and \mathcal{S}_{k_2} , respectively. Then their Wronskian W_{k_1, k_2} is defined as follows:

$$W_{k_1, k_2}(u_a, \xi) \equiv \xi^{\frac{2}{r+3}} \left(\Psi_{k_1}(z, u_a, \xi) \frac{d\Psi_{k_2}}{dz}(z, u_a, \xi) - \Psi_{k_2}(z, u_a, \xi) \frac{d\Psi_{k_1}}{dz}(z, u_a, \xi) \right). \quad (3.77)$$

With the definition of the Wronskians, let us then introduce the Y-functions:

Definition 3.29 Let W_{k_1, k_2} be the Wronskian of two solutions as in Def.3.28. Then, the Y-functions $Y_s(\xi, u_a)$, $s = 1, \dots, r$, are defined as follows:

$$\begin{aligned} Y_{2j}(\xi, u_a) &\equiv \frac{W_{-j, j} W_{-j-1, j+1}}{W_{-j-1, -j} W_{j, j+1}}(\xi, u_a) \\ Y_{2j+1}(\xi, u_a) &\equiv \frac{W_{-j-1, j} W_{-j-2, j+1}}{W_{-j-2, -j-1} W_{j, j+1}}\left(e^{\frac{i\pi}{2}} \xi, u_a\right), \end{aligned} \quad (3.78)$$

with $j \in \mathbb{Z}$, $1 \leq 2j < 2j+1 \leq r$.

The Y-functions in Def.3.29 obey to the following Y-system:

$$Y_s\left(e^{\frac{i\pi}{2}} \xi, u_a\right) Y_s\left(e^{-\frac{i\pi}{2}} \xi, u_a\right) = (1 + Y_{s+1}(\xi, u_a))(1 + Y_{s-1}(\xi, u_a)), \quad (3.79)$$

where $Y_0 = Y_{r+1} \equiv 0$ by definition. This Y-system is obtained using identities for the Wronskians that may be derived using their definition and the Symanzik rotation in Eq.3.72. In addition, one needs also to evaluate the asymptotic expansion for the Y's, along the lines of [AMSV10]. This will select the right solution for the Y-system in Eq.3.79, with the asymptotics representing the classical limit and encapsulating the specific dynamics of the system. Specifically, using the WKB expansion to approximate

the solutions for $\xi \rightarrow 0$, the Y-functions may be found to enjoy the following asymptotic expansion:

$$\begin{aligned} \log Y_{2j+1}(\xi, u_a) &\sim -\frac{1}{\xi} \oint_{\gamma_{r-2j}} \sqrt{E-V(z)} dz \equiv -\frac{m_{r-2j}}{\xi} \\ \log Y_{2j}(\xi, u_a) &\sim -\frac{i}{\xi} \oint_{\gamma_{r+1-2j}} \sqrt{E-V(z)} dz \equiv -\frac{m_{r+1-2j}}{\xi}, \end{aligned} \quad (3.80)$$

for $\xi \rightarrow 0^+$, $|\arg(\xi)| < \pi$, and where γ_a are the simple periods previously defined in Sect.3.5 and m_a the associated masses in Def.3.24. From the expansions above, it is clear that the Y_k function corresponds to the cycle $r+1-k$. Then, by relabelling $Y_k \rightarrow Y_{r+1-k}$, the pairing between Y-functions and cycles is the same as in Def.3.24. Finally, we are ready to translate the Y-system in Eq.3.79 to a TBA system. Following [AMSV10], using the function $l_a(\xi) \equiv \log Y_a(\xi) + m_a/\xi$ analytic in the physical strip $|\arg(\xi)| < \pi$, the Y-system is first translated to:

$$l_a\left(e^{\frac{i\pi}{2}}\xi\right) + l_a\left(e^{-\frac{i\pi}{2}}\xi\right) = \log\left((1+Y_{a+1}(\xi))(1+Y_{a-1}(\xi))\right). \quad (3.81)$$

Then, having defined

$$\xi = e^{-\theta}, \quad Y_a(\xi) = e^{-\varepsilon_a(\theta)}, \quad K(\theta) = \frac{1}{2\pi} \frac{1}{\cosh(\theta)}, \quad (3.82)$$

the equation Eq.3.81 may be convoluted with K :

$$\begin{aligned} K * \log\left((1+Y_{a+1}(\theta))(1+Y_{a-1}(\theta))\right) &= K * \left(l_a\left(\theta + i\frac{\pi}{2}\right) + l_a\left(\theta - i\frac{\pi}{2}\right)\right) = \\ &= \int_{\mathbb{R}} \frac{d\theta'}{2\pi} \frac{l_a\left(\theta' + i\frac{\pi}{2}\right) + l_a\left(\theta' - i\frac{\pi}{2}\right)}{\cosh(\theta - \theta')} = \\ &= \oint_{\gamma} \frac{d\theta'}{2\pi i} \frac{l_a(\theta')}{\sinh(\theta - \theta')} = l_a(\theta), \end{aligned} \quad (3.83)$$

where γ is the rectangle corresponding to the physical strip. The last two passages follow from the analytic properties of l_a described above, with a particularly important role played by the absence of singularities within the physical strip. With the result above at hand, it is a trivial matter to substitute the Y-functions with the corresponding pseudoenergies, and to get the TBA in Eq.3.57:

$$\varepsilon_a(\theta) = m_a e^\theta - K * L_{a-1}(\theta) - K * L_{a+1}(\theta). \quad (3.84)$$

The two derivations of the TBA system are equivalent, and the Y-functions associated, even though arising from different mathematical descriptions of the problem, do coincide. The reason for this is that they satisfy the same TBA system, or the same Y-system

with the same asymptotics. The main advantage of the derivation presented in this section lies in its more direct approach, and in providing a generalization of the traditional ODE-IM correspondence tools briefly presented in Chpt.2. Using this perspective, quantum periods emerge considering the algebraic relations obeyed by the Wronskian of solutions of the Schrödinger equation with prescribed asymptotics. Another potential advantage of this approach is that the periodicity properties of the Y-functions may find a more fundamental interpretation, as arising from the combined properties of the underlying Wronskians and with possible links with TQ-systems and TT-systems. This is a consequence of the already mentioned connection with the ODE-IM correspondence techniques of Chpt.2, and it could open to a deeper understanding of the principles at the basis of quantization.

3.8 Brief Overview of Exact Quantisation Conditions

For the sake of completeness, let us mention the final step it should be taken to solve a spectral Schrödinger problem, namely, imposing Exact Quantisation Conditions (EQCs). These constraints are typically transcendental equations for the Borel resummed Voros multipliers (or, equivalently, the Borel resummed quantum periods), and they allow to single out the energy spectrum of the system. The general shape of an EQC may be expressed as a single functional equation involving in principle all the Voros multipliers:

$$\mathcal{Q}(\mathcal{V}_{\gamma_1}(\hbar), \dots, \mathcal{V}_{\gamma_r}(\hbar)) = 0, \quad (3.85)$$

where $\{\gamma_a\}_{a=1}^r$ is the set of relevant simple cycles described in the previous sections. In case Voros symbols are not Borel summable in the needed direction due to the presence of saddle trajectories, a saddle reduction process must be considered. If so, the EQC above depends on which prescription is chosen to define the Borel resummation of the associated Voros symbol. Exact quantisation conditions may be derived in different alternative ways, whose equivalence may be non-trivial to prove. The approach that we shall present in the following is based on the exact WKB analysis described in Sect.3.3, and, in particular, on the connection formulae in Th.3.4. Let us briefly describe the method in general. Let us consider the Schrödinger problem as formulated in Eq.3.3. Taking into account an exact WKB approach, for a saddle free Stokes graph G , a solution may be given in terms of the Borel sum of the formal WKB solutions Ψ_a^\pm normalized at a turning point a (see Eq.3.14). To each Stokes region D of G is associated a pair of solutions $\Psi_{a,D}^\pm$, and the discontinuities from a region to an adjacent one are expressed in terms of the connection formulae in Th.3.4. The starting point to find EQCs is to recognize that a wave function is a legitimate eigenfunction associated to an eigenvalue $E \in \mathbb{C}$ if it is normalizable: more precisely, this translates into the requirement that the restriction of the wave function to the real axis is in $L^2(\mathbb{R})$, the set of square summable functions on the real axis. Then, considering a solution decaying in the $x \equiv \Re z \rightarrow -\infty$

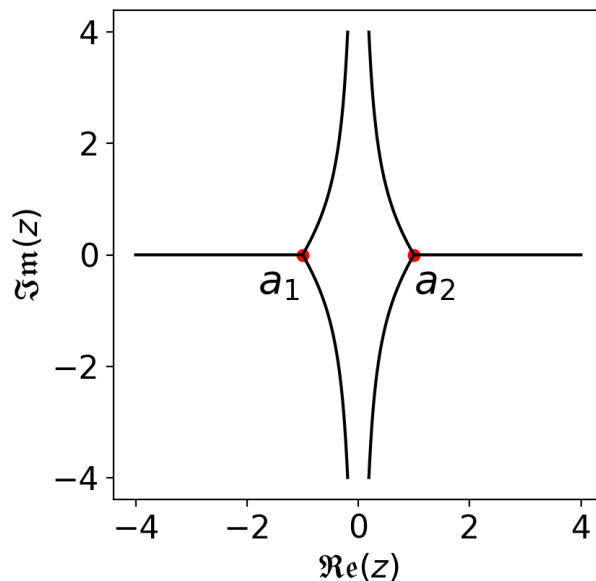


Figure 3.2: Stokes graph G_0 in the direction $\theta = 0$ for $V(z) = z^2$ and a real and positive energy.

limit, it is necessary to ask that the solution still vanishes as $x \rightarrow +\infty$. However, due to the Stokes regions that need to be crossed to get from the Stokes region containing the negative real axis to that containing the positive real axis, the connection formulae imply the presence of both decaying and exponentially increasing components. Thus, the normalizability condition is imposed by setting to zero all the prefactors of exponentially increasing terms, and this equation originates the EQC constraint in Eq.3.85. Along the lines of [ea20], let us present how EQCs are expressed in terms of Voros symbols for the simplest example of the harmonic oscillator. In this case, the potential is $V(z) = z^2$, with a Stokes graph G_0 in the direction $\theta = 0$ as in Fig.3.2 for a real and positive energy E . The turning points are two, and they correspond to the points $a_1 = -\sqrt{E}$ and $a_2 = \sqrt{E}$, lying on the real axis. Let us apply the procedure described above. Since two Stokes curve lie on the real axis for $\Re z < a_1$ and $\Re z > a_2$, Borel summability of the solutions is not guaranteed in general on these segments, hence they should be avoided. One may either think of adding a infinitesimally small imaginary part to move out of the real axis, or to pick a different direction infinitesimally apart from $\theta = 0$ of G_0 , so as to bend the Stokes trajectories away from the real axis. Following [ea20], we opt for the first approach, choosing to follow a path $\gamma_t \equiv \{z \in \mathbb{C} \mid z = t - i\delta, t \in [-\infty, \infty], \delta \in \mathbb{R}_+, \delta \ll 1\}$, slightly below the real axis. Let us consider the solutions Ψ_{a_1, D_1}^\pm in the region D_1 normalized at a_1 . Then, the analytic continuation from D_1 to D_2 is associated

to the following change in the wave functions (see Th.3.4):

$$\begin{pmatrix} \Psi_{a_1, D_1}^+ \\ \Psi_{a_1, D_1}^- \end{pmatrix} = M_+ \begin{pmatrix} \Psi_{a_1, D_2}^+ \\ \Psi_{a_1, D_2}^- \end{pmatrix}. \quad (3.86)$$

This is followed by a change of normalization from a_1 to a_2 , required to apply the connection formula to the next transition from D_2 to D_3 . This is expressed in Eq.3.30, and it may be encoded in the diagonal matrix

$$N_{a_1 \rightarrow a_2} \equiv \text{diag} \left(\exp \left(+ \int_{a_1}^{a_2} S_{\text{odd}}(z, \hbar) dz \right), \exp \left(- \int_{a_1}^{a_2} S_{\text{odd}}(z, \hbar) dz \right) \right). \quad (3.87)$$

Then, the change in normalization reads:

$$\begin{pmatrix} \Psi_{a_1, D_2}^+ \\ \Psi_{a_1, D_2}^- \end{pmatrix} = N_{a_1 \rightarrow a_2} \begin{pmatrix} \Psi_{a_2, D_2}^+ \\ \Psi_{a_2, D_2}^- \end{pmatrix}. \quad (3.88)$$

With completely analogous steps, it is possible to first transition from D_2 to D_3 , and then to go back to the normalization at a_1 , so that the complete connection problem is as follows:

$$\begin{aligned} \begin{pmatrix} \Psi_{a_1, D_1}^+ \\ \Psi_{a_1, D_1}^- \end{pmatrix} &= M_+ N_{a_1 \rightarrow a_2} M_+ N_{a_2 \rightarrow a_1} \begin{pmatrix} \Psi_{a_1, D_3}^+ \\ \Psi_{a_1, D_3}^- \end{pmatrix} = \\ &= \begin{pmatrix} \Psi_{a_1, D_3}^+ + i \left(1 + e^{\oint_A S_{\text{odd}}(z, \hbar) dz} \right) \Psi_{a_1, D_3}^- \\ \Psi_{a_1, D_3}^- \end{pmatrix}, \end{aligned} \quad (3.89)$$

where A , is the counter-clockwise cycle encircling the turning points a_1 and a_2 . Given that both the Stokes curves lying on the real axis are negatively oriented, the decaying solutions in the first Riemann sheet correspond to the "+" ones in both D_1 and D_3 . Hence, starting with Ψ_{a_1, D_1}^+ in D_1 , we see that its continuation in D_3 contains also a diverging term Ψ_{a_1, D_3}^- . Thus, the normalization condition amounts to setting:

$$1 + e^{\oint_A S_{\text{odd}}(z, \hbar) dz} = 1 + \mathcal{V}_A(\hbar) = 0. \quad (3.90)$$

This is an example of the general EQC presented in Eq.3.85, and it contains the only Voros symbol that may be associated to this problem. The last EQC is equivalent to:

$$\oint_A S_{\text{odd}}(z, \hbar) dz = -2\pi i \left(n + \frac{1}{2} \right), n \in \mathbb{Z}. \quad (3.91)$$

An explicit computation allows to get $\oint_A S_{\text{odd}}(z, \hbar) dz$ in closed form:

$$\oint_A S_{\text{odd}}(z, \hbar) dz = \oint_A S_{-1}(z, \hbar) dz = -2\pi i \frac{E}{\hbar\sqrt{2}}. \quad (3.92)$$

Hence, the well-known spectrum of the harmonic oscillator is obtained:

$$E = \hbar\sqrt{2} \left(n + \frac{1}{2} \right), n \in \mathbb{Z}_+, \quad (3.93)$$

where the restriction to \mathbb{Z}_+ comes from the fact that $E > 0$ must be required in order to have the Stokes graph G_0 we considered for the derivation.

In general, computing exact quantisation conditions is not an easy task. The reason for the very simple derivation above may be traced back to the specific properties of the harmonic oscillator potential. In particular, the possibility to explicitly compute the spectrum is due to the first relation in Eq.3.92, where the power series in S_{odd} truncates at zero-order. For generic potentials, on the other hand, one may hope to find functional relations as in Eq.3.85, which are implicit equations of both energy and the Planck's constant. For problems admitting a discrete energy spectrum, then it is possible to use the dependence on both E and \hbar to equivalently label the spectrum with discrete values of energy at fixed \hbar , or with discrete values of \hbar at fixed energy. The latter approach is more natural in the context of EQCs, due to the fact that Voros symbols are power series in \hbar , whereas the energy dependence of $Q(z)$ is more difficult to treat and extract. Thus, the discrete spectrum associated to the Schrödinger problem is the set $\{\hbar_n\}_{n=0}^\infty$, which is referred to as the Voros spectrum. This is connected to the energy spectrum via the consistency relation:

$$E_n(\hbar_n) = E, \quad (3.94)$$

for a given energy value $E \in \mathbb{C}$. To conclude this brief overview, let us underline that the possibility to define EQCs in terms of Voros symbols is a fundamental complement to the TBA equations. Indeed, as anticipated in Sect.3.5, by solving the TBA system and imposing EQCs, one is able to find in principle the exact energy spectrum of the Schrödinger problem.

Chapter 4

TBA System for Polynomial Potentials Out of the Minimal Chamber

In this chapter, we shall describe the deformation of the TBA system for polynomial potentials out of the minimal chamber of Def.3.27. For convenience, let us report here the TBA system in the minimal chamber, as written in Eq.3.62:

$$\tilde{\varepsilon}_a(\theta) = |m_a|e^\theta - \int_{\mathbb{R}} \frac{\tilde{L}_{a-1}(\theta')}{\cosh(\theta - \theta' + i(\varphi_{a-1} - \varphi_a))} \frac{d\theta'}{2\pi} - \int_{\mathbb{R}} \frac{\tilde{L}_{a+1}(\theta')}{\cosh(\theta - \theta' + i(\varphi_{a+1} - \varphi_a))} \frac{d\theta'}{2\pi}. \quad (4.1)$$

As pointed out in Sect.3.6, by leaving the minimal chamber of the problem, the poles in the kernels of Eq.4.1 move across the real line of integration. As a consequence, one is forced to consider a deformation of the integration path out of the singularity, which results in taking the residue of the integrand on that point. The process we just described is referred to as to a wall-crossing, and it produces a deformation of the TBA system due to the appearance of the residue at the pole.

In the following, we will start with the simplest example of wall-crossing, appearing at $r = 2$ for a cubic potential. In that context, we shall see most of the typical issues and techniques connected to a TBA deformation, with a relatively pedagogical approach. We will also try to make contact with the analysis of TBA triangulations described in Sect.3.4, connecting the rather ad-hoc definition of "new" pseudoenergies to the mutations in the spectrum of relevant cycles. This will be the first notable use of the Python code developed for this thesis, which is introduced in Appendix A. In addition, the Y-system in the maximal chamber is introduced and its periodicity properties are analyzed numerically. Next, the case of a quartic potential is analyzed, with a particular attention to the appearance of intermediate chambers between the minimal and the maximal

one. Analogously to the cubic case, a Y-system is introduced in each chamber, and its periodicity properties are described numerically.

4.1 Warm Up: the Cubic Potential

Let us start with an example of wall-crossing arising from the simplest non-trivial TBA system, namely that associated to a cubic potential. In this case, assuming to be in the minimal chamber, the TBA system has two equations, and it reads:

$$\tilde{\varepsilon}_1(\theta) = |m_1|e^\theta - K_{2,1} * \tilde{L}_2(\theta) \quad (4.2)$$

$$\tilde{\varepsilon}_2(\theta) = |m_2|e^\theta - K_{1,2} * \tilde{L}_1(\theta) . \quad (4.3)$$

Thinking of moving inside \mathcal{M} and out of the minimal chamber $A = \{p \in \mathcal{M} \mid |\varphi_2(p) - \varphi_1(p)| < \pi/2\}$, then the wall is crossed when $|\Delta\varphi_{2,1}(p)| \equiv |\varphi_2(p) - \varphi_1(p)| = \pi/2$. Indeed, for example, let us consider the equation for the poles of the kernel $K_{2,1}$:

$$\theta'_p = \theta + i \left[\Delta\varphi_{2,1} \mp \left(\frac{\pi}{2} + k\pi \right) \right] , \quad k \in \mathbb{Z} \quad (4.4)$$

Given that θ' is integrated over \mathbb{R} , for θ'_p to cross the integration path, one needs to ask that $\theta'_p \in \mathbb{R}$. This reduces to the equation $\Delta\varphi_{2,1} = \pm \left(\frac{\pi}{2} + k\pi \right)$, for $k \in \mathbb{Z}$. Now, since the starting point p in the moduli space \mathcal{M} is a special point of the minimal chamber A , $\Delta\varphi_{2,1}$ starts from 0 and may either increase or decrease: in either cases, the first poles hitting the integration path are those corresponding to $k = 0$, namely, $\Delta\varphi_{2,1} = \pm\pi/2$. So, let us assume for definiteness that $\Delta\varphi_{2,1} > \pi/2$ as the wall is crossed: then, the TBA system is deformed by picking the residues of the kernel. Let us see as an example the effect on the first equation in Eq.4.2, the one for $\tilde{\varepsilon}_1$. The position of the pole that crossed the integration path is $\theta'_p = \theta + i[\Delta\varphi_{2,1} - \pi/2]$, corresponding to the configuration depicted in Fig.4.1: in the same figure, the path deformation is shown, too. The deformed equation then reads as follows:

$$\tilde{\varepsilon}_1(\theta) = |m_1|e^\theta - K_{2,1} * \tilde{L}_2(\theta) + 2\pi i \text{Res} \left[\frac{1}{2\pi} \frac{\tilde{L}_2(\theta')}{\cosh(\theta - \theta' + i\Delta\varphi_{2,1})} \right] \Bigg|_{\theta'=\theta_p} , \quad (4.5)$$

where the sign in front of the residue is due to the clockwise direction on the path encircling the pole in Fig.4.1. Expanding the denominator around its zero θ_p :

$$\begin{aligned} \cosh(\theta - \theta' + i\Delta\varphi_{2,1}) &= -\sinh(\theta - \theta_p + i\Delta\varphi_{2,1})(\theta' - \theta_p) + \mathcal{O}\left((\theta' - \theta_p)^3\right) \\ &= -i(\theta' - \theta_p) + \mathcal{O}\left((\theta' - \theta_p)^3\right) , \end{aligned}$$

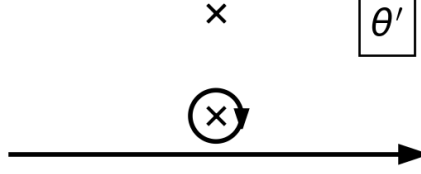


Figure 4.1: Pole configuration and deformation of the integration path after wall crossing. The position of the pole is given here by $\theta'_p = \theta + i[\Delta\varphi_{2,1} - \pi/2]$, with $\Delta\varphi_{2,1} > \pi/2$.

then, the residue may be obtained as follows:

$$\begin{aligned} \text{Res} \left[\frac{1}{2\pi \cosh(\theta - \theta' + i\Delta\varphi_{2,1})} \frac{\tilde{L}_2(\theta')}{\theta' - \theta_p} \right] \Bigg|_{\theta'=\theta_p} &= \lim_{\theta' \rightarrow \theta_p} \frac{\theta' - \theta_p}{2\pi} \frac{\tilde{L}_2(\theta')}{i(\theta_p - \theta') (1 + \mathcal{O}((\theta' - \theta_p)^2))} \\ &= -\frac{1}{2\pi i} L_2 \left(\theta - i\frac{\pi}{2} - i\varphi_1 \right) . \end{aligned}$$

The deformed equation reads then:

$$\tilde{\varepsilon}_1(\theta) = |m_1|e^\theta - K_{2,1} * \tilde{L}_2(\theta) - L_2 \left(\theta - i\frac{\pi}{2} - i\varphi_1 \right) . \quad (4.6)$$

With totally analogous steps, one obtains the deformed equation for $\tilde{\varepsilon}_2$. The only difference one should take care of is the fact that the pole responsible for crossing the integration path is now the upper one, and that the resulting integration circle is oriented in the counter-clockwise direction. The deformed TBA is as follows:

$$\tilde{\varepsilon}_1(\theta) = |m_1|e^\theta - K_{2,1} * \tilde{L}_2(\theta) - L_2 \left(\theta - i\frac{\pi}{2} - i\varphi_1 \right) \quad (4.7)$$

$$\tilde{\varepsilon}_2(\theta) = |m_2|e^\theta - K_{1,2} * \tilde{L}_1(\theta) - L_1 \left(\theta + i\frac{\pi}{2} - i\varphi_2 \right) . \quad (4.8)$$

Looking at Eq.4.7, it is apparent that the system is not functionally closed, due to the residues being calculated at shifted points. As a consequence, one is forced to add two more equations by conveniently shifting the first two ones so as to make the TBA system closed. While doing so, one should also be careful to the resulting displacement of the poles, so as to avoid the situation of poles lying on the integration path. For this reason, we introduce a small displacement in θ in the residues of Eq.4.7, so that the closed,

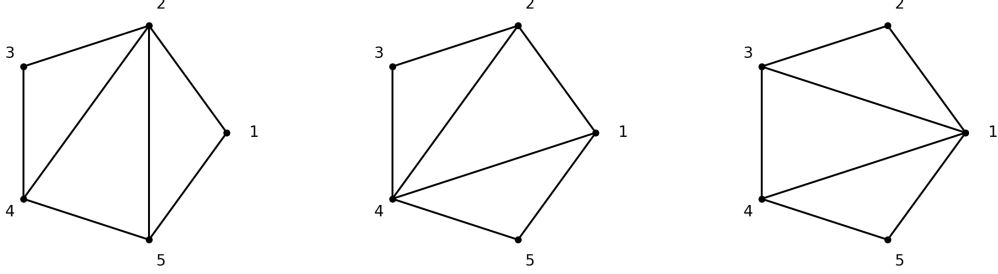


Figure 4.2: Mutations of the WKB triangulation for a cubic potential in the minimal chamber. The abstract triangulations in this figure were obtained from the analysis in Fig.4.3.

deformed TBA system reads as follows:

$$\begin{aligned}
\tilde{\varepsilon}_1(\theta) &= |m_1|e^\theta - K_{2,1} * \tilde{L}_2(\theta) - \tilde{L}_2\left(\theta + i\Delta\varphi_{2,1} - i\frac{\pi}{2} + i\delta\right) \\
\tilde{\varepsilon}_2(\theta) &= |m_2|e^\theta - K_{1,2} * \tilde{L}_1(\theta) - \tilde{L}_1\left(\theta + i\Delta\varphi_{1,2} + i\frac{\pi}{2} - i\delta\right) \\
\tilde{\varepsilon}_1\left(\theta + \Delta\varphi_{1,2} + i\frac{\pi}{2} - i\delta\right) &= i|m_1|e^\theta - K_{2,1} * \tilde{L}_2\left(\theta + \Delta\varphi_{1,2} + i\frac{\pi}{2} - i\delta\right) - \tilde{L}_2(\theta) \\
\tilde{\varepsilon}_2\left(\theta + \Delta\varphi_{2,1} - i\frac{\pi}{2} + i\delta\right) &= -i|m_2|e^\theta - K_{1,2} * \tilde{L}_1\left(\theta + \Delta\varphi_{2,1} - i\frac{\pi}{2} + i\delta\right) - \tilde{L}_1(\theta) ,
\end{aligned} \tag{4.9}$$

where the limit $\delta \rightarrow 0^+$ is understood. The TBA system in Eq.4.9 is a four-equations system. However, it is possible to reduce the number of equations to three, defining a new mass $m_{12} \equiv m_1 - im_2 = |m_{12}|e^{i\varphi_{12}}$. This is consistent with the new spectrum of simple cycles after wall-crossing, which contains the cycles γ_1 , γ_2 and the new cycle $\gamma_{12} \equiv \gamma_1 + \gamma_2$. We can explicitly check the spectra of simple cycles using the Python script described in Appendix A. For definiteness, let us choose a cubic potential $V(z) \equiv -z^3 + 3z$, initially at energy $E = 0$, so that $Q(z) = V(z)$. In this situation, the three turning points a_1 , a_2 and a_3 lie on the real axis, with $a_1 = -\sqrt{3}$, $a_2 = 0$ and $a_3 = \sqrt{3}$, the first interval being a classically allowed one. This choice of parameters in the moduli space corresponds then to a special point in the minimal chamber of the system. The spectrum of simple cycles may be then found by studying the $S^1(\theta)$ -action on the quadratic differential Φ associated to $Q(z)$, as explained at the end of Sect.3.4. The sequence of WKB triangulations over a π -wide interval in θ is shown in Fig.4.2, whereas in Fig.4.3, the corresponding sequence of Stokes graphs is shown. It is clear that the only two flips are those associated with the simple cycles γ_1 at $\theta_1 = \pi/2$ and γ_2 at $\theta_2 = 0$. Hence, using the analysis in Sect.3.5, the associated quantum periods are the only ones experiencing non-trivial discontinuities in their Borel resummation across the directions θ_1 and θ_2 . Now, let us move inside the

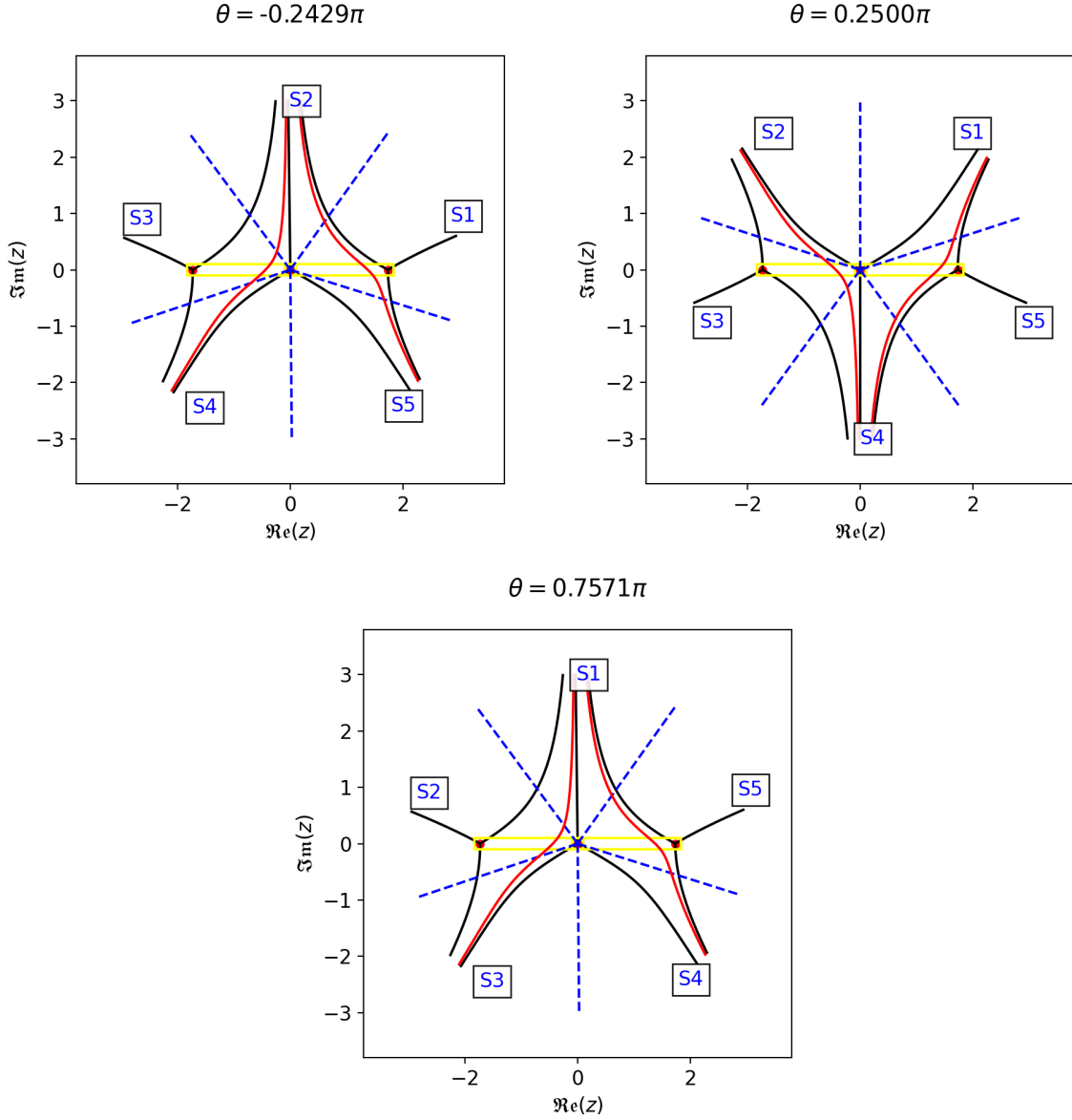
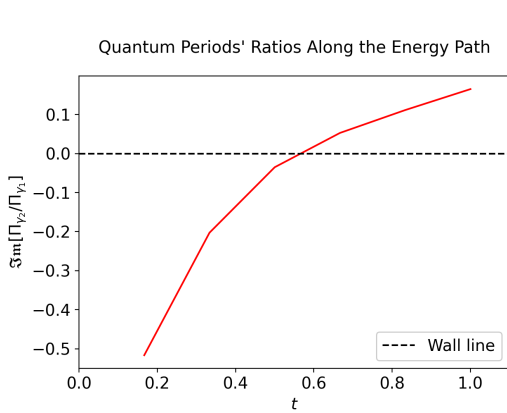
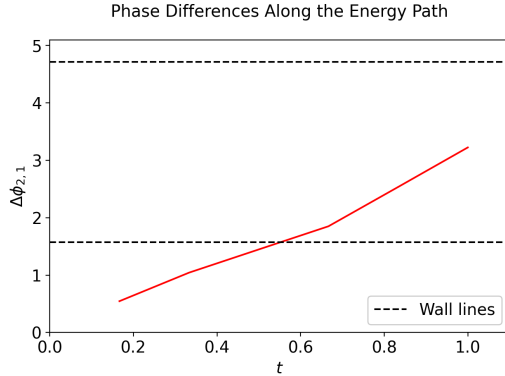


Figure 4.3: Mutations of the Stokes graphs of a cubic potential in the minimal chamber. The dashed blue lines delimit the Stokes sectors defined in Eq.A.4 and labeled with the corresponding integer number. Representatives of the class of arcs in the regular horizontal strips of the Stokes graph are shown as red lines. Finally, the yellow rectangular boxes denote the simple cycles associated to the Stokes graph. For the necessary background, see Sect.3.4, and, in particular, Procedure 3.1 and the following paragraphs.



(a) Ratio $\Im\mathfrak{m}(\Pi_{\gamma_2}^0/\Pi_{\gamma_1}^0)$ over $t \in [0, 1]$. The dashed line indicates the wall line for $\Im\mathfrak{m}(\Pi_{\gamma_2}^0/\Pi_{\gamma_1}^0) = 0$.

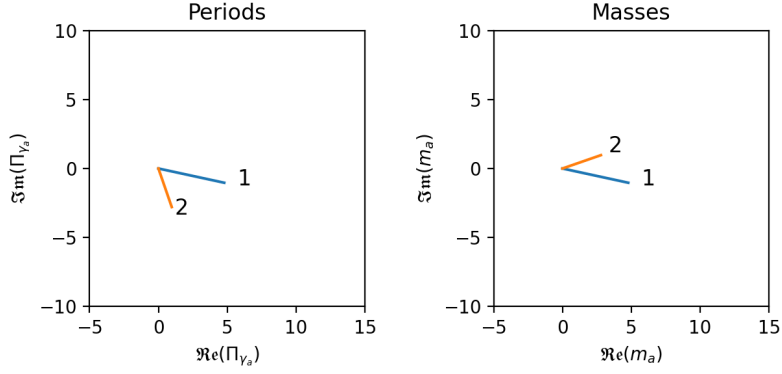


(b) Phase difference $\Delta\varphi_{2,1} = \varphi_2 - \varphi_1$ over $t \in [0, 1]$. The dashed line indicates the wall line corresponding to $\Im\mathfrak{m}(\Pi_{\gamma_2}^0/\Pi_{\gamma_1}^0) = 0$ in Fig.4.4a.

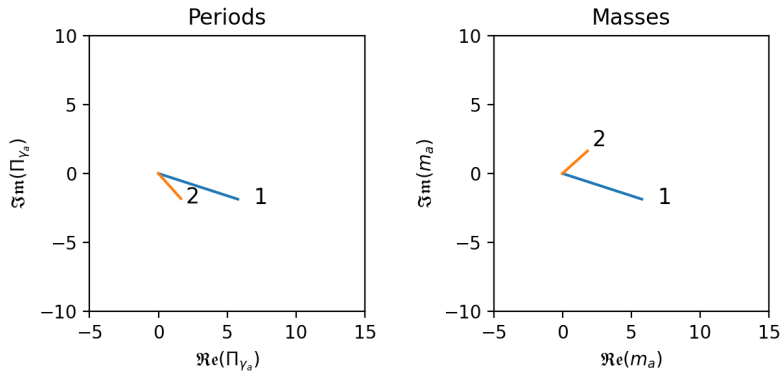
moduli space, keeping fixed the parameters of $V(z)$ and modifying the energy E . By inspecting the restriction of V to the real line, we expect that increasing the energy from 0 to any real value above 2 will result in a wall-crossing around $E = 2$. However, as pointed out in Sect.3.5, we shall avoid that point in the moduli space, since two zeros of the potential would coalesce to a single point. For this reason, let us connect the points $E_i = 0$ to $E_f = 3$ with a path E_t in the energy complex plane, parameterized as follows:

$$E_t = \{ E \in \mathbb{C} \mid E = E_i + t(E_f - E_i) + \frac{i}{10} \sin(i\pi t), t \in [0, 1] \}. \quad (4.10)$$

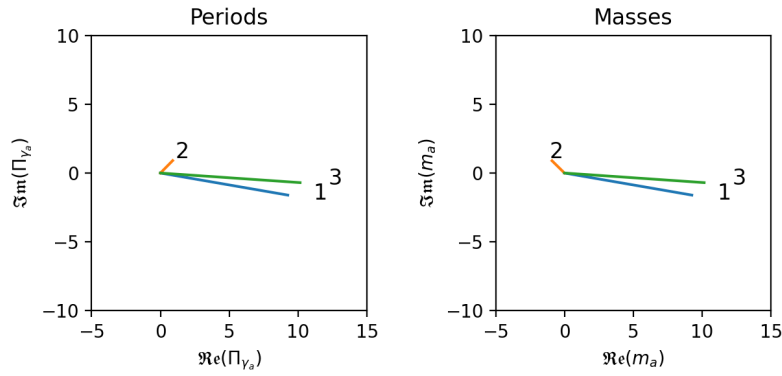
From the analysis above, at $t = 0$ the spectrum of simple cycles is given by $\{\gamma_1, \gamma_2\}$. Then, let us plot the ratio $\Im\mathfrak{m}(\Pi_{\gamma_2}^0/\Pi_{\gamma_1}^0)$ over $t \in [0, 1]$, where $\Pi_{\gamma_i}^0$, $i = 1, 2$, are the zero-order quantum periods associated to the simple cycles. The condition $\Im\mathfrak{m}(\Pi_{\gamma_2}^0/\Pi_{\gamma_1}^0) = 0$ corresponds to the alignment (or anti-alignment) of the zero-order quantum periods: using the definitions of the masses (Def.3.24), this is trivially equivalent to a wall-crossing, where $|\varphi_2 - \varphi_1| = \pi/2$. The result is shown in Fig.4.4a. In Fig.4.4b, the phase difference $\Delta\varphi_{2,1} = \varphi_2 - \varphi_1$ is shown. The presence of a zero for some $t \in [0.5, 0.667]$ in Fig.4.4a indicates the wall crossing has occurred at some energy between $E = 1.5 - i$ and $E = 2 - 0.866i$ along E_t . This is consistent with the hypothesis of a wall at $E = 2$. In principle, by mapping many curves connecting E_i to E_f , one could determine the locus of points where a wall crossing takes place: this curve is known as the curve of marginal stability (see [IMS19] and [BF96]), and it is known to go through $E = 2$, where one of the zero-order quantum periods vanishes. In addition, Fig.4.4b confirms that the wall crossing occurs with $\Delta\varphi_{2,1} < \pi/2 \rightarrow \Delta\varphi_{2,1} > \pi/2$, as assumed above during the derivation. Looking at the periods and mass rotations in Fig.4.5, we explicitly verify that this corresponds to the alignment of the zero-order quantum periods. Finally, let



(a) $E = (1 - i)/2$



(b) $E = 1 - i\sqrt{3}/2$



(c) $E = (5 - i)/2$

Figure 4.5: Zero-order quantum periods $\Pi_{\gamma_i}^0$, $i = 1, 2$, associated to the simple cycles. The sequence shows their rotation along the path E_t in the energy plane: wall crossing here occurs as the periods align, and it produces a new cycle $\gamma_{12} = \gamma_1 + \gamma_2$.

us check the spectrum of simple cycles after wall crossing, at $E = E_f$. The sequence of WKB triangulations and Stokes graphs over a π -wide interval is shown in Fig.4.6 and Fig.4.7, respectively. In this case, as expected, three flips occur, and an additional simple cycle encircling a_1 and a_3 appears in the spectrum: we shall provisionally call it γ_{new} , and we verify now that it actually coincides with the γ_{12} defined above. Indeed, by construction, the angle θ_{new} associated to the flip coincides with the phase φ_{new} of the corresponding zero-order quantum period, so that we can easily cross-check that γ_{new} does correspond to $\Pi_{\gamma_{12}}^0$; in addition, the other two zero-order quantum periods are such that $\Pi_{\gamma_{12}}^0 = \Pi_{\gamma_1}^0 + \Pi_{\gamma_2}^0$. In turn, this is equivalent to $\gamma_{12} \equiv \gamma_1 + \gamma_2$, from which the identification with γ_{12} above is verified. The passages briefly summarized here to correctly identify the new cycle γ_{12} are automatically performed by the Python code in Appendix A. The outcome had already been included in Fig.4.5, where $\Pi_{\gamma_{12}}^0$ appears after wall crossing and it coincides with $\Pi_{\gamma_1}^0 + \Pi_{\gamma_2}^0$.

The analysis above serves as a motivation to the otherwise seemingly ad-hoc procedure to get from the 4-equations TBA in Eq.4.9 to a 3-equations one. Let us now consider the steps in detail. Since the ultimate goal is to recover a TBA-like system after wall crossing, the first step is to define new pseudoenergies $\tilde{\varepsilon}_{1,2}^n$ absorbing the residues appearing on the right hand side of Eq.4.7:

$$\begin{aligned}\tilde{\varepsilon}_1^n(\theta) &= \tilde{\varepsilon}_1(\theta) + L_2 \left(\theta - i\frac{\pi}{2} - i\varphi_1 \right) \\ \tilde{\varepsilon}_2^n(\theta) &= \tilde{\varepsilon}_2(\theta) + L_1 \left(\theta + i\frac{\pi}{2} - i\varphi_2 \right) .\end{aligned}\tag{4.11}$$

Then, considering the presence of the additional simple cycle $\gamma_{12} \equiv \gamma_1 + \gamma_2$ out of the minimal chamber, we expect that the quantum periods get coupled to the new quantum period $\Pi_{\gamma_{12}}$ accordingly. This is consistent with the Delabaere-Pham formula in Eq.3.38, and it translates into the following Ansatz:

$$\begin{aligned}L_1(\theta) &= L_1^n(\theta) + L_{12}^n(\theta + i\alpha) \\ L_2(\theta) &= L_2^n(\theta) + L_{12}^n(\theta + i\beta) ,\end{aligned}\tag{4.12}$$

for some $\alpha, \beta \in \mathbb{R}$. Let us now fix α and β imposing the self-consistency between the Ansatz and the definitions of the new pseudoenergies in Eq.4.11. It is convenient to express both constraints in terms of the associated Y-functions, so that the Ansatz in Eq.4.12 reads

$$\begin{aligned}1 + Y_1(\theta) &= [1 + Y_1^n(\theta)] [1 + Y_{12}^n(\theta + i\alpha)] \\ 1 + Y_2(\theta) &= [1 + Y_2^n(\theta)] [1 + Y_{12}^n(\theta + i\beta)] ,\end{aligned}\tag{4.13}$$

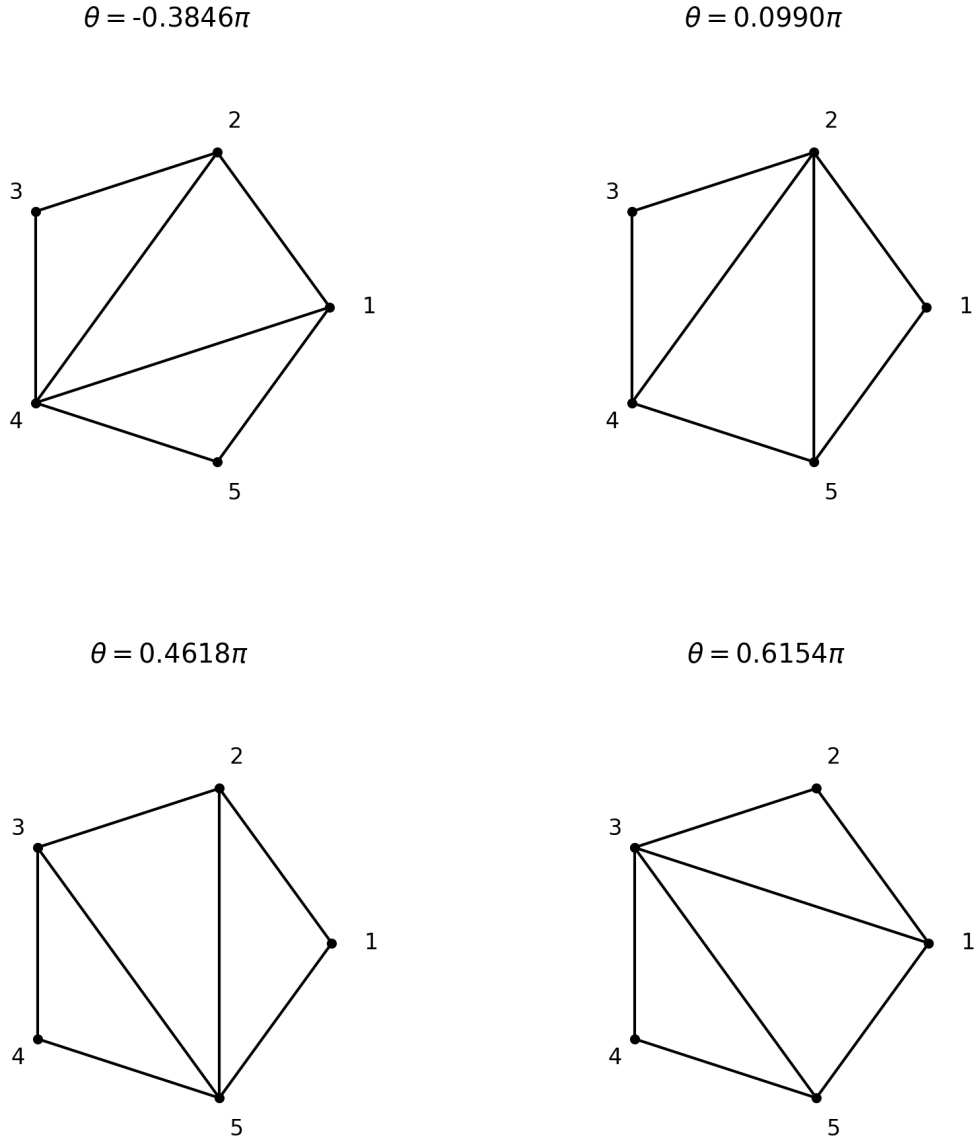


Figure 4.6: Mutations of the WKB triangulation for a cubic potential in the maximal chamber. The abstract triangulations in this figure were obtained from the analysis in Fig.4.7.

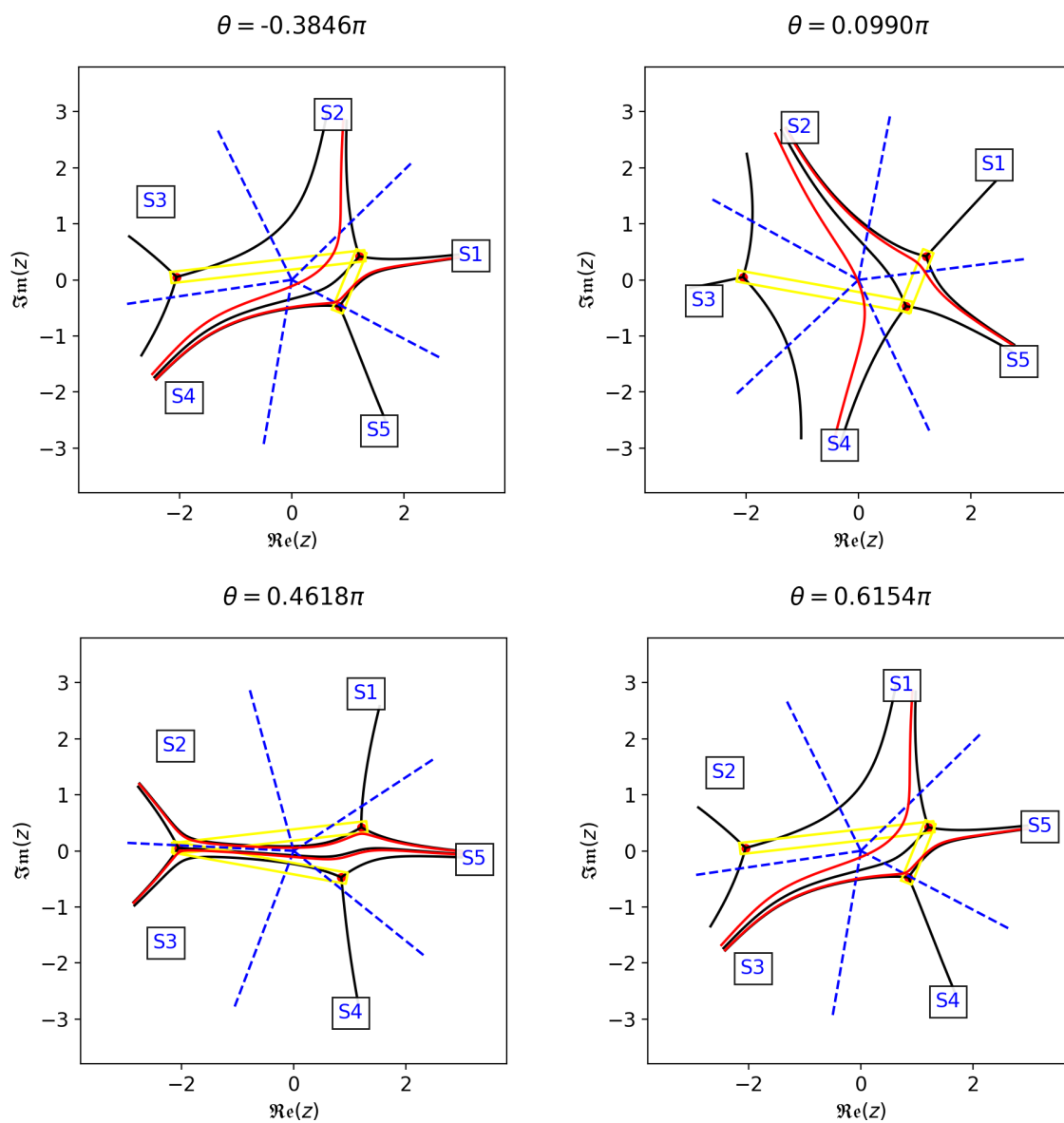


Figure 4.7: Mutations of the Stokes graphs of a cubic potential in the maximal chamber. For the content of this figure, see Fig.4.3.

and the definitions in Eq.4.11 are recast as follows:

$$\begin{aligned} Y_1^n(\theta) &= \frac{Y_1(\theta)}{1 + Y_2(\theta - i\frac{\pi}{2})} \equiv \frac{Y_1}{1 + Y_2^-} \\ Y_2^n(\theta) &= \frac{Y_2(\theta)}{1 + Y_1(\theta + i\frac{\pi}{2})} \equiv \frac{Y_2}{1 + Y_1^+} \end{aligned} \quad (4.14)$$

where the $(\cdot)^\pm$ notation has been introduced to indicate $\pm i\pi/2$ shifts in the argument of the function. Then, plugging in the definitions of the new pseudoenergies in terms of Y functions, one gets to the following consistency constraint:

$$\begin{aligned} Y_{12}^n(\theta + i\alpha) &= \frac{Y_1(\theta) Y_2^-(\theta)}{1 + Y_1(\theta) + Y_2^-(\theta)} \\ Y_{12}^n(\theta + i\beta) &= \frac{Y_1^+(\theta) Y_2(\theta)}{1 + Y_1^+(\theta) + Y_2(\theta)} \end{aligned} \quad (4.15)$$

so that $\beta - \alpha$ clearly is to be set to $\pi/2$. Finally, β and α are fixed by requiring that the classical limit associated to Y_{12}^n coincides with the correct one: in this case $m_{12} = m_1 - im_2$, so that $\beta = \pi/2$ and $\alpha = 0$. The correct values may be easily read off looking at the relative shifts between Y_1 and Y_2 on the right hand side of Eq.4.15: the reason for this will be clear in a moment, when the TBA equation for ε_{12}^n and its driving term are obtained in a single step. Either of the equations in Eq.4.15 also yields the expression of Y_{12}^n in terms of the old Y-functions:

$$Y_{12}^n = \frac{Y_1 Y_2^-}{1 + Y_1 + Y_2^-} \quad (4.16)$$

where the dependence on θ has been suppressed to lighten the notation. The definitions of the new Y-functions in Eq.4.14 and Eq.4.16 will be used in the next chapter to obtain the Y-system out of the minimal chamber. Using the definitions above, the TBA equations for $\tilde{\varepsilon}_{1,2}^n$ then read:

$$\begin{aligned} \tilde{\varepsilon}_1^n &= |m_1|e^\theta - K_{2,1} * \tilde{L}_2^n - K_{12,1}^+ * \tilde{L}_{12}^n \\ \tilde{\varepsilon}_2^n &= |m_2|e^\theta - K_{1,2} * \tilde{L}_1^n - K_{12,2} * \tilde{L}_{12}^n \end{aligned} \quad (4.17)$$

We are now ready to take the last step to find the third equation for the new mass m_{12} . To do so, let us sum the equations for $\tilde{\varepsilon}_{1,2}^n$ in Eq.4.7, with $\tilde{\varepsilon}_1$ shifted to $\theta \rightarrow \theta + i\varphi_1 - i\varphi_{12}$ and $\tilde{\varepsilon}_2$ to $\theta \rightarrow \theta + i\varphi_2 - i\varphi_{12} - i\pi/2$. The reason for the shifts may be traced back to the definition of \tilde{Y}_{12}^n in terms of the old Y-functions with the \sim -notation:

$$\tilde{Y}_{12}^n(\theta) = \frac{\tilde{Y}_1(\theta + i\varphi_1 - i\varphi_{12}) \tilde{Y}_2(\theta + i\varphi_2 - i\varphi_{12} - i\frac{\pi}{2})}{1 + \tilde{Y}_1(\theta + i\varphi_1 - i\varphi_{12}) + \tilde{Y}_2(\theta + i\varphi_2 - i\varphi_{12} - i\frac{\pi}{2})} \quad (4.18)$$

The correct shifts may be read off from the points of evaluation on the right hand side, and they are the only possible choice if one tries to match the expression of $\tilde{\varepsilon}_{12}^n$ (or, equivalently, \tilde{Y}_{12}^n) in terms of $\tilde{\varepsilon}_1$ and $\tilde{\varepsilon}_2$ (or \tilde{Y}_1 and \tilde{Y}_2). Then sum reads as follows:

$$\begin{aligned} \tilde{\varepsilon}_1(\theta + i\varphi_1 - i\varphi_{12}) + \tilde{\varepsilon}_2\left(\theta + i\varphi_2 - i\varphi_{12} - i\frac{\pi}{2}\right) &= \\ &= |m_1 - im_2|e^\theta - \int_{\mathbb{R}} \frac{d\theta'}{2\pi} \frac{\tilde{L}_1(\theta')}{\cosh(\theta - \theta' + i\Delta\varphi_{1,12} - i\frac{\pi}{2})} + \\ &\quad - \int_{\mathbb{R}} \frac{d\theta'}{2\pi} \frac{\tilde{L}_2(\theta')}{\cosh(\theta - \theta' + i\Delta\varphi_{2,12})} - L_2\left(\theta - i\varphi_{12} - i\frac{\pi}{2}\right) - L_1(\theta - i\varphi_{12}) . \end{aligned} \quad (4.19)$$

We already see here that the correct mass $m_{12} = m_1 - im_2$ has appeared, as a consequence of the correct choice of the shifts α and β above in Eq.4.15. Then, using the Ansatz in Eq.4.12, the two convolutions involving \tilde{L}_{12}^n combine and yield the following:

$$- \int_{\mathbb{R}} \frac{d\theta'}{2\pi} \left[\frac{1}{\cosh(\theta - \theta' - i\frac{\pi}{2})} + \frac{1}{\cosh(\theta - \theta' + i\frac{\pi}{2})} \right] \tilde{L}_{12}^n(\theta') = \tilde{L}_{12}^n(\theta) , \quad (4.20)$$

where the result has been obtained by combining the residues from the deformation of the integration path to avoid the pole θ_p . The integrals over $\mathbb{R} \setminus \{\theta_p\}$ vanish due to the anti-periodicity of the kernel over an interval $i\pi$. Then, plugging this result back into Eq.4.19 and bringing all the residues to the left hand side, one gets the following:

$$\begin{aligned} \tilde{\varepsilon}_1(\theta + i\varphi_1 - i\varphi_{12}) + \tilde{\varepsilon}_2\left(\theta + i\varphi_2 - i\varphi_{12} - i\frac{\pi}{2}\right) - L_{12}(\theta - i\varphi_{12}) + \\ + L_2\left(\theta - i\varphi_{12} - i\frac{\pi}{2}\right) + L_1(\theta - i\varphi_{12}) &= \\ &= |m_1 - im_2|e^\theta - \left(K_{1,12}^- * \tilde{L}_1^n\right)(\theta) - \left(K_{2,12} * \tilde{L}_2^n\right)(\theta) . \end{aligned} \quad (4.21)$$

Now, let us consider just the left hand side of the equation above. To lighten a bit the notation, let us momentarily shift $\theta \rightarrow \theta + i\varphi_{12}$. Then, simply applying Eq.4.11 and Eq.4.16, and using the relations $\varepsilon_a \equiv -\log(Y_a)$, the following identity holds:

$$\varepsilon_1(\theta) + \varepsilon_2\left(\theta - i\frac{\pi}{2}\right) - L_{12}(\theta) + L_2\left(\theta - i\frac{\pi}{2}\right) + L_1(\theta) = -\log(Y_{12}^n(\theta)) \equiv \varepsilon_{12}^n(\theta) . \quad (4.22)$$

Finally, substituting this identity back into Eq.4.21, we find the following equation for the new pseudoenergy $\tilde{\varepsilon}_{12}^n$:

$$\tilde{\varepsilon}_{12}^n(\theta) = |m_{12}|e^\theta - \left(K_{1,12}^- * \tilde{L}_1^n\right)(\theta) - \left(K_{2,12} * \tilde{L}_2^n\right)(\theta) . \quad (4.23)$$

Then, Eq.4.17 and Eq.4.23 represent the deformed TBA system after wall crossing in the direction $\Delta\varphi_{2,1} > \pi/2$.

Let us briefly comment on the derivation above, trying to make contact with the mutation in the simple cycle spectrum occurring at a wall crossing. First, it should be underlined that the Ansatz in Eq.4.12 depends on the direction of the wall crossing, which is consistent with the possible new cycles that may appear in the new chamber. Indeed, for example, if the wall crossing involves the cycles 1 and 2, then the possible new cycles would be $\gamma_1 + \gamma_2$ if $\Delta\varphi_{2,1} > \pi/2$ or $\gamma_1 - \gamma_2$ if $\Delta\varphi_{1,2} > \pi/2$. Accordingly, using the Ansatz in Eq.4.12, in the first case the new pseudoenergy ε_{12}^n is associated to a mass $m_{12} \equiv m_1 - im_2 = \Pi_{\gamma_1}^0 + \Pi_{\gamma_2}^0 = \Pi_{\gamma_1+\gamma_2}^0$, whereas in the second one to a mass $m_{12} \equiv m_1 + im_2 = \Pi_{\gamma_1}^0 - \Pi_{\gamma_2}^0 = \Pi_{\gamma_1-\gamma_2}^0$. Second, the same Ansatz also provides the correct convolution terms in Eq.4.17 and Eq.4.23. Indeed, by looking at the Stokes graphs in Fig.4.7, and recalling the general Delabaere-Pham formula in Eq.3.38, it is clear that the non-vanishing intersections between the new γ_{12} and $\gamma_{1,2}$ find a good correspondence with the interactions $1 \rightarrow \{2, 12\}$, $2 \rightarrow \{1, 12\}$ and $12 \rightarrow \{1, 2\}$ in Eq.4.17 and Eq.4.23. This comparison should serve as a justification for the deformation of the original TBA in the minimal chamber, and it should motivate its general application to tackle the problem of finding the correct TBA system for the simple cycles spectrum associated to a generic point in the moduli space.

As a final comment, let us focus on the chamber it was reached after wall crossing and on the possible directions of wall crossing. The number of equations and associated cycles in the spectrum is 3 in the new chamber, which coincides with the maximum number of simple cycles that could appear in the spectrum for a cubic potential (see Sect.3.4). Indeed, the graph of turning points and simple cycles is complete, as all pairs of turning points have an associated cycle in the spectrum encircling them. We shall then refer to such chamber as the maximal one:

Definition 4.1 *Let \mathcal{M} be the moduli space of the Schrödinger problem for a polynomial potential of degree $r + 1$. The subspace $\Omega \subset \mathcal{M}$ where the spectrum of simple cycles of the problem has the maximum number of elements $r(r + 1)/2$ is called the maximal chamber of the problem.*

Let us now take into account the two possible directions for the wall crossing involving the masses m_1 and m_2 . As mentioned above, these correspond to $\Delta\varphi_{2,1} > \pi/2$ or $\Delta\varphi_{1,2} > \pi/2$. Both these directions correspond to the same maximal chamber as defined above, yet they are associated with different TBA deformations and cycles. The reason for this discrepancy may be traced back to the polydromies introduced in the problem when deforming the parameters of the potential. Let us consider the condition for a wall crossing in Eq.3.63. This constraint defines a codimension one subspace in \mathcal{M} , whose hypersurface necessarily intersects the points in $C \subset \mathcal{M}$ where coalescence of turning points occurs. In turn, for a polynomial potential, the elements of C may be found as zeros of the discriminant Disc_z of $Q(z)$. Thus, in general, to each point in C will be associated a branch cut for the corresponding polydromy (see [GMN11]). For example,

considering the potential $V(z) = -z^3 + 3z$ above, with \mathcal{M} corresponding to the complex plane of the energy E , then

$$C \equiv \{ E \in \mathbb{C} \mid \text{Disc}_z [Q(z)] = 0 \} = \{ E \in \mathbb{C} \mid E^2 = 4 \} = \{ -2, 2 \} . \quad (4.24)$$

Thus, the monodromy around each point in C is of square root type, and this is in fact the type of monodromy associated to a single wall-crossing. From these considerations, it seems that the two possible directions of a wall crossing are associated to the different deformation paths in the moduli space around branching points in C . Once a determination in the Riemann surface is chosen, then the deformation path is uniquely fixed and the TBA description in the non-minimal chambers is determined accordingly. The alignment or anti-alignment of zero-order quantum periods may be also considered as a guiding prescription. For example, if wall crossings are all single wall crossings (i.e., the path in \mathcal{M} is such that at each wall crossing point, only two masses are involved), then asking that legitimate wall crossings produce the sum of the simple cycles involved uniquely resolves the ambiguity.

Let us now apply the same techniques described in this section to the case of a quartic potential ($r = 3$). Though a few more difficulties in the computation will arise due to the presence of intermediate chambers between the minimal one (with 3 TBA equations) and the maximal one (with 6 equations), the derivation will follow the same steps as for the cubic case.

4.2 Quartic Potential

Let us now move on to describe the case of a quartic potential. Assuming to start from a point in the minimal chamber (α -chamber), the TBA equations involve 3 pseudoenergies:

$$\tilde{\varepsilon}_1^\alpha(\theta) = |m_1|e^\theta - K_{2,1} * \tilde{L}_2^\alpha(\theta) \quad (4.25)$$

$$\tilde{\varepsilon}_2^\alpha(\theta) = |m_2|e^\theta - K_{1,2} * \tilde{L}_1^\alpha(\theta) - K_{3,2} * \tilde{L}_3^\alpha(\theta) \quad (4.26)$$

$$\tilde{\varepsilon}_3^\alpha(\theta) = |m_3|e^\theta - K_{2,3} * \tilde{L}_2^\alpha(\theta) . \quad (4.27)$$

Now, in this case, we know that the maximal chamber is associated with 6 simple cycles in the spectrum, so that the corresponding TBA system has 6 equations as well. Thus, two intermediate chambers lie between the minimal and the maximal ones. At each of the three wall crossings involved in the process, a new mass (or cycle) appears, which is a linear superposition of the masses participating to the wall crossing. As described at the end of the last section, the path to get from the minimal chamber to the maximal one is not unique. For the purpose of getting the corresponding deformation of the TBA system, it is fully specified once the sequence of oriented wall crossings is provided. In the following, we shall assume the following sequence:

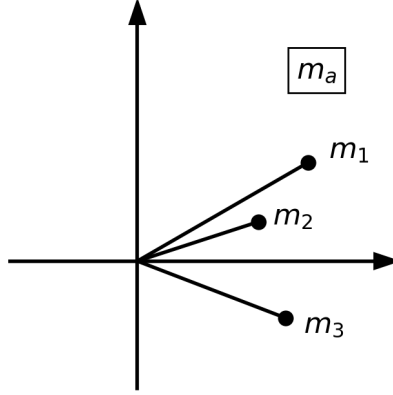


Figure 4.8: Possible diagram for the masses of a quartic potential in the minimal chamber (or α -chamber).

1. Masses 2 and 3: $\Delta\varphi_{2,3} > \frac{\pi}{2} \Rightarrow$ new mass m_{23} ;
2. Masses 1 and 2: $\Delta\varphi_{2,1} > \frac{\pi}{2} \Rightarrow$ new mass m_{12} ;
3. Masses 1 and 23: $\Delta\varphi_{23,1} > 0 \Rightarrow$ new mass m_{123} .

The sequence above is chosen so as to reproduce the final result in [IMS19], Eq.3.84. It is important to notice that this pattern corresponds to the following definitions of the new cycles and new masses:

$$\begin{array}{lll} \gamma_{23} = \gamma_2 + \gamma_3 & \gamma_{12} = \gamma_1 + \gamma_2 & \gamma_{123} = \gamma_1 + \gamma_{23} \\ m_{23} = m_3 - im_2 & m_{12} = m_1 - im_2 & m_{123} = m_1 + m_{23} \end{array}$$

so that the prescription of alignment of quantum periods is satisfied. The geometric consistency of the wall crossing sequence above may be checked step by step with diagrams representing masses as two-dimensional vectors rotating in the complex plane. As an example, a possible diagram for the masses of a quartic potential in the minimal chamber may be found in Fig.4.8. In addition, the necessity of these wall crossings is also clear by looking at the position of the poles in the kernels, as one transitions from a chamber to the next one. The steps to follow for the derivation are completely analogous to those for the cubic potential, so we will report just the essential passages. Let us start from the first wall crossing $\Delta\varphi_{2,3} > \pi/2$. A possible geometric configuration for the associated masses is shown in Fig.4.9. Then, in this case, the Ansatz in Eq.4.12 reads as follows:

$$\begin{aligned} L_2^\alpha(\theta) &= L_2^\beta(\theta) + L_{23}^\beta\left(\theta + i\frac{\pi}{2}\right) \\ L_3^\alpha(\theta) &= L_3^\beta(\theta) + L_{23}^\beta(\theta) \ , \end{aligned} \tag{4.28}$$

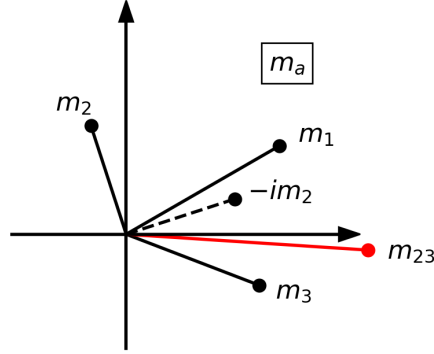


Figure 4.9: Possible diagram for the masses of a quartic potential in the β -chamber, after a wall crossing with $\Delta\varphi_{2,3} > \pi/2$.

while the definitions for the new pseudoenergies $\varepsilon_{2,3}^\beta$ may be obtained picking up the residues coming from the path deformation:

$$\begin{aligned}\varepsilon_2^\beta(\theta) &= \varepsilon_2^\alpha(\theta) + L_3^\alpha\left(\theta + i\frac{\pi}{2}\right) \\ \varepsilon_3^\beta(\theta) &= \varepsilon_3^\alpha(\theta) + L_2^\alpha\left(\theta - i\frac{\pi}{2}\right) .\end{aligned}\tag{4.29}$$

With the definitions above, the following TBA system in the β -chamber may be obtained:

$$\begin{aligned}\tilde{\varepsilon}_1^\beta &= |m_1|e^\theta - K_{2,1} * \tilde{L}_2^\beta - K_{23,1}^+ * \tilde{L}_{23}^\beta \\ \tilde{\varepsilon}_2^\beta &= |m_2|e^\theta - K_{1,2} * \tilde{L}_1^\beta - K_{23,2} * \tilde{L}_{23}^\beta - K_{3,2} * \tilde{L}_3^\beta \\ \tilde{\varepsilon}_3^\beta &= |m_3|e^\theta - K_{2,3} * \tilde{L}_2^\beta - K_{23,3}^+ * \tilde{L}_{23}^\beta \\ \tilde{\varepsilon}_{23}^\beta &= |m_{23}|e^\theta - K_{1,23}^- * \tilde{L}_1^\beta - K_{2,23} * \tilde{L}_2^\beta - K_{3,23}^- * \tilde{L}_3^\beta\end{aligned}\tag{4.30}$$

Let us underline that the definitions of the masses not involved in a wall crossing are left unchanged, since no residue has to be reabsorbed: for example, in this case, $\varepsilon_1^\beta \equiv \varepsilon_1^\alpha$, so as to keep the notation consistent throughout the chambers. Moving on to the next chamber, the Ansatz for the second wall crossing $\Delta\varphi_{2,1} > \pi/2$ reads as follows:

$$\begin{aligned}L_1^\beta(\theta) &= L_1^\gamma(\theta) + L_{12}^\gamma(\theta) \\ L_2^\beta(\theta) &= L_2^\gamma(\theta) + L_{12}^\gamma\left(\theta + i\frac{\pi}{2}\right) ,\end{aligned}\tag{4.31}$$

while the new pseudoenergies $\varepsilon_{1,2}^\beta$ are defined as follows:

$$\begin{aligned}\varepsilon_1^\beta(\theta) &= \varepsilon_1^\gamma(\theta) + L_2^\beta\left(\theta - i\frac{\pi}{2}\right) \\ \varepsilon_2^\beta(\theta) &= \varepsilon_2^\gamma(\theta) + L_1^\beta\left(\theta + i\frac{\pi}{2}\right) .\end{aligned}\tag{4.32}$$

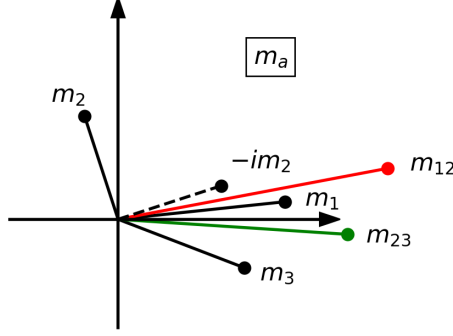


Figure 4.10: Possible diagram for the masses of a quartic potential in the γ -chamber, after a wall crossing with $\Delta\varphi_{2,1} > \pi/2$.

The mass diagram may be checked in Fig.4.10. With the definitions above, the following TBA system in the γ -chamber may be obtained:

$$\begin{aligned}
\tilde{\varepsilon}_1^\gamma &= |m_1|e^\theta - K_{2,1} * \tilde{L}_2^\gamma - K_{23,1}^+ * \tilde{L}_{23}^\gamma - K_{12,1}^+ * \tilde{L}_{12}^\gamma \\
\tilde{\varepsilon}_2^\gamma &= |m_2|e^\theta - K_{1,2} * \tilde{L}_1^\gamma - K_{12,2} * \tilde{L}_{12}^\gamma - K_{3,2} * \tilde{L}_3^\gamma - K_{23,2} * \tilde{L}_{23}^\gamma \\
\tilde{\varepsilon}_3^\gamma &= |m_3|e^\theta - K_{2,3} * \tilde{L}_2^\gamma - K_{12,3}^+ * \tilde{L}_{12}^\gamma - K_{23,3}^+ * \tilde{L}_{23}^\gamma \\
\tilde{\varepsilon}_{23}^\gamma &= |m_{23}|e^\theta - K_{1,23}^- * \tilde{L}_1^\gamma - K_{2,23} * \tilde{L}_2^\gamma - K_{3,23}^- * \tilde{L}_3^\gamma \\
\tilde{\varepsilon}_{12}^\gamma &= |m_{12}|e^\theta - K_{1,12}^- * \tilde{L}_1^\gamma - K_{2,12} * \tilde{L}_2^\gamma - K_{3,12}^- * \tilde{L}_3^\gamma,
\end{aligned} \tag{4.33}$$

where two simplifications occurred in the equations for $\tilde{\varepsilon}_{12}^\gamma$ and $\tilde{\varepsilon}_{23}^\gamma$ between the terms that couple the masses m_{12} and m_{23} , due to the antiperiodicity of the kernel over an interval $i\pi$. This is very much consistent with the cycle configuration for this chamber in Fig.4.11, from which it is clear that no intersection occurs between the cycles γ_{12} and γ_{23} . Finally, let us consider the third wall crossing shown in Fig.4.12, with $\Delta\varphi_{23,1} > 0$. As this case is associated to a different wall condition, let us see the process in detail, starting from the TBA equations in the γ -chamber. By direct inspection of the convolution products in Eq.4.33, it may be easily checked that the only terms whose poles have not yet crossed the integration path are precisely those that couple the masses m_{23} and m_1 , namely $K_{23,1}^+ * \tilde{L}_{23}^\gamma$ and $K_{1,23}^- * \tilde{L}_1^\gamma$. Indeed, for example, let us look at $K_{23,1}^+ * \tilde{L}_{23}^\gamma$:

$$K_{23,1}^+ * \tilde{L}_{23}^\gamma = \int_{\mathbb{R}} \frac{d\theta'}{2\pi} \frac{\tilde{L}_{23}^\gamma(\theta')}{\cosh(\theta - \theta' + i\Delta\varphi_{23,1} + i\frac{\pi}{2})}. \tag{4.34}$$

The poles in kernel that are the closest to the integration path are located at:

$$\theta'_p = \theta + i\Delta\varphi_{23,1} + i\frac{\pi}{2} \mp i\frac{\pi}{2}. \tag{4.35}$$

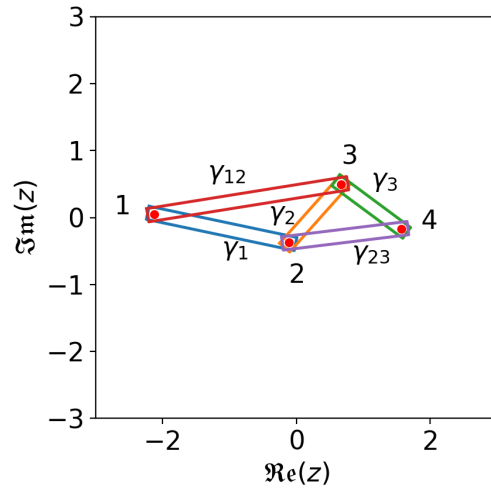


Figure 4.11: Spectrum of simple cycles in the γ -chamber.

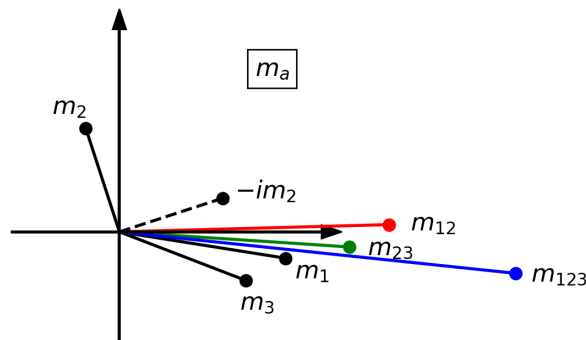


Figure 4.12: Possible diagram for the masses of a quartic potential in the δ -chamber, after a wall crossing with $\Delta\varphi_{23,1} > 0$.

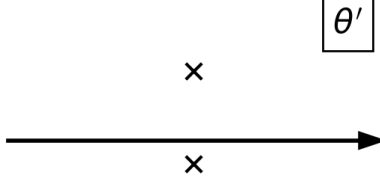


Figure 4.13: Poles configuration of $K_{23,1}^+ * \tilde{L}_{23}^\gamma$ in the γ -chamber. Here, $\Delta\varphi_{23,1} < 0$, and a wall crossing is still possible if $\Delta\varphi_{23,1}$ becomes positive.

Thus, since $\Delta\varphi_{23,1} < 0$ from Fig.4.13, it is still possible to get a wall crossing if $\Delta\varphi_{23,1}$ becomes positive. Let us now observe the following:

Observation 4.1 *From the equation for the poles, it is apparent that the reason for the different wall condition $\Delta\varphi_{23,1} > 0$ may be traced back to the presence of a $\pi/2$ shift in the kernel. In turn, this is due to m_{23} being a derived mass, with $m_{23} = m_3 - im_2$. The $-\pi/2$ rotation of m_2 in the complex plane eliminates the relative shift $\pi/2$ between the original adjacent masses m_a and m_{a+1} with respect to the zero-order quantum periods, and it is such that $m_{23} = m_3 - im_2 \equiv \Pi_{\gamma_{23}}^0$. On the other hand $m_1 \equiv \Pi_{\gamma_1}^0$. Thus, the wall crossing condition in this case directly corresponds to the condition in terms of quantum periods, i.e. alignment or anti-alignment. This observation suggests that the most natural approach when looking for wall crossings is to study the condition in terms of quantum periods first, and then possibly to translate it back in the language of masses.*

We shall go back to this observation in the next chapter. As usual, a residue is picked up and this may be easily evaluated, obtaining a contribution $-L_1^\gamma(\theta - i\varphi_{23})$. An analogous analysis for $K_{1,23}^- * \tilde{L}_1^\gamma$ produces a term $-L_{23}^\gamma(\theta - i\varphi_1)$. The new pseudoenergies in the δ -chamber are then defined by bringing the residues to the left hand side of the deformed TBA equations, and they read:

$$\begin{aligned} \varepsilon_{23}^\delta(\theta) &= \varepsilon_{23}^\gamma(\theta) + L_1^\gamma(\theta) \\ \varepsilon_1^\delta(\theta) &= \varepsilon_1^\gamma(\theta) + L_{23}^\gamma(\theta) . \end{aligned} \tag{4.36}$$

The absence of relative shifts in the new pseudoenergies definitions produces the following Ansatz

$$\begin{aligned} L_{23}^\delta(\theta) &= L_{23}^\gamma(\theta) + L_{123}^\gamma(\theta) \\ L_1^\delta(\theta) &= L_1^\gamma(\theta) + L_{123}^\gamma(\theta) , \end{aligned} \tag{4.37}$$

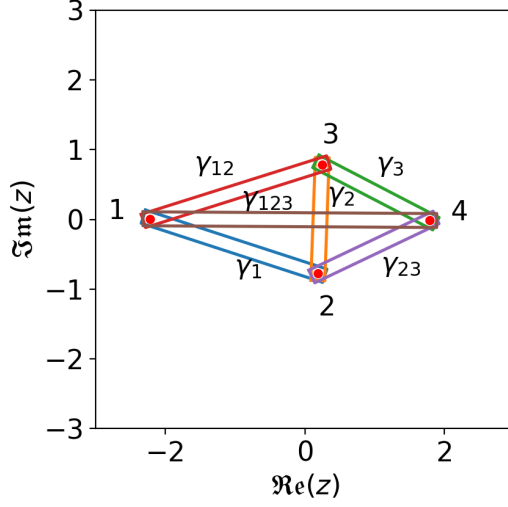


Figure 4.14: Spectrum of simple cycles in the δ -chamber. The associated graph is complete, indicating that this chamber is the maximal chamber.

so that the TBA system in the δ -chamber reads as follows:

$$\begin{aligned}
\tilde{\varepsilon}_1^\delta &= |m_1|e^\theta - K_{2,1} * \tilde{L}_2^\delta - K_{23,1}^+ * \tilde{L}_{23}^\delta - K_{12,1}^+ * \tilde{L}_{12}^\delta - K_{123,1}^+ * \tilde{L}_{123}^\delta \\
\tilde{\varepsilon}_2^\delta &= |m_2|e^\theta - K_{1,2} * \tilde{L}_1^\delta - 2K_{123,2} * \tilde{L}_{123}^\delta - K_{12,2} * \tilde{L}_{12}^\delta - K_{3,2} * \tilde{L}_3^\delta - K_{23,2} * \tilde{L}_{23}^\delta \\
\tilde{\varepsilon}_3^\delta &= |m_3|e^\theta - K_{2,3} * \tilde{L}_2^\delta - K_{12,3}^+ * \tilde{L}_{12}^\delta - K_{23,3}^+ * \tilde{L}_{23}^\delta - K_{123,3}^+ * \tilde{L}_{123}^\delta \\
\tilde{\varepsilon}_{12}^\delta &= |m_{12}|e^\theta - K_{1,12}^- * \tilde{L}_1^\delta - K_{2,12} * \tilde{L}_2^\delta - K_{3,12}^- * \tilde{L}_3^\delta - K_{123,12}^- * \tilde{L}_{123}^\delta \\
\tilde{\varepsilon}_{23}^\delta &= |m_{23}|e^\theta - K_{1,23}^- * \tilde{L}_1^\delta - K_{2,23} * \tilde{L}_2^\delta - K_{3,23}^- * \tilde{L}_3^\delta - K_{123,23}^- * \tilde{L}_{123}^\delta \\
\tilde{\varepsilon}_{123}^\delta &= |m_{123}|e^\theta - K_{1,123}^- * \tilde{L}_1^\delta - 2K_{2,123} * \tilde{L}_2^\delta - K_{23,123}^+ * \tilde{L}_{23}^\delta - K_{12,123}^+ * \tilde{L}_{12}^\delta - K_{3,123}^- * \tilde{L}_3^\delta .
\end{aligned} \tag{4.38}$$

The δ -chamber reached with the last wall crossing coincides with the maximal chamber of the system. Indeed, looking at Fig.4.14, the cycles diagram is a complete graph, and the number of cycles therein is maximum and equal to $r(r+1)/2 \equiv 6$. Thus, the full range of possible TBA deformations for a quartic potential has been covered. In analogy to the cubic case, we will present a specific example, using a suitable deformation path in the moduli space, considering the complex energy as the only free parameter in $Q(z)$. The potential is chosen as

$$V(z) = z^4 - \frac{7}{2}z^2 + 2z + \frac{1}{5}, \tag{4.39}$$

so that, for a real energy $-0.380 \leq \bar{E} \leq 0.493$, the turning points are all real and the leftmost interval between them is a classically allowed one. Hence, such point $\bar{E} \in \mathcal{M}$ is

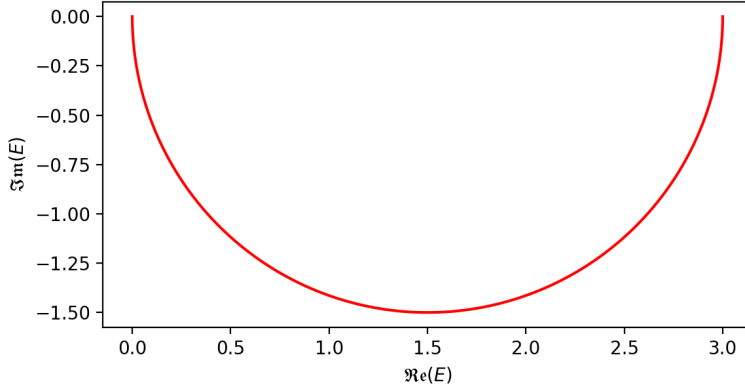
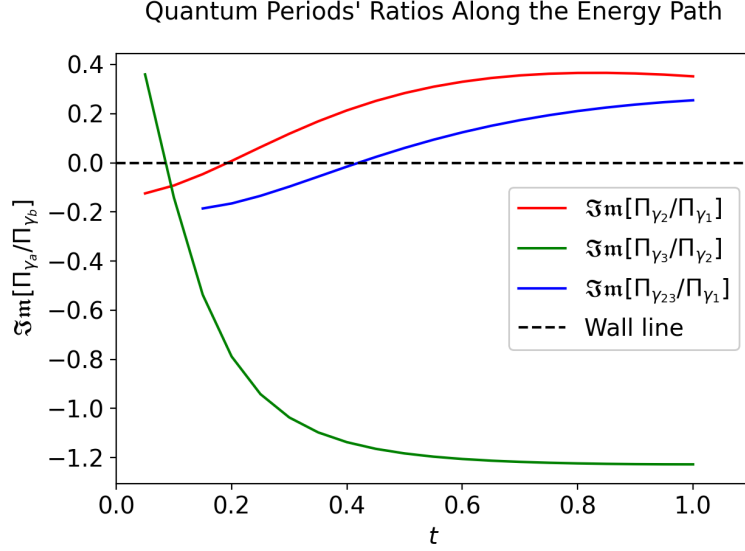


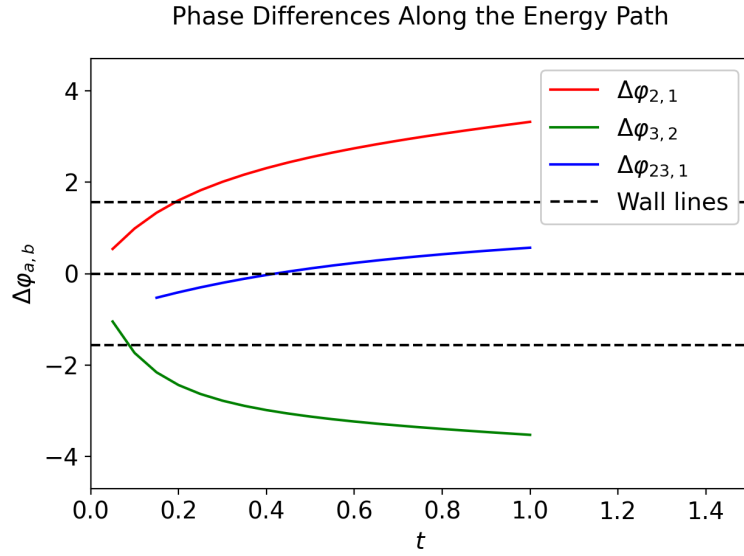
Figure 4.15: Deformation path E_t in the energy complex plane.

a special point of the minimal chamber. Let us now check the set $C \subset \mathcal{M}$ of points where turning points coalesce. For the choice of potential above, this coincides with $\{E_i\}_{i=1}^3$, where $E_1 \approx -5.638$, $E_2 \approx -0.380$ and $E_3 \approx 0.493$. The path E_t , $t \in [0, 1]$ in the complex plane is then chosen so as to avoid them, and also to guarantee single wall crossings: its shape is shown in Fig.4.15. As we can see in Fig.4.16a and Fig.4.16b, three wall crossings occur at three distinct points along the path, and the rotations of the masses and quantum periods do coincide with the behavior assumed in the deformed TBA derivation above. The changes in the spectrum of simple cycles are motivated in Fig.4.17, 4.18, 4.19, 4.20, 4.21 and 4.22, showing the mutations of the WKB triangulations and Stokes graphs in the β , γ and δ -chamber. In particular, the number of flips increases by one in each adjacent chamber, with the new saddle classes precisely corresponding with the expected new cycles. With a completely analogous analysis as for the cubic case, it is verified that the new periods emerging do satisfy the relations in terms of the old masses, as assumed at the beginning of this section. To be precise, the following relations are found to hold: $m_{23} = m_3 - im_2$, $m_{12} = m_1 - im_2$ and $m_{123} = m_1 + m_{23}$. This analysis is one of the main outputs of the code in Appendix A.

Let us now translate the analysis of this chapter in terms of Y-systems. We will see in the next chapter how these systems get deformed after wall crossings, checking whether any periodicity survives. Finally, a simplified procedure to obtain the Y-system in a given chamber is proposed, taking advantage of the Python code in Appendix A, and of the power of the exact results presented in this chapter and in the next one.



(a) Ratios $\Im\mathfrak{m}(\Pi_{\gamma_a}^0/\Pi_{\gamma_b}^0)$ over $t \in [0,1]$. The dashed line indicates the wall line for $\Im\mathfrak{m}(\Pi_{\gamma_a}^0/\Pi_{\gamma_b}^0) = 0$. The pairings considered correspond to the cycles having non-vanishing intersections with each other. The pairs (a, b) reported here are the only ones that cross the wall line.



(b) Phase differences of the masses $\Delta\varphi_{a,b} = \varphi_a - \varphi_b$ over $t \in [0,1]$. The dashed line indicates the wall line corresponding to $\Im\mathfrak{m}(\Pi_{\gamma_a}^0/\Pi_{\gamma_b}^0) = 0$ in Fig.4.16a.

Figure 4.16

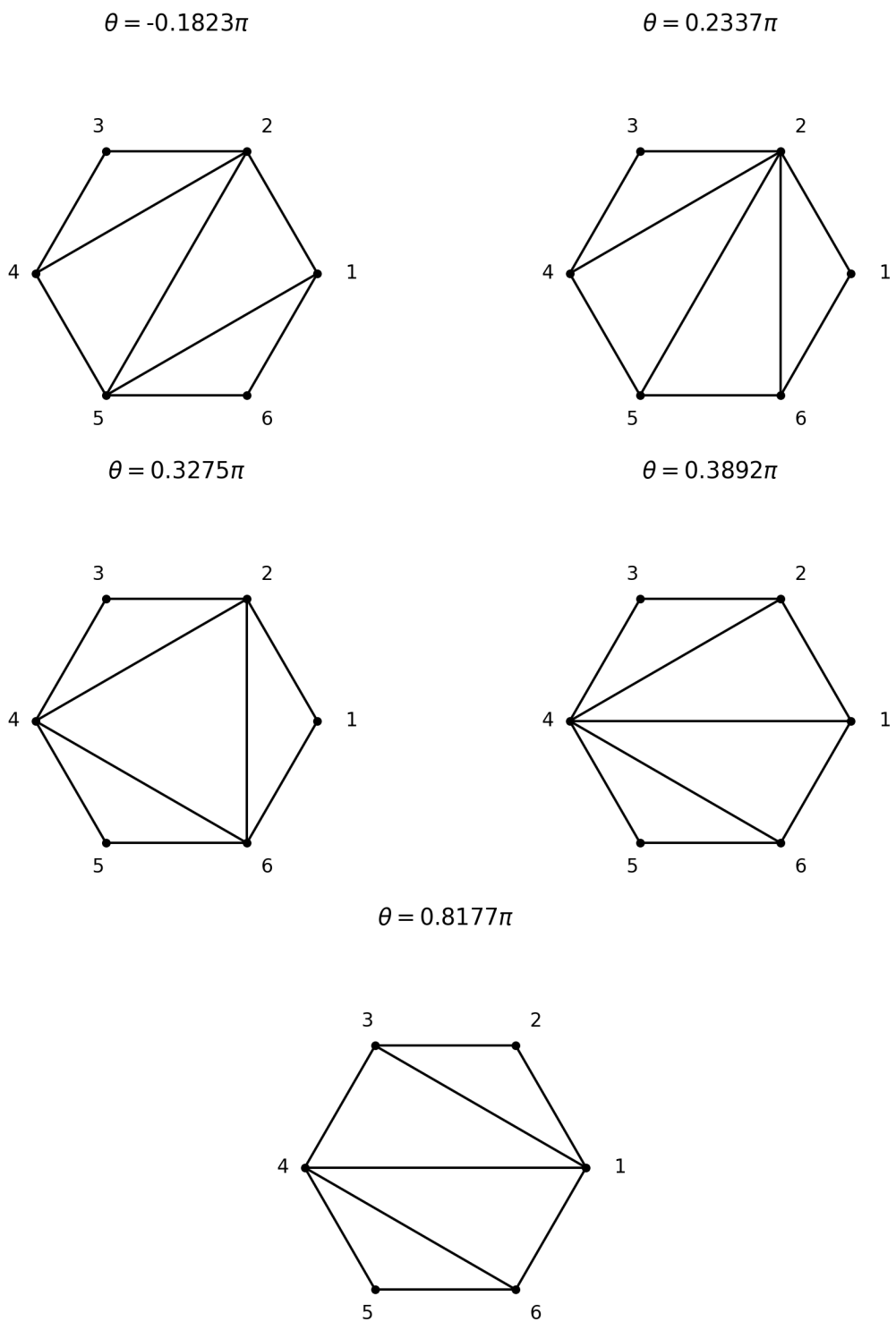


Figure 4.17: Mutations of the WKB triangulations in the β -chamber.

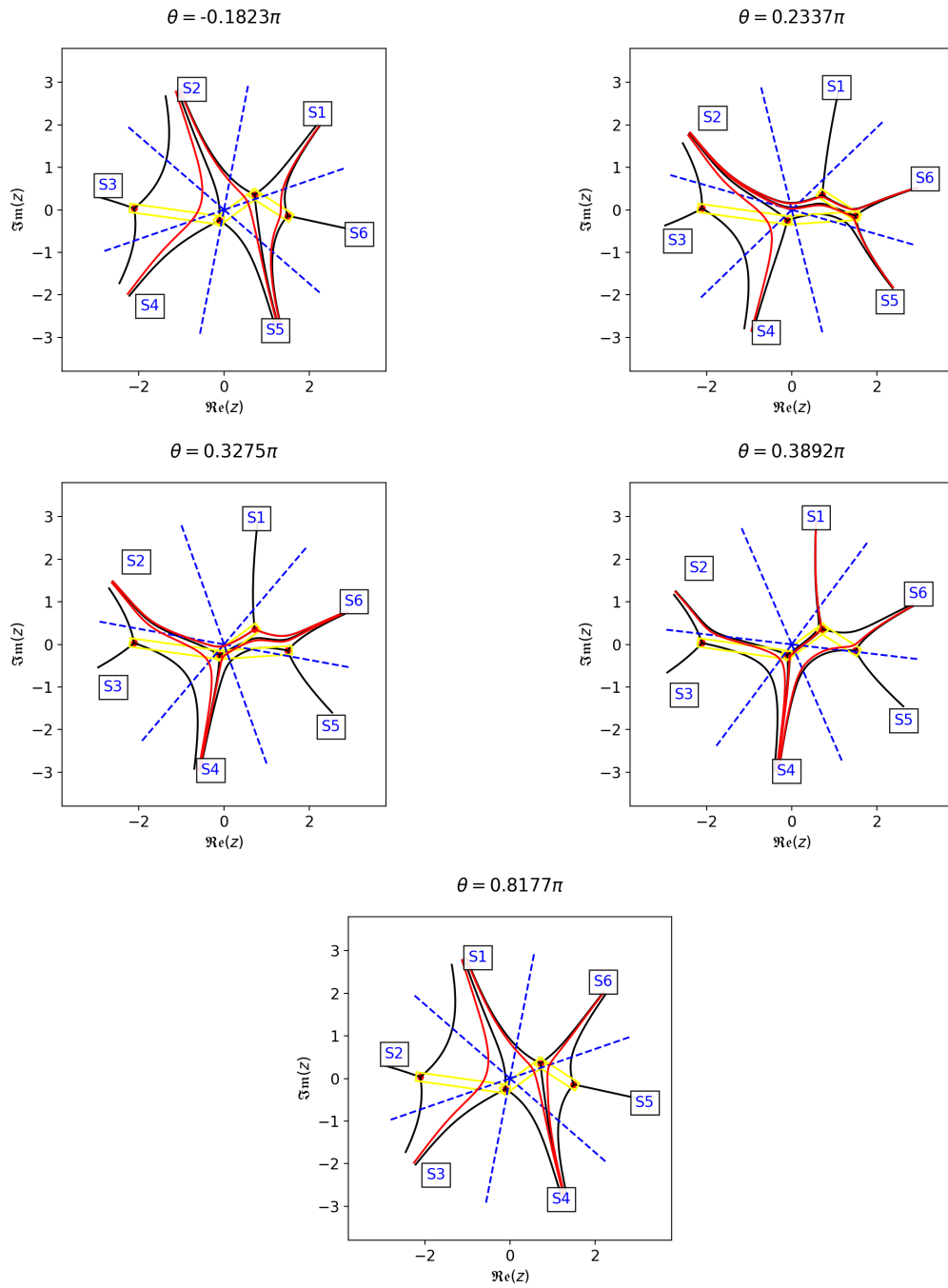


Figure 4.18: Mutations of the Stokes graphs in the β -chamber. For the content of this figure, see Fig.4.3.

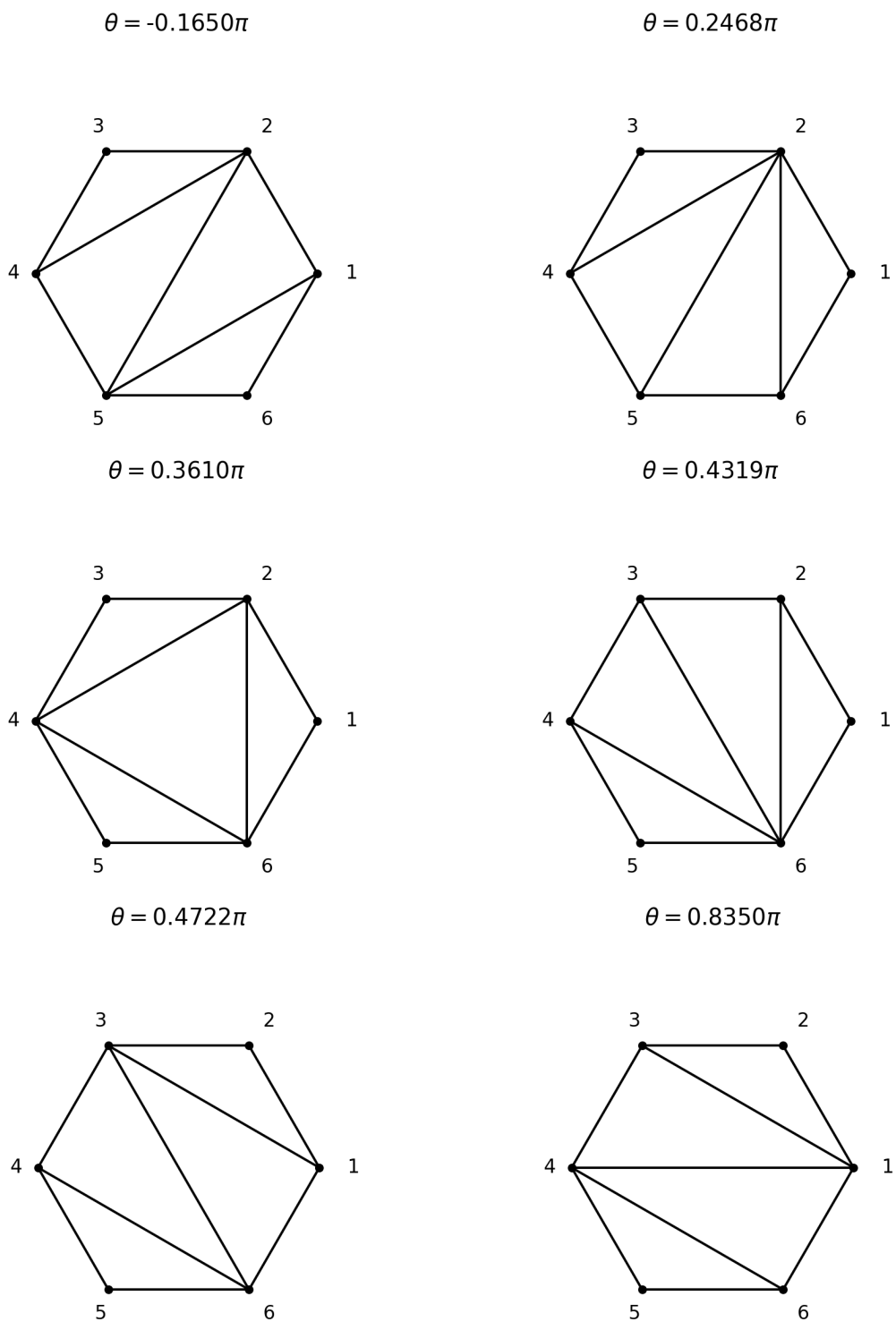


Figure 4.19: Mutations of the WKB triangulations in the γ -chamber.

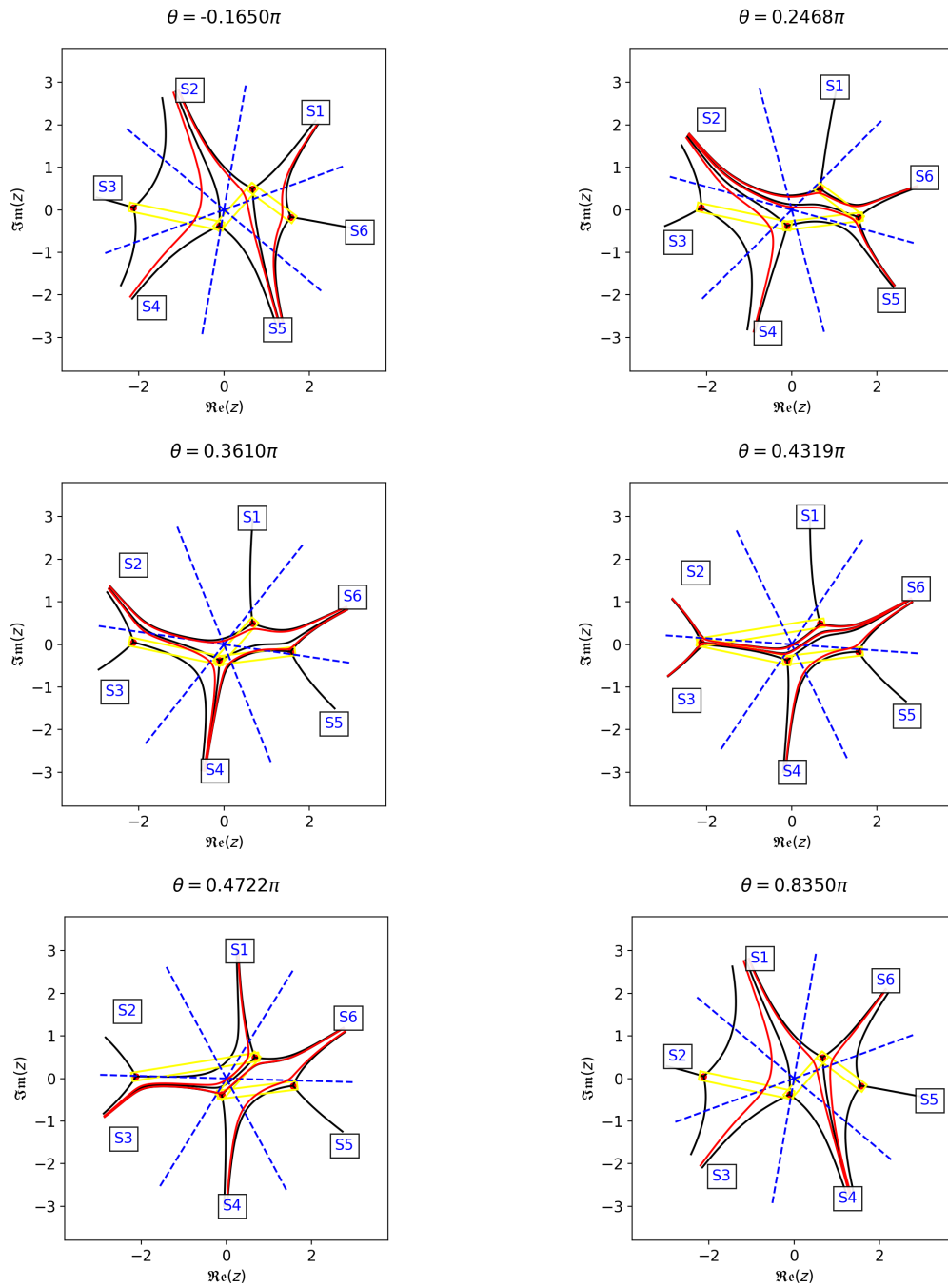


Figure 4.20: Mutations of the Stokes graphs in the γ -chamber. For the content of this figure, see Fig.4.3.

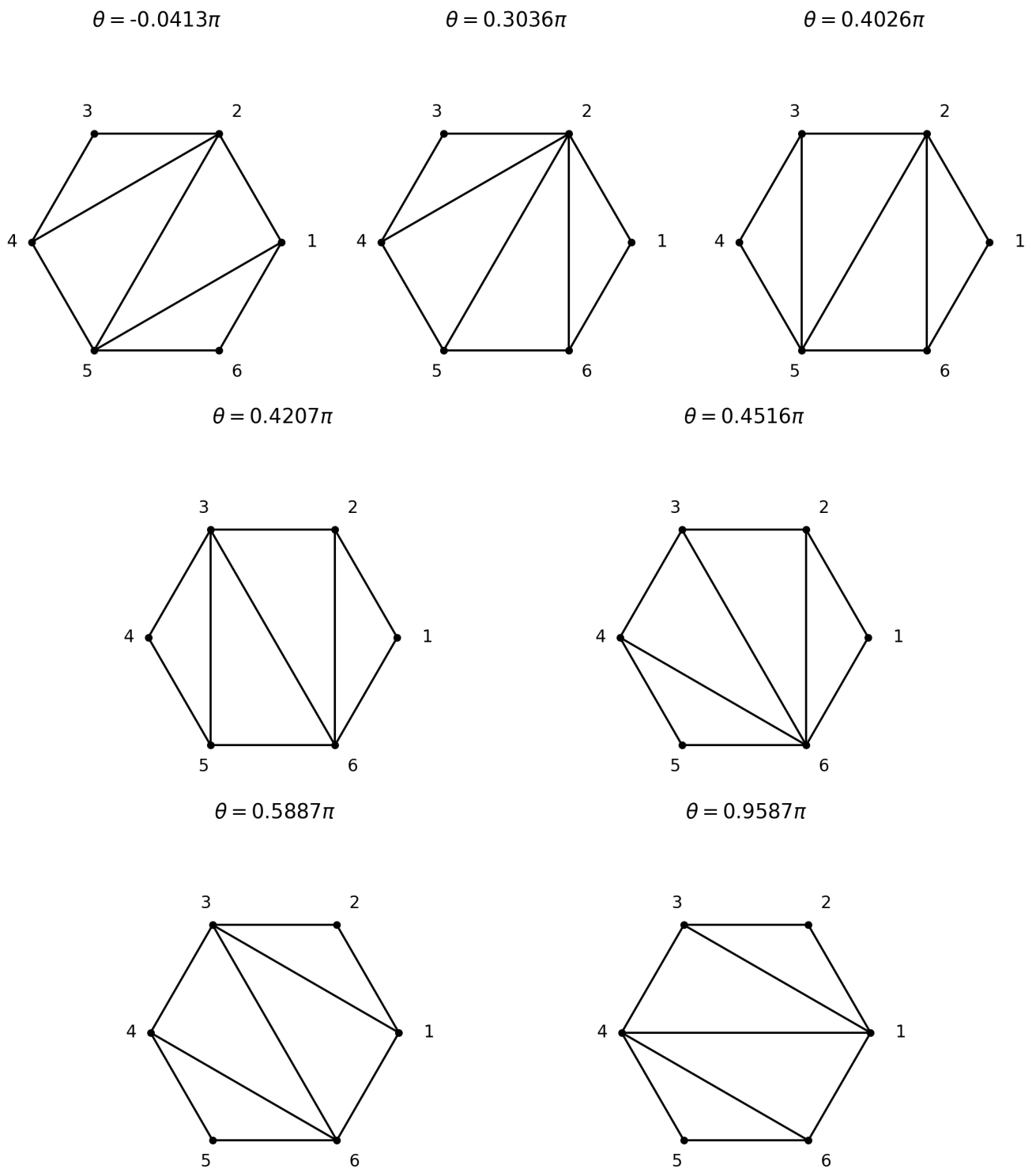


Figure 4.21: Mutations of the WKB triangulations in the δ -chamber.

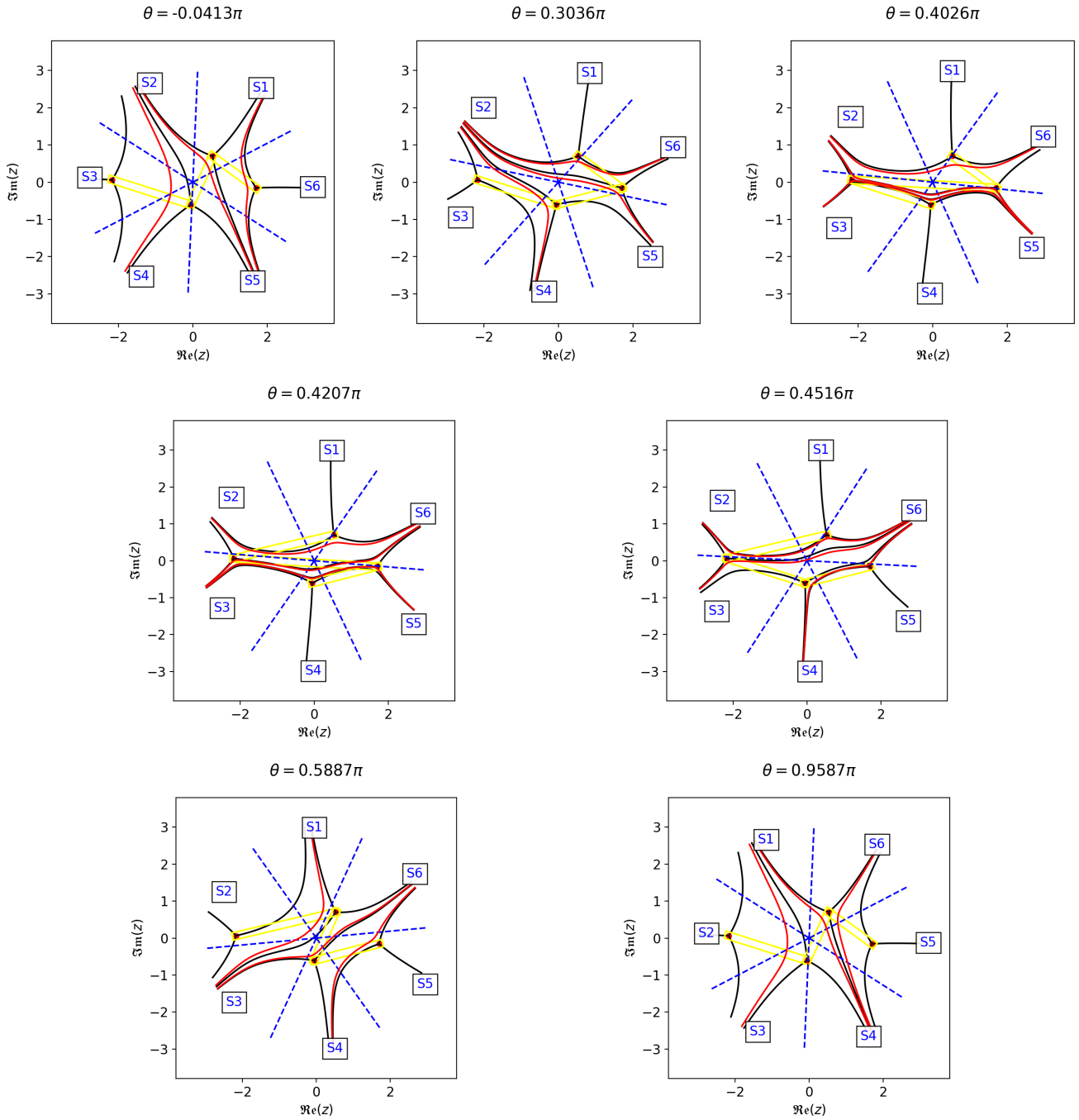


Figure 4.22: Mutations of the Stokes graphs in the δ -chamber. For the content of this figure, see Fig.4.3.

Chapter 5

Y-System Out of the Minimal Chamber

In this final chapter, the analysis of the Y-systems in non-minimal chambers described in the previous chapter is generalized to the case of a generic polynomial potential. In particular, we propose a general and simplified procedure to consistently obtain the Y-system and the TBA of a system in an arbitrary point of its moduli space. This will translate to a rather mechanical algorithm, whose only required ingredient is the sequence of wall crossings needed to transition from a special point in the minimal chamber to the required arbitrary point, avoiding coalescence points. To determine the sequence, a Python code is implemented, that is able to keep track of wall crossings, and that determines the spectra of simple cycles within each chamber. Let us start by looking at the Y-system deformation for the cubic potential in Sect.5.1: an analogous procedure will also apply to the quartic potential (see Sect.5.2). In these sections, the periodicity will be studied numerically. Finally, we will present the general procedure in Sect.5.3.

5.1 Y-System Deformation: Cubic Potential

Let us start considering the case of a cubic potential. As shown in Sect.4.1, the chambers for this system are just two, namely, the minimal and the maximal one. The Y-system in the minimal chamber is known, and it was given in Eq.3.58: let us now determine the one in the maximal chamber using two different methods. First, let us find the Y-system with the standard procedure, namely, by smoothly shifting the pseudoenergies to $\pm i\pi/2$: we will call this method the standard procedure. As an example, let us apply the procedure to $\tilde{\varepsilon}_1^n$, obeying to the deformed TBA in Eq.4.17. Its TBA equation is as follows:

$$\tilde{\varepsilon}_1^n = |m_1|e^\theta - K_{2,1} * \tilde{L}_2^n - K_{12,1}^+ * \tilde{L}_{12}^n . \quad (5.1)$$

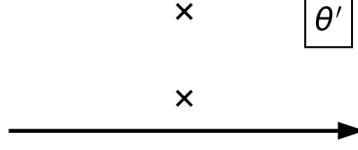


Figure 5.1: Pole configurations for the kernels $K_{2,1}$ and $K_{12,1}^+$ in Eq.5.1.

The positions of the poles in the kernels that are the closest to the integration path read

$$\begin{aligned}\theta_p^{1,2} &= \theta + i\Delta\varphi_{2,1} \mp i\frac{\pi}{2} \\ \theta_p^{12,2} &= \theta + i\Delta\varphi_{12,1} + i\frac{\pi}{2} \mp i\frac{\pi}{2},\end{aligned}\tag{5.2}$$

where $\theta_p^{1,2}$ and $\theta_p^{12,2}$ correspond to $K_{2,1}$ and $K_{12,1}^+$, respectively. Given that $\Delta\varphi_{2,1} > \pi/2$ and $\Delta\varphi_{12,1} > 0$ in that chamber, then in both cases the poles configuration is as shown in Fig.5.1. Let us then consider the sum of $\tilde{\varepsilon}_1^n$ shifted by $\pm i\pi/2$: from Fig.5.1, it is clear that no poles cross the integration path in the $+i\pi/2$ shift (the other poles below are more than $i\pi/2$ apart from the path), whereas in the $-i\pi/2$ one, both kernels have one pole each that goes through the integration path. Hence, picking up the residues with the correct signs, one gets:

$$\tilde{\varepsilon}_1^n \left(\theta + i\frac{\pi}{2} \right) + \tilde{\varepsilon}_1^n \left(\theta - i\frac{\pi}{2} \right) = \tilde{L}_2^n \left(\theta + i\Delta\varphi_{2,1} - i\pi \right) + \tilde{L}_{12}^n \left(\theta + i\Delta\varphi_{12,1} - i\frac{\pi}{2} \right), \tag{5.3}$$

which is equivalent to

$$Y_1^{n+} Y_1^{n-} = [1 + Y_2^{n--}]^{-1} [1 + Y_{12}^{n-}]^{-1}. \tag{5.4}$$

A completely analogous derivation may be carried out to find the Y-system equations also for Y_2^n and Y_{12}^n . The complete Y-system in the maximal chamber then reads as follows:

$$\begin{aligned}Y_1^{n+} Y_1^{n-} &= [1 + Y_2^{n--}]^{-1} [1 + Y_{12}^{n-}]^{-1} \\ Y_2^{n+} Y_2^{n-} &= [1 + Y_1^{n++}]^{-1} [1 + Y_{12}^{n++}]^{-1} \\ Y_{12}^{n+} Y_{12}^{n-} &= [1 + Y_1^{n+}]^{-1} [1 + Y_2^{n--}]^{-1}.\end{aligned}\tag{5.5}$$

It is crucial now to study the periodicity properties of the Y-system in the maximal chamber. To do so, we use a numerical approach, converting the Y-system in Eq.5.5 into

the following coupled sequences by recursion:

$$\begin{aligned}
a_{n+1}a_{n-1} &= [1 + b_{n-2}]^{-1} [1 + c_{n-1}]^{-1} \\
b_{n+1}b_{n-1} &= [1 + a_{n+2}]^{-1} [1 + c_{n+2}]^{-1} \\
c_{n+1}c_{n-1} &= [1 + a_{n+1}]^{-1} [1 + b_{n-2}]^{-1} ,
\end{aligned} \tag{5.6}$$

where $n \in \mathbb{N}$. If they exist finite, the periodicities of a_n , b_n and c_n are defined as usual as the smallest numbers $N_a, N_b, N_c \in \mathbb{N}$ such that $a_{n+N_a} \equiv a_n$, $b_{n+N_b} \equiv b_n$ and $c_{n+N_c} \equiv c_n$ for any $n \in \mathbb{N}$. Considering arbitrary starting points, the Y-system in Eq.5.5 is found to be non-periodic. Let us now consider a different approach to the derivation of Eq.5.5. This procedure seems to be much more straightforward, since it is just algebraic: hence, we will refer to it as to the algebraic method. It takes advantage of the known Y-system in the previous chamber (the minimal one, in this case), using the definitions of the new Y-functions in terms of the old ones, and the Ansatz in Eq.4.12. The Y-system is then computed simply by multiplying a given new Y-function evaluated at $\pm i\pi/2$, and then using the expressions in terms of the old Y-function and the old Y-system relations. As an example, let us show the passages for the Y_{12}^n functional relation:

$$\begin{aligned}
Y_{12}^{n+} Y_{12}^{n-} &= \frac{Y_1^+ Y_2}{1 + Y_1^+ + Y_2} \frac{Y_1^- Y_2^{--}}{1 + Y_1^- + Y_2^{--}} = \frac{(1 + Y_2) (1 + Y_1^-)}{(1 + Y_1^+ + Y_2) (1 + Y_1^- + Y_2^{--})} = \\
&= [1 + Y_1^{n+}]^{-1} [1 + Y_2^{n--}]^{-1} ,
\end{aligned} \tag{5.7}$$

where, in the first step Eq.4.14 was used, in the second one the Y-system in Eq.3.58, and in the third one again Eq.4.14. Finally, let us also mention that the non-derived Y-functions (i.e., those associated with masses 1 and 2) in the maximal chamber may be easily expressed in terms of their original counterpart in the minimal chamber:

$$\begin{aligned}
Y_1^n &= [Y_1^{--}]^{-1} \\
Y_2^n &= [Y_2^{++}]^{-1} ,
\end{aligned} \tag{5.8}$$

where the Y-system in Eq.3.58 was used. No analogous relation seems to hold for the derived mass 12.

Let us conclude this section introducing a procedure to directly obtain a TBA system from its associated Y-system, assuming the masses (or the zero modes) and the wall crossing's past history are known. The rules may be derived by following in reverse the traditional derivation of a Y-system out of its TBA system, and they may be stated as follows:

Procedure 5.1 *Let λ be a generic chamber in the moduli space \mathcal{M} , where a Y-system $Y_b^{\lambda+} Y_b^{\lambda-} = F_b(Y_1^\lambda, \dots, Y_n^\lambda)$ is known, for some functionals F_b where imaginary shifts in*

the arguments are possible, and $b = 1, \dots, n$. Let the classical limit of $-\log Y_b^\lambda$ be some $m_b \in \mathbb{C}$ for $b = 1, \dots, n$. In addition, the wall crossing sequence from the minimal chamber to the λ -chamber is assumed to be known. Then, a TBA equation for a pseudoenergy $\tilde{\varepsilon}_b^\lambda(\theta)$ may be associated in the following way.

1. The driving term is given by $|m_b|e^\theta$.
2. For each term $(1 + Y_a^{\lambda, \pm k})^{\pm m}$ ($k, m \in \mathbb{N}$)¹ in $F_b(Y_1^\lambda, \dots, Y_n^\lambda)$, a corresponding convolution term appears in the TBA equation:
 - (a) if the term $(1 + Y_a^{\lambda, \pm k})^{\pm m}$ is in the form $(1 + Y_a^{\lambda, \pm k})^{+m}$, then the convolution term is $mK_{a,b}^{\pm k} * \tilde{L}_a^\lambda$. This situation corresponds to the case in which the poles in the kernel $K_{a,b}^{\pm k}$ have not crossed the integration path;
 - (b) if the term $(1 + Y_a^{\lambda, \pm k})^{\pm m}$ is in the form $(1 + Y_a^{\lambda, \pm k})^{-m}$, then the convolution term is $m \left(K_{a,b}^{\pm k} * \tilde{L}_a^\lambda \right) (\theta \pm i\pi)$, where \pm in $\theta \pm i\pi$ is chosen so that the resulting shift in the kernel $K_{a,b}$ is either 0, $\pm i\pi/2$. This situation corresponds to the case in which poles have already crossed the integration path.

Despite the appearances, the procedure described above is very convenient to derive the deformed TBA system, in particular to guess the TBA equation associated to the new mass arising after a wall crossing. In addition, it turns out to be crucial when trying to adopt a Y-system-oriented perspective on the derivation of TBA deformations, as it will be clear in Sect.5.3.

5.2 Y-System Deformation: Quartic Potential

Let us now apply the same procedure to the quartic potential, so as to derive the Y-systems in the intermediate and in the maximal chambers. Since the definitions of the Y-functions in each chamber and the Ansatzes for the new masses arising are known, it is much more convenient to follow the algebraic method. Let us start from the β -chamber, defining the Y-functions in the chamber as follows:

$$Y_2^\beta \equiv \frac{Y_2^\alpha}{1 + Y_3^{\alpha+}}, \quad Y_3^\beta \equiv \frac{Y_3^\alpha}{1 + Y_2^{\alpha-}}, \quad Y_{23}^\beta \equiv \frac{Y_3^\alpha Y_2^{\alpha-}}{1 + Y_3^\alpha + Y_2^{\alpha-}}. \quad (5.9)$$

¹Here, $\pm k$ is a shorthand for $\pm \pm \dots \pm$, k -times. The \pm signs in front of k and m are completely independent.

Then, the β -chamber Y-system reads:

$$\begin{aligned}
Y_1^{\beta+} Y_1^{\beta-} &= [1 + Y_2^\beta] [1 + Y_{23}^{\beta+}] \\
Y_2^{\beta+} Y_2^{\beta-} &= [1 + Y_3^{\beta++}]^{-1} [1 + Y_{23}^{\beta++}]^{-1} [1 + Y_1^\beta] \\
Y_3^{\beta+} Y_3^{\beta-} &= [1 + Y_2^{\beta--}]^{-1} [1 + Y_{23}^{\beta-}]^{-1} \\
Y_{23}^{\beta+} Y_{23}^{\beta-} &= [1 + Y_3^{\beta+}]^{-1} [1 + Y_2^{\beta--}]^{-1} [1 + Y_1^{\beta-}] .
\end{aligned} \tag{5.10}$$

In the γ -chamber, the Y-functions are defined as

$$Y_1^\gamma \equiv \frac{Y_1^\beta}{1 + Y_2^{\beta-}} , \quad Y_2^\gamma \equiv \frac{Y_2^\beta}{1 + Y_1^{\beta+}} , \quad Y_{12}^\gamma \equiv \frac{Y_1^\beta Y_2^{\beta-}}{1 + Y_1^\beta + Y_2^{\beta-}} , \tag{5.11}$$

so that the Y-system reads:

$$\begin{aligned}
Y_1^{\gamma+} Y_1^{\gamma-} &= [1 + Y_{23}^{\gamma+}] [1 + Y_2^{\gamma--}]^{-1} [1 + Y_{12}^{\gamma-}]^{-1} \\
Y_2^{\gamma+} Y_2^{\gamma-} &= [1 + Y_3^{\gamma++}]^{-1} [1 + Y_{23}^{\gamma++}]^{-1} [1 + Y_1^{\gamma++}]^{-1} [1 + Y_{12}^{\gamma++}]^{-1} \\
Y_3^{\gamma+} Y_3^{\gamma-} &= [1 + Y_2^{\gamma--}]^{-1} [1 + Y_{12}^{\gamma-}]^{-1} [1 + Y_{23}^{\gamma-}]^{-1} \\
Y_{23}^{\gamma+} Y_{23}^{\gamma-} &= [1 + Y_3^{\gamma+}]^{-1} [1 + Y_2^{\gamma--}]^{-1} [1 + Y_1^{\gamma-}] \\
Y_{12}^{\gamma+} Y_{12}^{\gamma-} &= [1 + Y_3^{\gamma+}]^{-1} [1 + Y_2^{\gamma--}]^{-1} [1 + Y_1^{\gamma+}]^{-1} .
\end{aligned} \tag{5.12}$$

Finally, in the δ -chamber, the Y-functions are introduced as

$$Y_1^\delta \equiv \frac{Y_1^\gamma}{1 + Y_{23}^\gamma} , \quad Y_{23}^\delta \equiv \frac{Y_{23}^\gamma}{1 + Y_1^\gamma} , \quad Y_{123}^\delta \equiv \frac{Y_1^\gamma Y_{23}^\gamma}{1 + Y_1^\gamma + Y_{23}^\gamma} , \tag{5.13}$$

so that the Y-system reads:

$$\begin{aligned}
Y_1^{\delta+} Y_1^{\delta-} &= [1 + Y_2^{\delta--}]^{-1} [1 + Y_{23}^{\delta-}]^{-1} [1 + Y_{12}^{\delta-}]^{-1} [1 + Y_{123}^{\delta-}]^{-1} \\
Y_2^{\delta+} Y_2^{\delta-} &= [1 + Y_1^{\delta++}]^{-1} [1 + Y_{23}^{\delta++}]^{-1} [1 + Y_{12}^{\delta++}]^{-1} [1 + Y_3^{\delta++}] [1 + Y_{123}^{\delta++}]^{-2} \\
Y_3^{\delta+} Y_3^{\delta-} &= [1 + Y_2^{\delta--}]^{-1} [1 + Y_{23}^{\delta-}]^{-1} [1 + Y_{12}^{\delta-}]^{-1} [1 + Y_{123}^{\delta-}]^{-1} \\
Y_{12}^{\delta+} Y_{12}^{\delta-} &= [1 + Y_1^{\delta+}]^{-1} [1 + Y_2^{\delta--}]^{-1} [1 + Y_3^{\delta+}]^{-1} [1 + Y_{123}^{\delta+}]^{-1} \\
Y_{23}^{\delta+} Y_{23}^{\delta-} &= [1 + Y_1^{\delta+}]^{-1} [1 + Y_2^{\delta--}]^{-1} [1 + Y_3^{\delta+}]^{-1} [1 + Y_{123}^{\delta+}]^{-1} \\
Y_{123}^{\delta+} Y_{123}^{\delta-} &= [1 + Y_2^{\delta--}]^{-2} [1 + Y_{23}^{\delta-}]^{-1} [1 + Y_1^{\delta+}]^{-1} [1 + Y_3^{\delta+}]^{-1} [1 + Y_{12}^{\delta-}]^{-1} .
\end{aligned} \tag{5.14}$$

Analogously to the cubic case, the non-derived Y-functions (i.e., those for the masses 1, 2 and 3) in the maximal chamber may be expressed in terms of their original counterpart

in the minimal chamber:

$$\begin{aligned} Y_1^\delta &= [Y_1^{\alpha--}]^{-1} \\ Y_2^\delta &= [Y_2^{\alpha++}]^{-1} \\ Y_3^\delta &= [Y_3^{\alpha--}]^{-1} , \end{aligned} \tag{5.15}$$

so that the pattern for a generic non-derived mass m_a looks as follows:

$$Y_a^{max} = [Y_a^{min\pm\pm}]^{-1} . \tag{5.16}$$

Let us conclude this section checking the periodicity properties of the Y-systems in Eq.5.10, 5.12 and 5.14. Converting them into systems of sequences by recursion like in Eq.5.6, it is possible to look for finite periodicities numerically. The problem was tackled with a Python code, and the result is that no finite periodicity is found in the Y-systems out of the minimal chamber. This is consistent with the analogous behavior of the Y-system in the maximal chamber for a cubic potential.

5.3 General Procedure

Let us now generalize the methods described above to the case of a generic polynomial potential, so as to devise a general procedure based on wall-crossings and Y-systems to efficiently find the deformed Y-systems and TBAs. Let Q be built out of a generic polynomial potential in the complex coordinate z and of a complex energy E . Let us take the moduli space \mathcal{M} as to coincide with the complex plane of the energy, considering then the parameters of the potential to be fixed. This is physically reasonable, since the main objective is to find the Voros spectrum for a given potential: hence, the TBA deformation should occur along a path in the energy complex plane for the same potential. Let us further assume that the parameters of the potential are such that there exists some real value of the energy \bar{E} where the system lies in a special point $p_{\bar{E}} \in \mathcal{M}$ of the minimal chamber. This passage should not constitute a too sharp restriction, since one may first deform the potential parameters to meet this condition, while requiring to remain in the same chamber of the moduli space. The only condition it should be checked in this case is that the spectrum of simple cycles in the two points remains the same. Finally, let γ_E be a path in the energy moduli space, which connects $p_{\bar{E}}$ to a generic point $p_E \in \mathcal{M}$, avoiding the points in $C \subset \mathcal{M}$ where coalescence occurs. We shall restrict its shape so that only single wall crossings are involved. Then, the following procedure may be introduced.

Procedure 5.2 *Let us assume the hypothesis above. Then, the analysis of the WKB triangulation mutations provides the spectrum of simple cycles at each point on γ_E . Thus, the sequence of wall crossings $\{W_{a_i, b_i}\}_{i=1}^n$ is uniquely fixed. Labelling the chambers with $\alpha, \alpha_1, \dots, \alpha_n$, where α is the minimal chamber, W_{a_i, b_i} denotes the i -th wall crossing that*

involves the masses m_{a_i} and m_{b_i} , both appearing in the mass (or cycles) spectrum of the chamber α_i . With this notation, the Y -system in the α_i chamber may be iteratively obtained by computing the $i - 1$ previous ones. In particular, the i -th step from α_{i-1} to α_i through W_{a_i, b_i} reads as follows:

1. Considering the wall crossing W_{a_i, b_i} , we may distinguish two possible wall crossing conditions in terms of the phases φ_{a_i} and φ_{b_i} of the masses m_{a_i} and m_{b_i} :

(a) $\Delta\varphi_{b_i, a_i} > \pi/2$. Then, define the Y -functions in the α_i chamber as follows²:

$$Y_{b_i}^{(\alpha_i)} \equiv \frac{Y_{b_i}^{(\alpha_{i-1})}}{1 + Y_{a_i}^{(\alpha_{i-1})+}}, \quad Y_{a_i}^{(\alpha_i)} \equiv \frac{Y_{a_i}^{(\alpha_{i-1})}}{1 + Y_{b_i}^{(\alpha_{i-1})-}}, \quad Y_c^{(\alpha_i)} \equiv Y_c^{(\alpha_{i-1})}, \quad (5.17)$$

where c stands for any mass in the spectrum of α_{i-1} other than m_{a_i} and m_{b_i} . The Y -function for the new arising mass $m_{a_i b_i}$ is defined as

$$Y_{a_i b_i}^{(\alpha_i)}(\theta + i\omega) \equiv \frac{Y_{a_i}^{(\alpha_{i-1})} Y_{b_i}^{(\alpha_{i-1})-}}{1 + Y_{a_i}^{(\alpha_{i-1})} + Y_{b_i}^{(\alpha_{i-1})-}}, \quad (5.18)$$

where $\omega \in \mathbb{R}$ is chosen so that the classical limit of $-\log\left(Y_{a_i b_i}^{(\alpha_i)}\right)$ coincides with $m_{a_i b_i}$ coming from the WKB triangulation analysis. For example, if $m_{a_i b_i} \equiv m_{a_i} - im_{b_i}$, then $\omega \equiv 0$.

- (b) $\Delta\varphi_{b_i, a_i} > 0$. Then, define the Y -functions in the α_i chamber as follows:

$$Y_{b_i}^{(\alpha_i)} \equiv \frac{Y_{b_i}^{(\alpha_{i-1})}}{1 + Y_{a_i}^{(\alpha_{i-1})}}, \quad Y_{a_i}^{(\alpha_i)} \equiv \frac{Y_{a_i}^{(\alpha_{i-1})}}{1 + Y_{b_i}^{(\alpha_{i-1})}}, \quad Y_c^{(\alpha_i)} \equiv Y_c^{(\alpha_{i-1})}, \quad (5.19)$$

where c stands for any mass in the spectrum of α_{i-1} other than m_{a_i} and m_{b_i} . The Y -function for the new arising mass $m_{a_i b_i}$ is defined as

$$Y_{a_i b_i}^{(\alpha_i)} \equiv \frac{Y_{a_i}^{(\alpha_{i-1})} Y_{b_i}^{(\alpha_{i-1})}}{1 + Y_{a_i}^{(\alpha_{i-1})} + Y_{b_i}^{(\alpha_{i-1})}}. \quad (5.20)$$

2. With the definitions of the Y -functions in the α_i -chamber in terms of those in the α_{i-1} -chamber, and using the known Y -system in the α_{i-1} -chamber, the Y -system in the α_i -chamber is found with the algebraic method described in Sect.5.1.
3. The associated TBA system may be then directly obtained using the Procedure 5.1.

²If not explicitly specified, in the following, the Y -functions are intended to be evaluated at some θ .

The procedure above is general enough so as to cover most of the parameters and energy values in Q . If one momentarily extends the moduli space \mathcal{M} to include also the parameters in the potential, then the points in \mathcal{M} that cannot be reached are those corresponding to coalescing turning points. The reasons for this were anticipated at the end of Sect.3.5, and now we may summarize them as follows. Avoiding coalescence is necessary to keep the simple cycle deformation smooth and ruled by a canonical isomorphism. On the other hand, at coalescence points, no such isomorphism is available, and the labelling of cycles is singular. In turn, this prevents us from obtaining a well defined prescription for a deformation of either the Y-system or the TBA equations.

Conclusions and Outlook

In the present thesis we proposed an iterative, Y-system-based procedure to obtain the correct TBA governing the resummed quantum periods in an (almost) arbitrary point of its moduli space (see Procedure 5.3 in Sect.5.3). The analysis so far is limited to a quantum system with a polynomial potential, and the only points excluded from its moduli space are those where turning points coalesce. In the first phase of the procedure, one performs a numerical analysis of the WKB triangulation over the path in the moduli space to get the exact sequence of wall crossings involved and the spectrum of simple cycles in each chamber. The Python code developed for this thesis is suitable to perform such analysis, and it was successfully tested against the results shown in [IMS19], [IN14] and [GMN11]. Then, using the knowledge on the behavior of TBA and Y-system under analytic deformation, it is possible to first get algebraically the Y-system in the final chamber, and then directly read off the corresponding TBA system. By doing so, the analytic deformation is turned into an algebraic problem. The aim of the procedure above is to simplify the calculations and to try to single out, at the same time, the most basic working principles underlying TBA and Y-system deformation. It should be underlined that the approach could be applied to any problem whose description is based on WKB triangulations of polynomial functions. As a byproduct, the Python code here presented may be also used to compute the BPS spectra of the scaling limit of linear $SU(2)$ quivers in the context of $d = 4$, $\mathcal{N} = 2$ SUSY theories, as explained in [GMN11].

A natural continuation of the work presented in this thesis would be trying to generalize the set of allowed potentials. For example, it would be interesting to study the case of potentials with singularities at finite points (e.g., angular momentum terms like in Eq.2.21), or to extend the formalism to potentials with an infinite set of turning points, like for Liouville potentials. In the former case, one would have to deal also with "pops" in the WKB triangulations, while in the latter one, the main difficulty is represented by the appearance of an infinite number of cycles in the spectrum. Another line of research that builds on the results presented here consists in a systematic derivation of EQCs for arbitrary polynomial potentials, and generalizations thereof. This would be necessary to conclude the program of determining the spectra of Schrödinger problem using Y-systems and TBA systems presented in this thesis.

Acknowledgments

I would like to express my gratitude to Prof. Francesco Ravanini and Prof. Davide Fioravanti, for their support and their suggestions.

A heartfelt thanks goes to Francesco Mangialardi, for the collaboration we had during the first part of this thesis project, and for the helpful and productive conversations we shared.

I wish to express my warmest gratitude to my family and all my friends, for your endless and reassuring support. You all know what this means to me, and each of you carried me through this journey.

I would like to dedicate this Master's thesis to all my family and friends. In particular, a special thought goes to my grandmother, nonna Maria, who recently passed away.

Appendix A

Description of the Python Code

The numerical analysis was performed by developing a purpose-built Python code. This program provides functions to numerically compute, plot and analyze the Stokes graph of a generic potential in an arbitrary direction. The only assumption on the functional shape of the potential is that no singularities exist at finite points in the complex plane. The analysis presented in this thesis is specialized to the study of polynomial potentials, where the number of zeros is known and finite, and an essential singularity lies at infinity. This last aspect, as underlined in Chpt.3, is at the origin of the Stokes phenomenon that characterizes this problem, and it requires the definition of a suitable number of Stokes sectors (see Sect.3.4). The main purpose of the code is to determine the sequence of wall crossings for a given path in the energy complex plane, and to provide the correct wall crossing directions and the corresponding new masses in terms of the old ones. As explained in Sect.5.3, this is the required starting point to apply the general Procedure 5.2. The code provides three possible built-in functionalities, plus a fourth routine that may be fully customized. The three built-in ones are selected with boolean flags, and they correspond to the following:

1. "energy_boolean": determine the sequence of wall crossings for a given path in the energy complex plane, starting from the minimal chamber. The wall crossing directions are computed and the corresponding new masses are obtained in terms of the old ones. The mutations of the triangulations in each non-minimal chamber are provided, too, as they are necessary to get the spectrum of simple cycles in each chamber: this procedure is performed by the function "FindSpectrumOfCycles".
2. "theta_boolean": evaluate the $S^1(\theta)$ -action on the quadratic differential Φ associated to the polynomial potential at a fixed point in its moduli space. This routine essentially coincides with the content of the function "FindSpectrumOfCycles".
3. "just_one_theta_boolean": compute and plot the Stokes graph G_θ in a direction θ at a fixed point in the moduli space.

In the code, the standard mathematical Python libraries Numpy ([HMvdW⁺20]) and Scipy ([VGO⁺20]) are used, while plots are obtained with Matplotlib ([Hun07] and Seaborn ([Was21]). In addition, three open-source libraries are used at crucial stages in the code: "graph-tool" ([Pei14]) is employed for the analysis of the WKB triangulation from a graph's theory perspective, "cxroots" ([Par18]) to compute the zeroes (or turning points) of the function $Q(z)$ within a given contour in the complex plane, and "shapely" ([G⁺]) for the analysis of planar geometry features, like intersections between paths, or to check whether a point is contained in polygon or not.

Before turning to considering the validation of the code output, a brief description of the code is in order.

A.1 Code Description

Since the first option "energy_boolean" is the most complex one and it comprises all the features also contained in both "theta_boolean" and "just_one_theta_boolean", we shall concentrate on the first one. The most important inputs for this option are the energy path E_t in the energy complex plane, and the set of coefficients that fix the polynomial potential. The polynomial coefficients should be taken as real, so that the potential $V(z)$ is real for z real. The path E_t is assumed to start at a special point E_1 in the minimal chamber and to avoid the points where the turning points of the system coalesce. The main steps of the routine may be summarized as follows:

1. Starting from E_1 , find the roots of $Q(z)$ (all real roots) using "FindRootsQ0" and cxroots, and order them by their real part.
2. Define the cycles in the minimal chamber encircling adjacent roots using "RectangleBox": the direction on the path is fixed at this point by asking that the masses are all real and positive. The computation of the zero-order quantum periods is numerically performed using "PathIntegrationSqrt".
3. Enter a loop over the points in E_t . At each iteration, the roots positions are updated and the labeling is kept consistent with the previous step: the same label is associated to the root that is closest to a certain root from the previous step. To reduce the computational cost, the whole analysis of wall crossings and, possibly, WKB triangulations, is carried out every N_skip iterations. A generic analysis-iteration reads as follows:
 - (a) Update the known cycles and zero-order quantum periods using the new root positions.

- (b) If a wall crossing occurred in the last analysis-iteration, update the cycles spectrum with FindSpectrumOfCycles. Having recognized the already known cycles, append the new ones, and check whether they correspond to the sum or the subtraction between the cycles that produced the wall crossing. Fix the direction on the path accordingly.
- (c) Compute the ratios $\Im(\Pi_{\gamma_a}^0/\Pi_{\gamma_b}^0)$, for the pairings (a, b) in the spectrum having non-vanishing intersection between each other. Such pairs are considered for consistency with the Delabaere-Pham formula in Th.3, where discontinuities may arise only for intersecting simple cycles.
- (d) Check if a wall crossing occurred comparing the sign of each ratio with the corresponding one coming from the previous analysis-iteration.

The output of this routine consists then in the sequence of wall-crossings, including their directions, and with the definition of the new masses in terms of the old ones. In addition, the following plots and files are produced:

1. Plot of the energy path E_t in the energy complex plane (see for example Fig.4.15).
2. Sequence of roots configurations at each analysis-iteration.
3. Sequence of plots at each analysis-iteration with two subplots: on the left, the zero-order quantum periods, on the right, the masses (see for example Fig.4.5).
4. Mutations of the WKB triangulations and the underlying Stokes graphs for each non-minimal chamber.
5. Text file with all the ratios $\Im(\Pi_{\gamma_a}^0/\Pi_{\gamma_b}^0)$ and all the corresponding mass phase differences $\Delta\varphi_{a,b}$, for the intersecting pairings (a, b) . Such values are printed as functions of the parameter $t \in [0, 1]$ of the path E_t .

Due to their importance, let us briefly explain how the functions PathIntegrationSqrt and FindSpectrumOfCycles are implemented.

First, PathIntegrationSqrt integrates an arbitrary function in the form $\sqrt{f(z)}$ on a path on the Riemann surface of $\sqrt{f(z)}$. The only assumption is that no singularity is crossed along the path. The function f may also depend on an arbitrary set of parameters. The integration is approximated with a first order integration scheme, which reads as follows:

$$\int_{\gamma} dz \sqrt{f(z)} \approx \sum_{i=1}^N k_i f(z_i) (z_i - z_{i-1}) , \quad (\text{A.1})$$

where the set $\{z_i\}_{i=0}^N$ is a N -point discretization of the path γ , and $k_i = \pm 1$, with k_0 conventionally set to $+1$. The coefficients k_i for $i > 0$ are computed on the fly, and

they change sign if a discontinuity in the integrand is crossed along the integration path. Indeed, numerically, the square root is defined on a fixed determination of the square root. Hence, the discontinuities arising across the branch cuts are used to select the other appropriate leaf in the Riemann surface, so that the integration is performed over the whole Riemann surface. This is also crucial when dealing with the simple cycles and zero-order quantum periods, as simple cycles are closed paths only on the entire Riemann surface. A numerical subtlety arises in the analysis-iterations described above, while updating the previously known zero-order quantum periods. Indeed, the direction along the cycles is fixed once at the beginning, at the special point in the minimal chamber. However, it may happen that during the energy deformation, the starting point of the cycle crosses a branch cut: if so, the whole path integration would be performed starting from the other leaf of the Riemann surface, generating an overall minus sign discrepancy, and breaking the smooth deformation. To cure this problem, a corrective minus sign is picked if the quantum period is seen to discontinuously rotate by π with respect of the one computed at the previous analysis-iteration.

Now, let us consider `FindSpectrumOfCycles`. The purpose of this function is to get the spectrum of simple cycles at a given point of the moduli space. To do so, the $S^1(\theta)$ -action on the quadratic differential Φ associated to $Q(z)$ must be analysed. The first stage of the procedure aims at finding the optimal set of angles where to evaluate the WKB triangulation. Since, by construction, the angles where a flip occurs correspond to the phase of a zero-order quantum period, such set of phases is computed for all the cycles around any two turning points. It must be underlined that, if the point of the moduli space does not lie in the maximal chamber, some of these values will not correspond to simple cycles in the spectrum. Then, using the π -periodicity of the $S^1(\theta)$ -action, the opposite directions are added. Restricting to an arbitrary π -wide interval, the middle points between the angles in this set of phases are the optimal angles to use. Indeed, these angles maximize the saddle reductions, producing the widest Stokes regions possible and making the analysis less prone to numerical errors. In addition, they reduce to the minimum the number of angles where to evaluate the WKB triangulations, minimizing the computational cost. The second stage of the procedure consists in the loop over the optimal set of angles. At each iteration, a WKB triangulation is associated to the Stokes graph G_θ following the Procedure 3.1 for a polynomial $Q(z)$ of degree $r+1$. The circle cut out around the essential singularity at infinity has radius "max_distance", which is taken large enough so as to contain all the turning points and to allow to correctly describe the asymptotic behavior of the Stokes trajectories. Such parameter may be conveniently tuned by visual inspection with a preliminary run of the option `just_one_theta_boolean`. During an iteration at angle $\bar{\theta}$, the following operations are performed:

1. The Stokes graph is computed using "GetStokesCurves". This function finds the Stokes trajectories in the direction $\bar{\theta}$, using as starting points the turning points. The integration scheme is again a first order one, but with a backward implemen-

tation: by doing so, the vanishing of $Q(z)$ at the starting point is avoided, and the Stokes line may be determined more elegantly. The first step starting from the turning point z_0 reads as follows:

$$\int_{z_1}^{z_0} dz' \sqrt{Q(z')} = \int_{z_1}^{z_1 + \delta z_1} dz' \sqrt{Q(z')} \approx \sqrt{Q(z_0 - \delta z_1)} \delta z_1 \quad (\text{A.2})$$

Considering each turning point z_0 , a scan in every direction is performed using a small displacement δz_1 . The angles where

$$|I| \approx \left| \Im \left(e^{-i\theta} \sqrt{Q(z - \delta z_1)} \delta z_1 \right) \right| \quad (\text{A.3})$$

is minimized correspond to the directions of the Stokes trajectories emanating from z_0 . Then, a similar algorithm is iterated starting from each emanating trajectory, until the bounding circle at $|z| = \text{max_distance}$ is reached. At this stage, the scan is limited to the directions that are $\pi/6$ apart from the previous direction, so as to avoid the one turning back towards z_0 , and to reduce the computational cost.

2. The Stokes sectors are obtained using "GetStokesSectors". The bounding rays $z_j^{(+)}$ and $z_j^{(-)}$, $j = 1, \dots, r + 3$ are defined so as to contain the direction the Stokes trajectories are asymptotic to (see Eq.3.41), and they correspond to:

$$\begin{aligned} z_j^{(+)} &\equiv \left\{ z \in \mathbb{C} \mid \arg(z) = 2i \frac{\theta + \pi(2j + 1)/2}{r + 3} \right\} \\ z_j^{(-)} &\equiv \left\{ z \in \mathbb{C} \mid \arg(z) = 2i \frac{\theta + \pi(2j - 1)/2}{r + 3} \right\}, \end{aligned} \quad (\text{A.4})$$

if the polynomial coefficient of z^{r+1} is positive, and:

$$\begin{aligned} z_j^{(+)} &\equiv \left\{ z \in \mathbb{C} \mid \arg(z) = 2i \frac{\theta + \pi j}{r + 3} \right\} \\ z_j^{(-)} &\equiv \left\{ z \in \mathbb{C} \mid \arg(z) = 2i \frac{\theta + \pi(j - 1)}{r + 3} \right\}, \end{aligned} \quad (\text{A.5})$$

if the polynomial coefficient of z^{r+1} is negative.

3. A representative of the isotopy class of arcs is associated to each Stokes region with the function "GetStokesLinks". In this function, "GetStokesCurveThroughPoint" is used to get the Stokes trajectories going through an arbitrary point. The starting points here correspond to a suitably adapted version of the marked points \mathbf{M} in Procedure 3.1.

4. The abstract WKB triangulation is then computed with "BuildTriangulation", in terms of an undirected graph whose vertices are labelled using the Stokes sectors labelling. The path-finding algorithms in graph-tools are employed to find the internal edges of the triangulation and to associate the corresponding saddle class of cycles, as described at the end of Sect.3.4. This is done in the next step.
5. The set of simple cycles associated to the triangulation is obtained using "GetCyclesAndLabels"

After the loop over the set of optimal angles, the spectrum of simple cycles is finally obtained, by checking that a single flip is associated to each cycle.

Let us now conclude this Appendix presenting a brief validation of the code.

A.2 Code Validation

The numerical output of the program may be tested against the same computations performed in Mathematica ([Inc]). The root-finding function FindRootsQ0 was tested in this way, and also comparing its results with analytic solutions in the cases where analytic computations were possible. The integration routine PathIntegrationSqrt was tested against Mathematica, using $Q(z) = 2 - 5z + z^3$, with roots $z_1 = -1 - \sqrt{2}$, $z_2 = -1 + \sqrt{2}$ and $z_3 = 2$. The integration cycle is a rectangle encircling z_1 and z_2 counterclockwise. The result reads:

$$I_M = -10.8044 - 1.63936 \cdot 10^{-12}i . \quad (\text{A.6})$$

Using the same path and a discretization step along the path of 10^{-5} , PathIntegrationSqrt yielded:

$$I_{\text{PIS}} = -10.80438 + 1.8 \cdot 10^{-5}i , \quad (\text{A.7})$$

which is consistent with a real result, if one takes into account the first-order accuracy of the integration scheme. Now, let us present a visual validation of GetStokesCurves, with a direct comparison to Fig.3a, 3b, 3d, 3e and 3f in [IN14]. The results obtained with GetStokesCurves are shown in Fig.A.1, and they exhibit a good qualitative agreement with the ones in [IN14]. Finally, let us compare the abstract WKB triangulations for the cubic potential $Q(z) = z^3 - 3\lambda^2z + u$, as presented in Sect.9.4.4 of [GMN11]. Choosing $\lambda = i$, the mutations of the WKB triangulations are correctly reproduced using the option theta.boolean, and two energy values $u_1 = 0$ and $u_2 = 4i$: the first one corresponding to the minimal chamber is shown in Fig.A.2, whereas the second one lying in the maximal chamber is shown in Fig.A.3. Accordingly, in the maximal chamber, an additional flip is present, which is associated to the new cycle connecting non-adjacent turning points. The triangulations coincide with those presented in [GMN11] up to an irrelevant relabeling of the Stokes sectors.

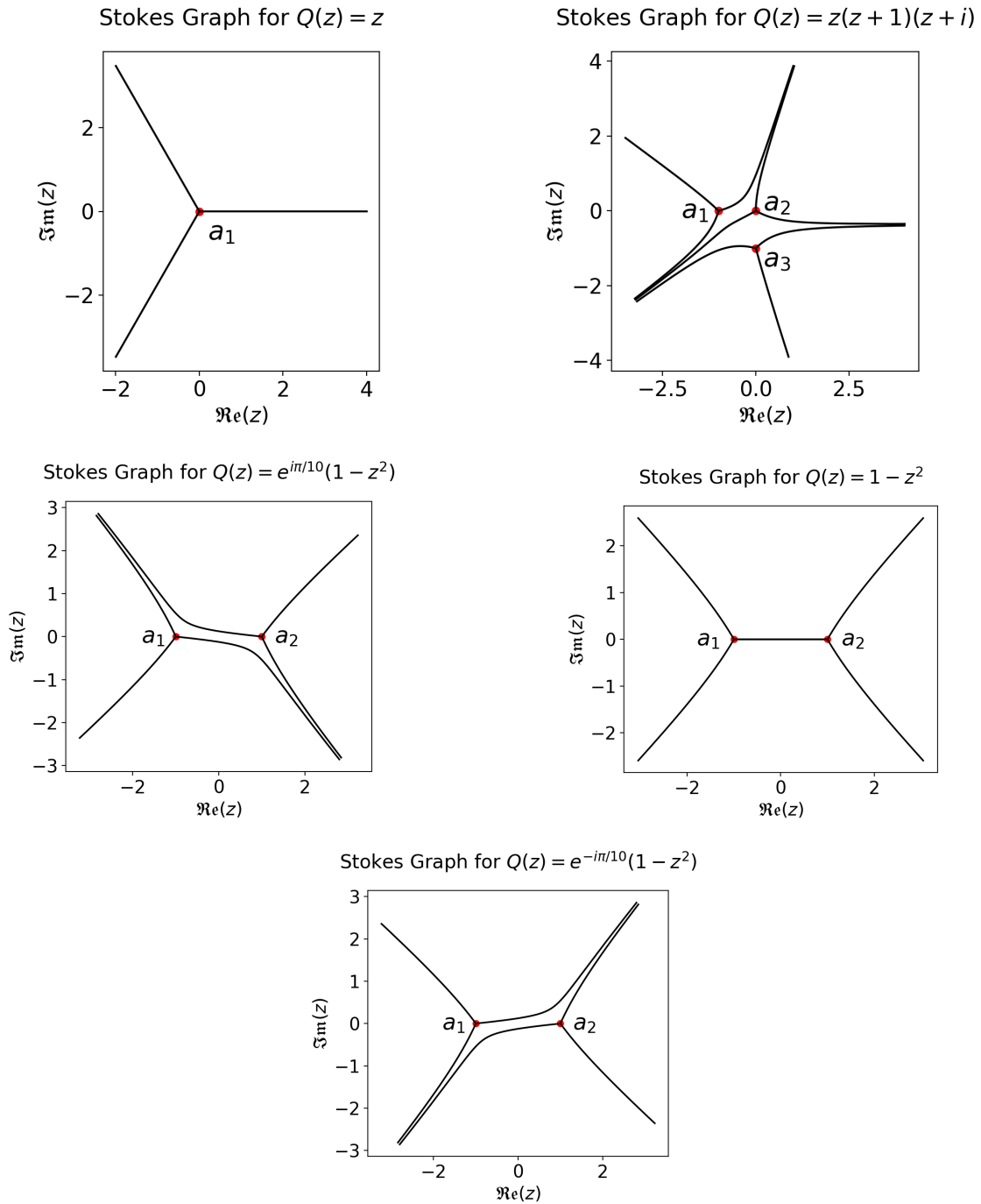


Figure A.1: Stokes graphs in the direction $\theta = 0$, as computed by GetStokesCurves. By visually comparing the results with those in Fig.3 in [IN14], a good qualitative agreement is found.

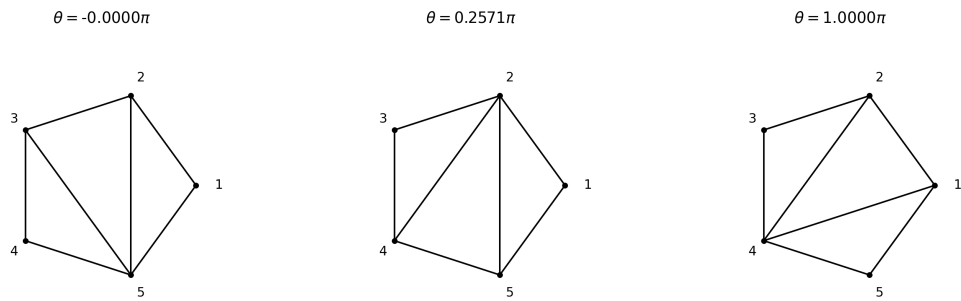


Figure A.2: WKB triangulations at $u = 0$ from the `theta_boolean` option.

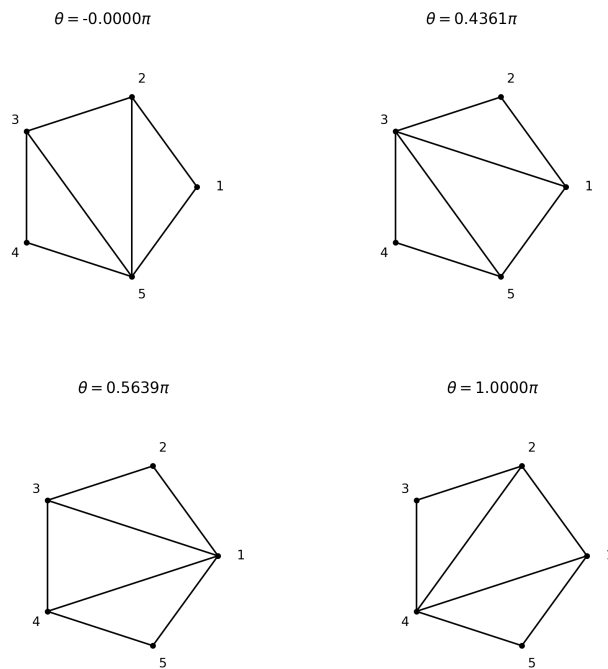


Figure A.3: WKB triangulations at $u = 4i$ from the `theta_boolean` option.

List of Figures

3.1	Signed flip $T' = \mu_k^{(\varepsilon)}(T)$ at k with sign ε	33
3.2	Stokes graph G_0 in the direction $\theta = 0$ for $V(z) = z^2$ and a real and positive energy.	48
4.1	Pole configuration and deformation of the integration path after wall crossing. The position of the pole is given here by $\theta'_p = \theta + i[\Delta\varphi_{2,1} - \pi/2]$, with $\Delta\varphi_{2,1} > \pi/2$	53
4.2	Mutations of the WKB triangulation for a cubic potential in the minimal chamber. The abstract triangulations in this figure were obtained from the analysis in Fig.4.3.	54
4.3	Mutations of the Stokes graphs of a cubic potential in the minimal chamber. The dashed blue lines delimit the Stokes sectors defined in Eq.A.4 and labeled with the corresponding integer number. Representatives of the class of arcs in the regular horizontal strips of the Stokes graph are shown as red lines. Finally, the yellow rectangular boxes denote the simple cycles associated to the Stokes graph. For the necessary background, see Sect.3.4, and, in particular, Procedure 3.1 and the following paragraphs.	55
4.5	Zero-order quantum periods $\Pi_{\gamma_i}^0$, $i = 1, 2$, associated to the simple cycles. The sequence shows their rotation along the path E_t in the energy plane: wall crossing here occurs as the periods align, and it produces a new cycle $\gamma_{12} = \gamma_1 + \gamma_2$	57
4.6	Mutations of the WKB triangulation for a cubic potential in the maximal chamber. The abstract triangulations in this figure were obtained from the analysis in Fig.4.7.	59
4.7	Mutations of the Stokes graphs of a cubic potential in the maximal chamber. For the content of this figure, see Fig.4.3.	60
4.8	Possible diagram for the masses of a quartic potential in the minimal chamber (or α -chamber).	65
4.9	Possible diagram for the masses of a quartic potential in the β -chamber, after a wall crossing with $\Delta\varphi_{2,3} > \pi/2$	66

4.10	Possible diagram for the masses of a quartic potential in the γ -chamber, after a wall crossing with $\Delta\varphi_{2,1} > \pi/2$	67
4.11	Spectrum of simple cycles in the γ -chamber.	68
4.12	Possible diagram for the masses of a quartic potential in the δ -chamber, after a wall crossing with $\Delta\varphi_{23,1} > 0$	68
4.13	Poles configuration of $K_{23,1}^+ * \tilde{L}_{23}^\gamma$ in the γ -chamber. Here, $\Delta\varphi_{23,1} < 0$, and a wall crossing is still possible if $\Delta\varphi_{23,1}$ becomes positive.	69
4.14	Spectrum of simple cycles in the δ -chamber. The associated graph is complete, indicating that this chamber is the maximal chamber.	70
4.15	Deformation path E_t in the energy complex plane.	71
4.16	72
4.17	Mutations of the WKB triangulations in the β -chamber.	73
4.18	Mutations of the Stokes graphs in the β -chamber. For the content of this figure, see Fig.4.3.	74
4.19	Mutations of the WKB triangulations in the γ -chamber.	75
4.20	Mutations of the Stokes graphs in the γ -chamber. For the content of this figure, see Fig.4.3.	76
4.21	Mutations of the WKB triangulations in the δ -chamber.	77
4.22	Mutations of the Stokes graphs in the δ -chamber. For the content of this figure, see Fig.4.3.	78
5.1	Pole configurations for the kernels $K_{2,1}$ and $K_{12,1}^+$ in Eq.5.1.	80
A.1	Stokes graphs in the direction $\theta = 0$, as computed by GetStokesCurves. By visually comparing the results with those in Fig.3 in [IN14], a good qualitative agreement is found.	95
A.2	WKB triangulations at $u = 0$ from the theta_boolean option.	96
A.3	WKB triangulations at $u = 4i$ from the theta_boolean option.	96

Bibliography

- [AMSV10] Luis F Alday, Juan Maldacena, Amit Sever, and Pedro Vieira. Y-system for scattering amplitudes. *Journal of Physics A: Mathematical and Theoretical*, 43(48):485401, nov 2010.
- [Bax72] Rodney J Baxter. Partition function of the eight-vertex lattice model. *Annals of Physics*, 70(1):193–228, 1972.
- [BB98] Carl M. Bender and Stefan Boettcher. Real spectra in non-hermitian hamiltonians having \mathcal{PT} -symmetry. *Physical Review Letters*, 80(24):5243–5246, jun 1998.
- [BF96] Adel Bilal and Frank Ferrari. Curves of marginal stability, and weak- and strong-coupling BPS spectra in $n = 2$ supersymmetric QCD. *Nuclear Physics B*, 480(3):589–619, dec 1996.
- [BLZ96] Vladimir V. Bazhanov, Sergei L. Lukyanov, and Alexander B. Zamolodchikov. Integrable structure of conformal field theory, quantum KdV theory and thermodynamic bethe ansatz. *Communications in Mathematical Physics*, 177(2):381–398, apr 1996.
- [BLZ97] Vladimir V. Bazhanov, Sergei L. Lukyanov, and Alexander B. Zamolodchikov. Integrable structure of conformal field theory II. q-operator and DDV equation. *Communications in Mathematical Physics*, 190(2):247–278, dec 1997.
- [BLZ99] Vladimir V. Bazhanov, Sergei L. Lukyanov, and Alexander B. Zamolodchikov. Integrable structure of conformal field theory III. the yang-baxter relation. *Communications in Mathematical Physics*, 200(2):297–324, feb 1999.
- [DDP97] E. Delabaere, H. Dillinger, and F. Pham. Exact semiclassical expansions for one-dimensional quantum oscillators. *Journal of Mathematical Physics*, 38(12):6126–6184, 12 1997.

- [DDT01] P. Dorey, C. Dunning, and R. Tateo. Spectral equivalences, bethe ansatz equations, and reality properties in pt-symmetric quantum mechanics. *Journal of Physics A: Mathematical and General*, 34(28):5679, jul 2001.
- [DDT07] Patrick Dorey, Clare Dunning, and Roberto Tateo. The ODE/IM correspondence. *Journal of Physics A: Mathematical and Theoretical*, 40(32):R205–R283, jul 2007.
- [DP99] Eric Delabaere and Frédéric Pham. Resurgent methods in semi-classical asymptotics. *Annales de l’Institut Henri Poincaré. Physique Théorique*, 71, 07 1999.
- [DT96] Patrick Dorey and Roberto Tateo. Excited states by analytic continuation of TBA equations. *Nuclear Physics B*, 482(3):639–659, dec 1996.
- [DT99a] P. Dorey and R. Tateo. On the relation between stokes multipliers and the t-q systems of conformal field theory. *Nuclear Physics B*, 563(3):573–602, dec 1999.
- [DT99b] Patrick Dorey and Roberto Tateo. Anharmonic oscillators, the thermodynamic bethe ansatz and nonlinear integral equations. *Journal of Physics A: Mathematical and General*, 32(38):L419–L425, sep 1999.
- [DT00] P. Dorey and R. Tateo. Differential equations and integrable models: the SU(3) case. *Nuclear Physics B*, 571(3):583–606, apr 2000.
- [ea20] N. Sueishi et al. On exact-wkb analysis, resurgent structure, and quantization conditions. *J. High Energ. Phys.*, 114, 2020.
- [FMS99] Philippe Di Francesco, Pierre Mathieu, and David Sénéchal. Conformal field theory. 1999.
- [G⁺] Sean Gillies et al. Shapely: manipulation and analysis of geometric objects, 2007–.
- [GMN11] Davide Gaiotto, Gregory W. Moore, and Andrew Neitzke. Wall-crossing, hitchin systems, and the wkb approximation, 2011.
- [HD93] F. Pham H. Dillinger, E. Delabaere. Résurgence de voros et périodes des courbes hyperelliptiques. *Annales de l’institut Fourier*, 43(1):163–199, 1993.
- [HMvdW⁺20] Charles R. Harris, K. Jarrod Millman, Stéfan J. van der Walt, Ralf Gommers, Pauli Virtanen, David Cournapeau, Eric Wieser, Julian Taylor, Sebastian Berg, Nathaniel J. Smith, Robert Kern, Matti Picus,

Stephan Hoyer, Marten H. van Kerkwijk, Matthew Brett, Allan Haldane, Jaime Fernández del Río, Mark Wiebe, Pearu Peterson, Pierre Gérard-Marchant, Kevin Sheppard, Tyler Reddy, Warren Weckesser, Hameer Abbasi, Christoph Gohlke, and Travis E. Oliphant. Array programming with NumPy. *Nature*, 585(7825):357–362, September 2020.

- [Hun07] J. D. Hunter. Matplotlib: A 2d graphics environment. *Computing in Science & Engineering*, 9(3):90–95, 2007.
- [IMS19] Katsushi Ito, Marcos Mariño, and Hongfei Shu. TBA equations and resurgent quantum mechanics. *Journal of High Energy Physics*, 2019(1), jan 2019.
- [IN14] Kohei Iwaki and Tomoki Nakanishi. Exact wkb analysis and cluster algebras, 2014.
- [Inc] Wolfram Research, Inc. Mathematica, Version 13.3. Champaign, IL, 2023.
- [KM90] Timothy R. Klassen and Ezer Melzer. Purely elastic scattering theories and their ultraviolet limits. *Nuclear Physics B*, 338(3):485–528, 1990.
- [KM91] Timothy R. Klassen and Ezer Melzer. The thermodynamics of purely elastic scattering theories and conformal perturbation theory. *Nuclear Physics B*, 350(3):635–689, 1991.
- [KT05] Takahiro Kawai and Yoshitsugu Takei. Algebraic analysis of singular perturbation theory. 2005.
- [Mus20] Giuseppe Mussardo. *Statistical Field Theory: An Introduction to Exactly Solved Models in Statistical Physics*. Oxford University Press, 03 2020.
- [Nik23] Nikita Nikolaev. Existence and uniqueness of exact WKB solutions for second-order singularly perturbed linear ODEs. *Communications in Mathematical Physics*, 400(1):463–517, jan 2023.
- [Par18] Robert Parini. cxroots: A Python module to find all the roots of a complex analytic function within a given contour, 2018.
- [Pei14] Tiago P. Peixoto. The graph-tool python library. *figshare*, 2014.
- [RVT93] F. Ravanini, A. Valleriani, and R. Tateo. DYNKIN TBA’s. *International Journal of Modern Physics A*, 08(10):1707–1727, apr 1993.
- [SC73] Yasutaka Sibuya and Robert H. Cameron. An entire solution of the functional equation $f(\lambda) + f(\omega\lambda)f(\omega^{-1}\lambda) = 1$, ($\omega^5 = 1$). 1973.

- [Sib75] Yasutaka Sibuya. Global theory of a second order linear ordinary differential equation with a polynomial coefficient. 1975.
- [VGO⁺20] Pauli Virtanen, Ralf Gommers, Travis E. Oliphant, Matt Haberland, Tyler Reddy, David Cournapeau, Evgeni Burovski, Pearu Peterson, Warren Weckesser, Jonathan Bright, Stéfan J. van der Walt, Matthew Brett, Joshua Wilson, K. Jarrod Millman, Nikolay Mayorov, Andrew R. J. Nelson, Eric Jones, Robert Kern, Eric Larson, C J Carey, İlhan Polat, Yu Feng, Eric W. Moore, Jake VanderPlas, Denis Laxalde, Josef Perktold, Robert Cimrman, Ian Henriksen, E. A. Quintero, Charles R. Harris, Anne M. Archibald, Antônio H. Ribeiro, Fabian Pedregosa, Paul van Mulbregt, and SciPy 1.0 Contributors. SciPy 1.0: Fundamental Algorithms for Scientific Computing in Python. *Nature Methods*, 17:261–272, 2020.
- [Vor83] A. Voros. The return of the quartic oscillator. the complex wkb method. *Annales de l'I.H.P. Physique théorique*, 39(3):211–338, 1983.
- [Vor93] André Voros. Résurgence quantique. *Annales de l'Institut Fourier*, 43(5):1509–1534, 1993.
- [Was21] Michael L. Waskom. seaborn: statistical data visualization. *Journal of Open Source Software*, 6(60):3021, 2021.
- [YY69] Chen Ning Yang and C. P. Yang. Thermodynamics of a one-dimensional system of bosons with repulsive delta-function interaction. *Journal of Mathematical Physics*, 10:1115–1122, 1969.
- [Zam90] Al.B. Zamolodchikov. Thermodynamic bethe ansatz in relativistic models: Scaling 3-state potts and lee-yang models. *Nuclear Physics B*, 342(3):695–720, 1990.
- [Zam91] Al.B. Zamolodchikov. On the thermodynamic bethe ansatz equations for reflectionless ade scattering theories. *Physics Letters B*, 253(3):391–394, 1991.